Properties of mesons and quarks under extreme conditions from Gauge/Gravity duality
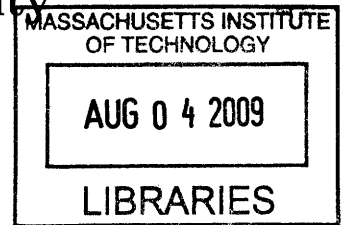
by

Thomas Faulkner

Submitted to the Department of Physics
in partial fulfillment of the requirements for the degree of

Doctor of Philosophy

at the

MASSACHUSETTS INSTITUTE OF TECHNOLOGY

June 2009

Author ....
Department of Physics
May 12, 2009

Certified by.....
Hong Liu
Associate Professor
Thesis Supervisor

Certified by
Krishna Rajagopal
Professor
Thesis Supervisor

Accepted by ....
Thomas J. Greytak
Associate Head for Education

Properties of mesons and quarks under extreme conditions from Gauge/Gravity duality

by

Thomas Faulkner

Submitted to the Department of Physics
on May 12, 2009, in partial fulfillment of the
requirements for the degree of
Doctor of Philosophy

Abstract

This thesis is concerned with the properties of mesons and quarks which live in the strongly coupled plasma of certain gauge theories which are similar to QCD. To study these plasmas we exploit gauge gravity duality which has been particularly useful for understanding QCD at temperatures above, but not far above, that at which quarks and gluons are deconfined.

For example we will show analytically that mesons propagating through these plasmas have a subluminal limiting velocity at non zero temperatures. This limiting velocity decreases with increasing temperature towards the dissociation temperature. We then argue that this behavior will be universal in gauge theories with a gravity dual. If this result applies in QCD it would have observable effects in future heavy ion collisions at RHIC and the LHC. We also study the width of these mesons by exploiting nonperturbative string effects which can destabilize them, a result we attribute on the gauge theory side to thermal fluctuations. We show that the lifetime of these mesons, described via nonperturbative string effects, decreases rapidly above the momentum at which the meson speed approaches its limiting velocity. This is further evidence for the universality of the limiting velocity and it sharpens the signature expected in heavy ion collisions, especially when the LHC starts colliding ions.

Finally the system that was used to study these mesons has an interesting phase structure in the plane of temperature and quark chemical potential. We find a third order phase transition line which ends at a tricritical point. We argue that this phase transition is driven by the same nonperturbative physics which contributed to the meson lifetime.

Thesis Supervisor: Hong Liu
Title: Associate Professor

Thesis Supervisor: Krishna Rajagopal
Title: Professor

Acknowledgments

Contents

List of Figures

15

Chapter 1

Introduction

In this chapter we will begin by motivating the strong coupling problem of QCD, focusing on attempts to understand the strongly coupled quark gluon plasma. Then we will introduce AdS/CFT as a tool for understanding features of strongly interacting theories, such as QCD. We will explain how to add fundamental degrees of freedom to pure gauge theories in AdS/CFT. The system we will arrive at will be the main focus of this thesis from which general properties of mesons and quarks in these AdS/CFT setups will be derived.

1.1 QCD and the quark gluon plasma

The vacuum of QCD looks nothing like the perturbative degrees of freedom (quarks and gluons) we use to define it. The reason for this is that the interactions are strong which leads to confinement of the perturbative degrees of freedom - the spectrum which results is that of hadrons. Thanks to asymptotic freedom, at large energies the coupling is weak and we may talk of quarks and gluons freely.

For QCD at finite T, one would expect a similar picture where at small temperatures the relevant degrees of freedom are hadrons and at very high temperatures one expects a free gas of quarks and gluons, the quark-gluon plasma. Somewhere in between there is a deconfinement transition T_d, which for real QCD at zero Baryon density is just a cross over.

What of the region in between: above the deconfinement transition, but not too far above it? Turning to experiment, an interesting picture has emerged over the last few years, of a deconfined yet strongly interacting phase of quarks and gluons (sometimes referred to as the strongly coupled QGP or sQGP.) Heavy ion experiments at RHIC collide Gold nuclei at energies of 200GeV per nucleon. The resulting fireball of quarks and gluons seems to behave collectively like an almost perfect liquid - a liquid which is well described by hydrodynamics.

The conclusion of collective behavior comes from examining the asymmetry of a collision around the collision axis. This is characterized by the elliptic flow parameter v_2 as a function of the impact parameter of the collision. v_2 is the second moment of the collision distribution around the collision axis. For a weakly interacting gas v_2 should be small, or dominated by fluctuations which go away for large number of individual nucleon collisions. This is not found. Instead, the degrees of freedom and hence the observable v_2 are found to be best modeled by ideal hydrodynamics [1, 2, 3]. Fitting the data on elliptic flow to hydrodynamic models gives a range for the viscosity to entropy density ratio η/s of $0 - 0.2$ [3].

Ideal hydrodynamics actually means strong interactions - the viscosity is a measure of the ability of the medium to transfer momentum, the stronger the interactions between constituents the harder it is for momentum to transfer across a fixed distance since the distance between collisions is small. For example, for weakly interacting $\lambda\phi^4$ theory $\eta/s \sim \lambda^{-2}$ [4], so one might imagine that the viscosity to entropy density ratio η/s is a good measure of the inverse coupling of the theory. As a result the observations of v_2 cannot be explained in perturbation theory.

We need new tools in order to understand analytically the properties of such a strongly interacting QGP. Lattice QCD is useful when it comes to strong coupling properties of QCD, however it is hard to extract dynamical quantities. On the lattice, properties are measured in Euclidean time: it is hard to rotate back to real time without analytic results. Certainly the sQGP is a "dynamic" environment, so such a program remains difficult[1].

---

[1]See [116] for recent progress in this direction.

There is one calculation of η/s in a class of strongly coupled quark gluon plasmas, for which the result is universally $1/4\pi$. [2] These plasmas are exactly those which are described by the AdS/CFT correspondence in the gravity approximation (to be explained below.) This result has spurred interest in AdS/CFT as a tool for understanding the quark gluon plasma of QCD, and a growing list of properties (some universal and some not) have been found for this class of theories in order to compare to experiment. This list includes: diffusion constants [5, 6], the diffusion of quarks through the plasma [7, 8], the opacity of the plasma to hard probes [9], etc. In the next section we will describe the screened quark anti-quark potential in QCD which has also been extensively investigated through AdS/CFT [10, 11, 12, 13].

1.1.1 The phenomenon of J/Ψ suppression

Electromagnetic interactions are screened by free electrons in an ordinary plasma. Through this the photon receives a mass called the Debye mass m_D. A similar mechanism is at play for the QCD plasma. It is not hard to see that this will have important consequences for bound states of quarks and anti-quarks (mesons) that live in such a plasma. The weakened interactions should suppress their survival probability, relative to if the mesons were simply found in vacuum. So it was suggested in [14] that this suppression for the J/Ψ meson is an ideal probe of properties of the medium itself.

The inverse Debye mass defines a scale called the screening length and characterizes the size of the interactions between a heavy quark antiquark pair. Lattice calculations [15] of this potential give an estimate of this length of around $L_s \sim 0.5/T$ as a function of temperature.

Dissociation is then simply a matter of scales [16]. For hadrons made of light quarks (including the strange quark) the screening length already at the deconfinement transition is smaller than their size, which is determined largely by the dynamical scale of QCD, of around 1fm. Hence they will not survive the deconfinement

---

[2]This is certainly small, in fact it has been conjectured to be a lower bound for any substance, [117, 118, 119].

transition, and so will not be useful as probes of the deconfined quark-gluon plasma. On the other hand the size of heavy quark bound states is determined largely by their heavy constituent quarks. Potential models, which work well for such states [16], suggest that the size of J/Ψ is about .25 fm much smaller than the size of hadrons made of lighter quarks. Equating this size to the screening length gives a dissociation temperature of around $T = 2T_c$. These states *do* survive above T_c and may provide a useful thermometer for this state of matter.

As we will discuss in more detail in Chapter 2, lattice calculations of meson spectral functions confirm this picture, suggesting that the J/Ψ meson in a thermal bath survives the deconfinement transition T_c, but dissociates (ceases to exist) at around $T = 1.5T_c$ [17]. However the QGP created at RHIC is not a static thermal bath, but rather a very dynamic environment. So it would be nice to understand the effects of a flowing plasma on the properties of the the J/Ψ meson. Lattice calculations are not suited to this, so we will examine this question using the AdS/CFT correspondence. From an examination of the screened quark anti-quark potential in a flowing plasma the authors of [10, 11] suggested that in fact the survival probability for a heavy quark meson moving relative to the plasma would further be suppressed.

This calculation will be summarized later in this chapter, as it provides motivation for going beyond the quark-antiquark potential and studying directly a system with dynamical quarks and real meson bound states. This will be the main focus of this thesis. Studying real meson bound states will further strengthen the predictions inferred from the quark anti-quark potential. In Chapter 2 we will find that the propagation of heavy quark mesons is dramatically modified by a limiting velocity which is less than the speed of light. We will also find in Chapter 3 that the widths of these mesons below their dissociation temperature increase dramatically as a function of momentum relative to the plasma.

1.2 The Gauge Gravity Duality

The large N_c limit of gauge theories is a useful approximation to the theory at finite N_c (that is $N_c = 3$ for QCD.) The limit must be carefully defined such that the Yang-Mills coupling g_{YM} is scaled appropriately, holding the 't Hooft coupling

$$\lambda = g_{\text{YM}}^2 N_c \tag{1.1}$$

fixed. Upon making the assumption of confinement, large N_c QCD was shown to yield a weakly interacting "classical" theory of mesons and glueballs, a good starting point for any understanding of the low energy dynamics of QCD. However, as opposed to large N vector models where the theory becomes free, matrix models cannot be directly solved in this limit. (For example the spectrum of mesons and glueballs in large-N_c QCD cannot be found.) Actually since we know QCD to be a strongly interacting theory at low energies this feature is a blessing - we have not lost one of the essential features of the theory. It was long believed that the appropriate theory to describe large N_c QCD was in fact a string theory, with $1/N_c$ playing the role of the string coupling g_s. The first realization of this idea was from [18], where a specific string theory constructed on Anti-de Sitter (AdS) space was conjectured to be dual to a special gauge theory which was in fact a Conformal Field Theory (CFT). This set of ideas is labeled the AdS/CFT correspondence.

This gives the simplest example of the AdS/CFT correspondence: the duality between $\mathcal{N} = 4$ super Yang-Mills (SYM) theory and classical gravity in $AdS_5 \times S_5$ [18, 19, 20, 21]. $\mathcal{N} = 4$ super Yang-Mills (SYM) theory is a conformally invariant theory with two parameters: the rank of the gauge group N_c and the 't Hooft coupling λ defined in (1.1). These parameters imprint themselves in the string theory via the string coupling and the curvature scale of AdS in string units $R/\sqrt{\alpha'}$,

$$4\pi g_s = \lambda/N_c, \qquad \frac{R^4}{(\alpha')^2} = \lambda \tag{1.2}$$

In the large-N_c limit, quantum effects can be neglected and in the large λ limit

the string length scale is small and stringy corrections can be ignored. Upon taking these limits gauge theory problems can be solved using classical gravity in $AdS_5 \times S_5$ geometry. Throughout this thesis we will mostly be concerned with this limit. In chapter 4 we will make some comments about relaxing the $\lambda \to \infty$ limit.

At finite temperature, $\mathcal{N} = 4$ SYM theory with a gauge group $SU(N_c)$ can be described by a string theory in the spacetime of a black hole in $AdS_5 \times S_5$, whose metric can be written as

$$ds^2 = \frac{r^2}{R^2}\left(-f dt^2 + d\vec{x}^2\right) + \frac{R^2}{r^2}\frac{dr^2}{f} + R^2 d\Omega_5^2 \tag{1.3}$$

where $\vec{x} = (x_1, x_2, x_3)$ and

$$f = 1 - \frac{r_0^4}{r^4} . \tag{1.4}$$

$d\Omega_5^2$ is the metric on a unit five-sphere S_5 and r_0 is the location of the black hole horizon. The temperature T of the YM theory is given by the Hawking temperature of the black hole,

$$T = \frac{r_0}{\pi R^2} . \tag{1.5}$$

One can think of the gauge theory as living at the boundary of AdS_5 at $r \to \infty$, with the spacetime coordinates $(t, \vec{x})$ which we will collectively denote x.

It is important to note that the existence of this black hole at any finite temperature T implies that $\mathcal{N} = 4$ SYM is always *deconfined* [22]. So we will only use it as a model of QCD above the deconfinement transition.

One of the basic maps in the dictionary between gauge theory and gravity is a correspondence between gauge invariant local operators $O(x)$ and fields in the bulk gravity theory $\phi(x, r)$. Correlators of such operators can be calculated using the GKPW formula [19, 20] which relates the generating functional of the field theory to the on-shell gravity action:

$$Z[\phi_0] \equiv \left\langle \exp\left(-\int d^4x \phi_0(x) O(x)\right) \right\rangle \sim \exp\left(-S_{\text{grav}}[\phi(r, x)]\right) \tag{1.6}$$

where $\phi(r, x)$ solves the appropriate field equation in the bulk subject to certain

boundary conditions. For simplicity we will work here in Euclidean time. To describe the boundary conditions we observe the behavior close to the boundary of AdS. This is quite generally,

$$\phi(r, k) = \phi_0(k)r^{\Delta-4}(1 + \mathcal{O}(r^{-1})) + \psi(k)r^{-\Delta}(1 + \mathcal{O}(r^{-1})) \qquad (1.7)$$

where we are now working in Fourier space for the spacetime directions $x \to k$. Δ is the dimension of the operator $O(x)$ which can be calculated from gravity. The two boundary conditions for a second order field equation are then: fix ϕ_0 at the boundary and demand regularity of the solution in the bulk of AdS. This will then fix $\psi(k)$ in (1.7) in terms of $\phi_0(k)$.

For example from (1.6) the two point function works out to be:

$$\langle O(k)O(-k)\rangle \sim \frac{\psi(k)}{\phi_0(k)} \qquad (1.8)$$

Care must be used when defining this in real time, especially in the presence of a horizon in the bulk. The correct prescription is to demand in-falling boundary conditions at the horizon [123]. Then the formula (1.8) computes the retarded Greens function in the gauge theory. We will come across real time issues in Chapter 3 of this thesis.

The reason we have introduced this machinery is that it allows us to study the spectrum of states in the gauge theory. We will be interested in meson bound states which will show up as poles in the retarded greens function of certain operators which we will discuss in the next section. From (1.8) we see that this occurs when $\phi_0(k) = 0$. Because the overall normalization of ϕ does not matter, the extra condition $\phi_0(k) = 0$ actually over specifies the problem and solutions of this form will only occur for a discrete set of energies $k^\mu = (\omega_n(\vec{k}), \vec{k})$. In fact if our bulk space is regular (and there are no annoying horizons) then the problem reduces to that of eigenvalues/eigenstates of some Schrödinger type problem. The potential of the resultant Schrödinger equation has no scattering states. The reason for this is that the boundary of AdS acts like an infinite box. This is the classic picture of confinement in AdS/CFT [22]: if the

bulk geometry is everywhere regular, correlators of gauge invariant operators will only have a discrete spectrum. This satisfies the expectation in the large-N limit (upon the assumption of confinement.) We will actually see, in chapter 2 of this thesis, such a spectrum for mesons in the *deconfined* phase of a gauge theory plasma, albeit with a dispersion relation $\omega_n(k)$ different from the relativistic one. The reason that, despite living in a deconfined plasma, the meson spectrum is discrete is essentially that the field dual to the meson operator lives in a smooth geometry which is asymptotically AdS.

If there was a horizon, then in general only solutions with complex $\omega(\vec{k})$ will exist. These are termed quasi-normal modes [23], however for our purposes they are really just mesons with a width. In chapter 3 we will demonstrate how this comes about for the mesons studied in chapter 2. The essential mechanism will be to generate a black hole horizon in the normally smooth geometry these mesons live in.

1.2.1   The philosophy - universality

Having introduced AdS/CFT at non-zero T we are now in a position to discuss how we can use this tool to make predictions for QCD without actually having a dual gravity theory for QCD.

Firstly we should mention that although in the vacuum $\mathcal{N} = 4$ SYM looks very different to QCD at finite-T they look very similar. In vacuum $\mathcal{N} = 4$ SYM is supersymmetric, conformal, not confining, has gapless excitations. Whereas QCD is certainly not supersymmetric and because of the dynamic scale Λ_{QCD} it is not conformal, it is confining and has a mass gap. At non-zero T all these differences disappear [24]. One clear remaining difference is the number of degrees of freedom, however for certain quantities there are ways to scale out this dependence - for example by taking ratios. An example of such a quantity is the energy density $\epsilon(T)$ of the plasma, which will clearly scale with the number of degrees of freedom. However taking the ratio of the energy density to that of the energy density of the same system at zero coupling (the usual Stefan Boltzmann law $\epsilon_{SB} \propto T^4$) we can make a useful comparison between QCD and $\mathcal{N} = 4$ SYM. The calculation in $\mathcal{N} = 4$ can

be done at strong coupling using gravity [25], and the result is $\epsilon/\epsilon_{SB} = .75$. Lattice calculations [26] also suggest that this ratio goes to a *constant* rapidly above the deconfinement temperature, taking a value of around $\epsilon/\epsilon_{SB} = .85$. The fact that this value is less than 1 is an indication of strong interactions, it is also interesting because it is consistent with the behavior of an interacting conformal field theory. The reason this should be the case is still not known.

Secondly, via the AdS/CFT correspondence a new notion of universality is emerging which goes beyond the standard condensed matter definition of universality (based on global symmetries.) The primary example of this is the universal quantity $\eta/s = 1/4\pi$, which is true for all theories with string theory duals in the large-N_c and strong coupling limit. We will present two more examples in this thesis. It is interesting to entertain the possibility that QCD is in this universality class, or at least close to it. We can then make predictions based on this.

Hence we will proceed, looking for quantities on the gravity side of the duality which are universal. The calculations done in Chapter 2 and 3 were mostly done in $\mathcal{N} = 4$ SYM. However we argue that they should apply to a large class of gauge theories with gravity duals, and so might also apply to QCD.

1.2.2 Thermal screening from gravity

One prediction of AdS/CFT for heavy ion collisions relates to the screened interactions of quarks and antiquarks bound together in a meson and moving relative to the rest frame of the QCD plasma. This prediction was made in [10, 11] by studying the potential between a *test* quark and anti-quark moving through an $\mathcal{N} = 4$SYM plasma. This calculation is summarized in Chapter 2, Section 2.2. Here we heuristically explain how such a potential may be obtained using semiclassical strings to compute Wilson loops. This will serve as a motivation for the introduction of dynamical quarks/flavors, the main subject of this thesis.

The heavy quark anti-quark potential (in a pure gauge theory) is defined generally

using a Wilson loop [27],

$$\langle W(C_L) \rangle = \left\langle \text{Tr} \mathcal{P} \exp \left(i \int_{C_L} A \right) \right\rangle \sim \exp(-iV(L)\tau) \qquad (1.9)$$

where the contour C_L is a rectangle with spatial separation L and temporal separation τ, and the trace is taken in the fundamental representation. The potential is extracted in the limit $\tau \gg L$. Ignoring the spacelike segments of the curve the Wilson loop calculates the action of an infinitely heavy quark anti-quark pair separated by L.

In the supergravity approximation of the string theory side of the duality, this Wilson loop is obtained by computing the action of an extremal string world sheet, ending at $r \to \infty$ (r being the fifth dimension of AdS_5) on the curve C_L. The heavy quarks are represented by the ends of the string and as such live on the boundary of AdS_5 separated by a distance L. The string then hangs down from the the boundary of AdS_5 towards smaller r and represents the interactions between the quark and anti-quark. Quantitatively the potential is then simply given by the renormalized action of this string $V(L)\tau = S(C_L)_{\text{ren}}$, where renormalization accounts for the infinite action of two infinitely massive and non interacting *test* quarks.

In $\mathcal{N} = 4$ SYM theory at zero temperature, the static potential between a heavy external quark and antiquark separated by a distance L is given in the large N_c and large λ limit by [28, 27]

$$V(L) = -\frac{4\pi^2}{\Gamma(\frac{1}{4})^4} \frac{\sqrt{\lambda}}{L} , \qquad (1.10)$$

where the $1/L$ behavior is required by conformal invariance.

At non-zero temperature a very nice picture of thermal screening from string theory emerges [29, 30]. The existence of a black hole at $r = r_0$ means there are now two possible saddle points to the area extremization problem. The new saddle point is simply two strings hanging down into the black hole unaware of each other. This solution will become dominant for separations above a critical length L_c, and hence indicates a complete loss of interaction for $L > L_c$. This situation is pictured in 1-1. For $\mathcal{N} = 4$ SYM it was found [29, 30] that $L_c = .24/T$.

In limit where the tension of the string is large (λ large) the potential has a
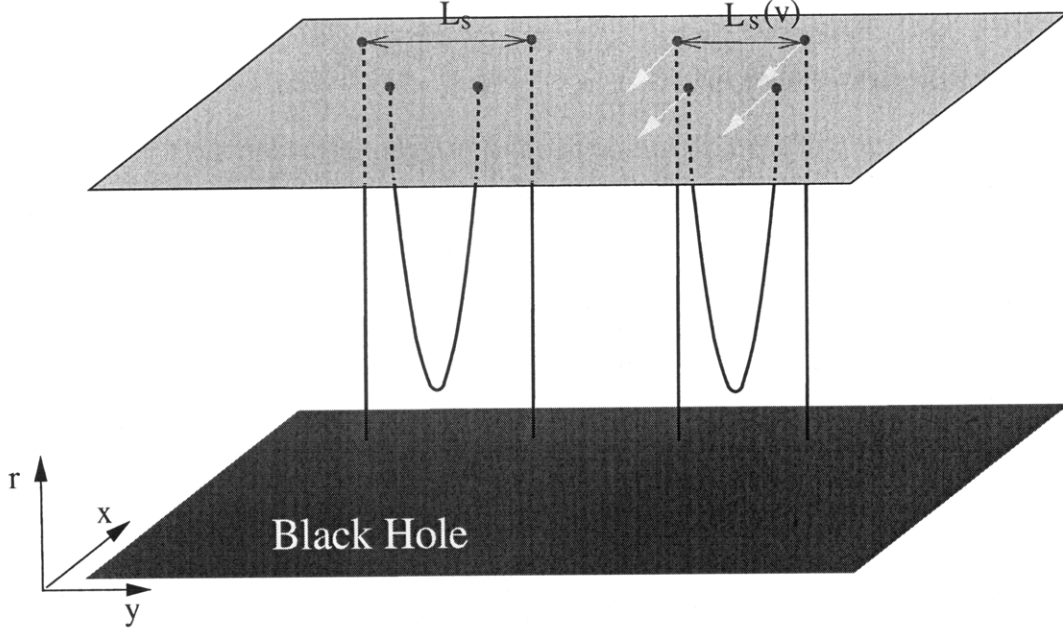
Figure 1-1: Schematic picture of the AdS_5 black hole and the computation of the screening length from hanging semiclassical strings. The calculation for moving quarks is very similar.

discontinuity at $L = L_c$.

$$
\begin{aligned}
V(L) &\approx \frac{\sqrt{\lambda} f(LT)}{L} \qquad L < L_c \\
&\approx 0 \qquad L > L_c .
\end{aligned}
\tag{1.11}
$$

This discontinuity should be smoothed out at finite λ. Of course it is natural to identify L_c as a screening length for gluon interactions. Or in other words the Debye mass at strong coupling satisfies $m_D = 1/L_c \approx 4T$. This should be compared with the screening length at weak coupling $\lambda \ll 1$ which is $m_d = \sqrt{\lambda} T$.

At non-zero velocity a similar picture of the two saddle points exists. However the critical length at which the change in dominance occurs is changed to [10, 11],

$$
L_s(v, T) \approx L_s(0, T)(1 - v^2)^{1/4} \propto \frac{1}{T}(1 - v^2)^{1/4} .
\tag{1.12}
$$

In words, the screening length decreases with increased motion relative to the plasma. As will be discussed in Chapter 2.6, this behavior fits into the usual universality

discussion of Section 1.2.1, in the sense that such a scaling exists in a large class of gauge theories with gravity duals.

For a *bound state* of a quark and anti-quark we can interpret the screening length in terms of meson dissociation. The temperature at which a meson dissociates can be estimated by the point at which the screening length becomes larger than the size of the meson.

Given this, the velocity dependence of the screening length (1.12) suggests that the dissociation temperature $T_{\text{diss}}(v)$, the temperature above which mesons with a given velocity do not exist, should scale with velocity as [10]

$$T_{\text{diss}}(v) \sim T_{\text{diss}}(v = 0)(1 - v^2)^{1/4} \ . \tag{1.13}$$

The scaling (1.13) then indicates that slower mesons can exist up to higher temperatures than faster ones.

The results (1.12) and (1.13) have a simple physical interpretation which suggests that they could be applicable to a wide class of theories regardless of specific details. First, note that since $L_s(0) \sim \frac{1}{T}$, both (1.12) and (1.13) can be interpreted as if in their rest frame the quark-antiquark dipole experiences a higher effective temperature $T\sqrt{\gamma}$. Although this is not literally the case in a weakly coupled theory, in which the dipole will see a redshifted momentum distribution of quasiparticles coming at it from some directions and a blueshifted distribution from others [31], we give an argument below for how this interpretation can nevertheless be sensible. The result (1.12) can then be seen as validating the relevance of this interpretation in a strongly coupled plasma. The argument follows from the *assumption* that quarkonium propagation and dissociation are mainly sensitive to the local energy density of the medium.[3] Now, in the rest frame of the dipole, the energy density (which we shall denote by ρ) is blue shifted by a factor $\sim \gamma^2$ and since $\rho \propto T^4$ in a conformal theory, the result (1.12) is as if quarks feel a higher effective temperature given by $T\sqrt{\gamma}$. As we have

---

[3]Note that it is not obvious that it should be energy density and not for example entropy density for which quarkonium dissociation is sensitive to, so one may alternatively interpret (1.13) as evidence in favor of this assumption.

already mentioned lattice calculations indicate that the quark-gluon plasma in QCD is nearly conformal over a range of temperatures $1.5T_c < T \lesssim 5T_c$, with an energy density $\rho \approx bT^4$ where b is a constant about 85% of the free theory value [26] (see also [32, 33].) So it does not seem far-fetched to imagine that (1.12) could apply to QCD. We should also note that AdS/CFT calculations in other strongly coupled gauge theories with a gravity description are consistent with the interpretation above [34] and that for near conformal theories the deviation from conformal theory behavior appears to be small [34, 35].

If a velocity scaling like (1.12) and (1.13) holds for QCD, it can potentially have important implications for quarkonium suppression in heavy ion collisions as we will discuss at the end of Chapter 2.

While the argument leading from (1.12) to (1.13) is plausible, it is important to have a set-up within which one can study mesons directly. Such a set-up will allow us to move one step closer to real QCD, allowing us to study properties of mesons which cannot be inferred from the study of the quark anti-quark potential. Dynamical properties such as their dispersion relations and widths. It is the purpose of Chapter 2 and Chapter 3 to examine this issue in a specific model with dynamical flavors. For now we simply introduce the AdS/CFT machinery that will make this study possible.

1.3 Adding flavors - the D3/D7 system

This brings us to a discussion of the main system of interest to us, the D3/D7 system. We want to add fundamental matter to the previously discussed gauge theory. The general picture of how to do this in string theory is to "add a D-brane" in the bulk. A D-brane is a soliton/defect of string theory which strings can end on. It will turn out that the strings which end on this D-brane have the interpretation of quarks.

To be more specific one can introduce "quarks"[4] to $\mathcal{N} = 4$ SYM theory by adding N_f $\mathcal{N} = 2$ hypermultiplets in the fundamental representation of the gauge group. In the limit of large N_c with N_f finite this can be described in the dual string theory

---

[4]Quarks in this system are both bosonic and fermionic, due to supersymmetry.

side by adding N_f D7-branes in the black hole geometry[5] (1.3) and to leading order in N_f/N_c, the back reaction of the D7-branes on the background geometry can be neglected. A fundamental "quark" in the YM theory can be described by an open string with one end on the D7-branes and the other end on the black hole. Strings corresponding to quarks and anti-quarks have opposite orientations. Open strings with both ends on the D7-branes can be considered as "bound states" of a quark and antiquark, thus describing meson-type excitations in the YM theory.

In the usual limit

$$N_c \to \infty, \qquad \lambda \to \infty, \qquad N_f = \text{finite} \qquad (1.14)$$

which corresponds to the limit $g_s \to 0$, $\frac{\alpha'}{R^2} \to 0$ in the string theory side, the geometric embedding and the dynamics of the D7-branes can be described using the Dirac-Born-Infeld (DBI) action

$$S = -N_f T_7 \int d^8\xi \sqrt{-\det\left(g_{mn} + 2\pi\alpha' F_{mn}\right)}. \qquad (1.15)$$

where g_{mn} denotes the induced metric on the D7-brane and $T_7 = \frac{1}{(2\pi)^7 g_s \alpha'^4}$ is the tension of a D7-brane.

To describe the embedding of the D7-branes in (1.3), it is more convenient to introduce a new radial coordinate u defined by

$$\frac{dr^2}{r^2 f(r)} = \frac{du^2}{u^2}, \quad \implies \quad r^2(u) = \frac{u^4 + u_0^4}{u^2} \text{ with } u_0 \equiv \frac{r_0}{\sqrt{2}} \qquad (1.16)$$

in terms of which (1.3) can be written as

$$\begin{aligned} ds^2 &= -\frac{r^2(u)}{R^2} f(u) dt^2 + \frac{r^2(u)}{R^2} d\vec{x}^2 + \frac{R^2}{u^2}(du^2 + u^2 d\Omega_5^2) \\ &= \frac{u^2}{R^2} q(u) \left(-f dt^2 + d\vec{x}^2\right) + \frac{R^2}{u^2}\left(d\rho^2 + \rho^2 d\Omega_3^2 + dy^2 + y^2 d\phi^2\right) \end{aligned} \qquad (1.17)$$

---

[5]See Chapter 2 Section 3.1 for a discussion of the D7 brane at zero temperature.

where

$$u^2 = y^2 + \rho^2, \qquad f(u) = \frac{(u^4 - u_0^4)^2}{(u^4 + u_0^4)^2}, \qquad q(u) \equiv \frac{r^2(u)}{u^2} = 1 + \frac{u_0^4}{u^4} . \qquad (1.18)$$

In (1.17), we have split the last term of the first line in terms of polar coordinates on $\mathbb{R}^4 \times \mathbb{R}^2$ with $d\Omega_3^2$ denoting the metric on a unit three-sphere. The D7-branes can be chosen to lie along the directions $\xi^\alpha = (t, \vec{x}, \Omega_3, \rho)$ and using the symmetries of the problem the embedding in the two remaining transverse directions can be taken as $\phi(\xi^\alpha) = 0$ and $y(\xi^\alpha) = y(\rho)$. $y(\rho)$ can be found by solving the equation of motion obtained from the DBI action (1.15) with the boundary condition

$$y(\infty) = L = (2\pi\alpha')m_q \qquad (1.19)$$

where m_q can be interpreted as the (bare) mass of the "quarks". We denote the resulting embedding function as $y_0(\rho)$, which were first obtained numerically in [43]. At a small temperature, the brane lies entirely outside the black hole, as indicated schematically in Fig. 1-2. The brane is closest to the black hole at $\rho = 0$, where the three-sphere in last term of (1.17) shrinks to a point. Denoting

$$y_0(\rho = 0) = L_0 \qquad (1.20)$$

then the shortest open string connecting the D7-brane to the horizon has a mass in the YM theory

$$m_q^{(T)} = \frac{1}{2\pi\alpha'} \int_{u_0}^{L_0} dy \, \sqrt{fq} \, \Big|_{\rho=0} . \qquad (1.21)$$

$m_q^{(T)}$ can be interpreted as the effective mass of the "quarks" at temperature T.

Note that $m_q^{(T)}$ decreases monotonically with T, since as we increase the temperature, the black hole becomes bigger and gravity attracts the brane more to the black hole. There exists a temperature T_d ($= 2.166 m_q/\sqrt{\lambda}$), after which the branes fall into the black hole (often called black hole embedding) through a first order phase transition [36, 37]. The physics of which was associated with the dissociation of mesons by

[38, 37]. For $T > T_d$ mesonic excitations, which we will describe in the next section, cease to exist. We will be interested in the temperature range smaller or of order T_d in which regime we always have $(\beta = \frac{1}{T})$

$$\beta m_q^{(T)} \sim O(\sqrt{\lambda}) \ . \tag{1.22}$$
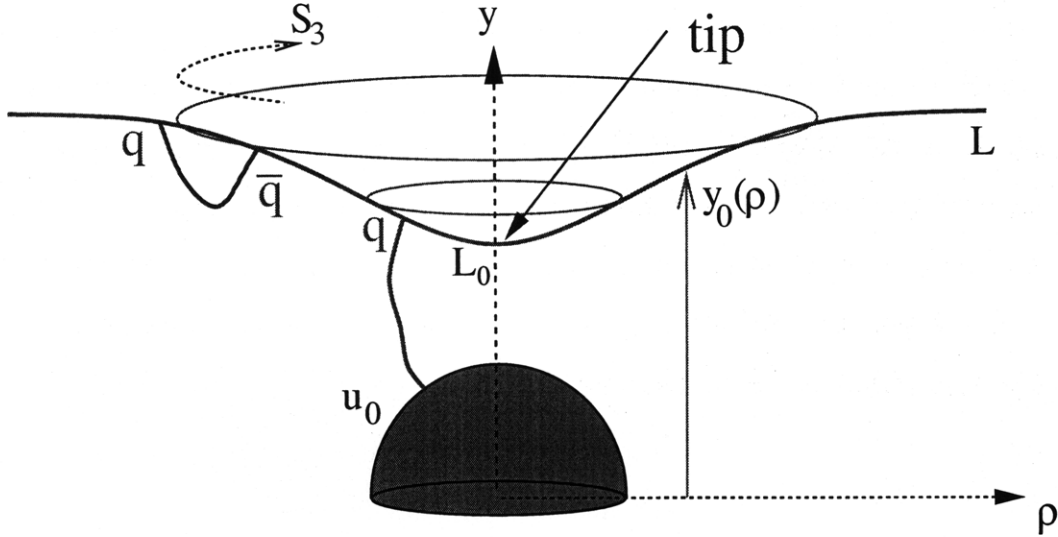
Figure 1-2: An embedding of the D7 brane (green) in the $AdS_5 \times S_5$ black hole geometry which lies entirely outside the black hole. The exact form of the embedding has been exaggerated to emphasize certain features.

1.3.1 Properties of mesons

As described above mesons correspond to the fields living on the D7 brane. For example the fields which encode the two transverse fluctuation of the brane are,

$$y(\rho, \vec{x}) = y_0(\rho) + \delta y(\rho, \vec{x}) \rightarrow [O_y(\vec{x})] = 3 \tag{1.23}$$

$$\phi(\rho, \vec{x}) = \delta\phi(\rho, \vec{x}) \rightarrow [O_\phi(\vec{x})] = 3 \tag{1.24}$$

where $O_{y,\phi}$ are quark bilinear operators in the gauge theory (including both scalar and fermionic quarks.) And the correspondence between field and operator is in the sense

of (1.7) with ρ now playing the role of the radial coordinate r. The problem of finding mesons is reduced to that of finding the eigenvalues of a certain Schrodinger problem for the fluctuations (1.23) living in the geometry of the D7 brane, which is essentially completely defined by the induced metric g_{mn} on the D7 brane. This induced metric for embeddings below the dissociation temperature satisfies the requirements of a confining gauge theory, hence the mesons have zero width.

In Chapter 2 we study the dispersion relations of the mesons created by the above operators by studying the spectrum of bound states in the dual gravity theory. We find that at large momentum k the dispersion relations become $\omega(k) \simeq v_0 k + a + b/k + \ldots$, where the limiting velocity v_0 is the same for mesons with any quantum numbers and depends only on the ratio of the temperature to the quark mass T/m_q. The limiting meson velocity v_0 becomes much smaller than the speed of light at temperatures below but close to T_{diss}. From our result for $v_0(T/m_q)$, we find that the temperature above which no meson bound states with velocity v exist is $T_{\text{diss}}(v) \simeq (1 - v^2)^{1/4} T_{\text{diss}}$, up to few percent corrections. We thus confirm by direct calculation of meson dispersion relations the result (1.13) inferred indirectly via analysis of the screening length between a static quark and antiquark in a moving plasma.

As we have already mentioned, one draw back of this system is that for a range of temperatures below the dissociation temperature T_d these mesons have exactly zero width. Of course this is not what one would expect for QCD, or for that matter a quark anti-quark bound state sitting in any *deconfined* plasma, since in a thermal environment one expects the meson to be bombarded with deconfined quarks and gluons. The reason *these* mesons have zero width, as we will show in Chapter 3, is that this is an artifact of the large λ approximation.

As already discussed, in the Large-N limit of a *confined* theory one expects mesons to have zero width. Since the glue of $\mathcal{N} = $ SYM is deconfined at finite-T we need another mechanism for confining the *quarks*. On the gravity side we already have a mechanism, that is the induced metric g_{mn} is smooth in the bulk and asymptotically AdS. On the gauge theory side the mechanism turns out to be Boltzmann suppression. The mesons in this theory, as we will see in Chapter 2, are actually very tightly bound

mesons. Their binding energy is of order $E_{BE} = \sqrt{\lambda}M$ where M is the mesons mass. Hence any process which breaks them apart[6] has a large energy cost. Such processes occur at a rate of order $\exp(-E_{BE}/T) = \exp(-\sqrt{\lambda}M/T)$. So it is exponentially small for large 't Hooft coupling.

In chapter 3 we show how to calculate such contributions to the meson width. We show that this can happen through nonperturbative worldsheet instantons, allowing mesons "living" on a D-brane which lies outside an AdS black hole to tunnel into the black hole. These instantons have a simple interpretation in terms of thermal quarks in the dual Yang-Mills (YM) theory. While the width of the meson is zero to all orders in the $1/\sqrt{\lambda}$ expansion with λ the 't Hooft coupling, it receives non-perturbative contributions in $1/\sqrt{\lambda}$ from worldsheet instantons. We find that the width increases quadratically with momentum at large momentum and comment on potential phenomenological implications of this enhancement for heavy ion collisions.

1.3.2   Finite quark density

The system possesses a $U(1)_B$ global baryon symmetry under which "quarks" transform non-trivially. In Chapter 4 we will examine the the effects of turning on a nonzero net quark density n_q. In order to achieve this we need to understand some more elements of the gauge gravity dictionary.

The associated conserved current J_B^μ is dual to the $U(1)$ gauge field A_μ on the D7-branes. Turning on a chemical potential μ_q for the charge density in the boundary theory then corresponds to imposing the following boundary condition[7] for A_μ

$$A_0(\rho = \infty) = \mu_q \; . \tag{1.25}$$

---

[6]At finite temperature there are process, suppressed by $1/N_c$, which do not break the mesons apart and still contribute to their width. This is essentially related to a diffusion type process. See [132].

[7]Also, if the D7-branes fall into the horizon there will also be a boundary condition that $A_0 = 0$ at the horizon.

The charged density n_q can be calculated from the bulk theory by

$$n_q = \Pi^0(\rho = \infty) \tag{1.26}$$

where Π^0 is the canonical momentum conjugate to A_0 (in terms of ρ-slicing) evaluated at the classical solution which satisfies the boundary condit ions (1.19) and (1.25). By symmetry we will take A_0 to depend only on ρ and the other components of the gauge field will be set to zero.

Turning on a chemical potential now allows us to study the phase structure of this theory in the $\mu - T$ phase plane. This has been studied previously by [36, 39, 40, 41, 42, 43, 44, 45] where a rich phase diagram was found. In the final chapter of this thesis we revisit the phase diagram of the $\mathcal{N} = 4$ $SU(N_c)$ super-Yang-Mills theory coupled to N_f fundamental "quarks" at strong coupling using the gauge-gravity correspondence. We show that in the plane of temperature vs. baryon chemical potential there is a critical line of third order phase transitions which ends at a tricritical point after which the transition becomes first order. Close to the critical line there is an intriguing logarithmic behavior, which cannot follow from a mean field type of analysis. We argue that on the string theory side the third order phase transition is driven by the condensation of worldsheet instantons and that this transition might become a smooth crossover at finite 't Hooft coupling.

Chapter 2

Properties of mesons I - dispersion relations

2.1 Introduction

The radii of the tightly bound heavy quark-antiquark systems of the charmonium (J/Ψ, Ψ', χ_c, ...) and bottomonium (Υ, Υ', ...) families provide a unique set of decreasing length scales in strong interaction physics. On general grounds, it is expected that the attraction between a heavy quark and an anti-quark is sensitive to the medium in which the bound state is embedded, and that this attraction weakens with increasing temperature. In the context of ultra-relativistic nucleus-nucleus collisions, the radii of some quarkonia states correspond to fractions of the natural length scale displayed by the medium produced in heavy ion collisions, namely fractions of its inverse temperature $1/T$. Such scale considerations support the idea that measurements of the medium-modification or dissociation of quarkonia can characterize properties of the QCD matter produced in heavy ion collisions.

Matsui and Satz were the first to highlight the role of quarkonium in the study of hot QCD matter [14]. They suggested that J/Ψ-suppression is a signature for the formation of deconfined quark-gluon plasma (QGP). More precisely, they argued that in comparison to proton-proton or proton-nucleus collisions, the production of J/Ψ mesons should be suppressed if quark-gluon plasma is formed in sufficiently ener-

getic nucleus-nucleus collisions, since the screened interaction of a c and a $\bar{c}$ in QGP would not bind them [14]. The theoretical basis for this argument has been clarified considerably within the last two decades [16]. Model-independent calculations of the static potential between a heavy quark and anti-quark have been performed in lattice-regularized QCD, valid at strong coupling [47, 48, 49, 50, 51, 52, 15, 53, 54]. In lattice calculations without dynamical quarks, at temperature $T = 0$ and large separation L this potential rises linearly with L, consistent with confinement. At nonzero temperature, the potential weakens and levels off at large distances; with increasing temperature, the distance at which this screening occurs decreases. This behavior of the static potential has been mapped out for hot QCD matter both without [51] and with [52, 15] dynamical quarks. However, the physical interpretation of static potentials at finite temperature rests on additional assumptions. For instance, even if a potential supports a bound state with several MeV binding energy, it remains unclear which physics can be attributed to such a state in a heat bath of $\sim$ 200 MeV temperature. Such issues do not arise in a discussion of quarkonium mesons based directly on their Minkowski space spectral functions or dispersion relations. In recent years, the spectral functions have been characterized by lattice calculations of the Euclidean correlation functions to which they are analytically related, again in hot QCD matter both without [55, 56, 57, 58, 59, 60, 61] and with [62, 63, 64, 65] dynamical quarks. The use of these calculations of finitely many points on a Euclidean correlator to constrain the Minkowski space spectral function of interest via the Maximum Entropy Method requires further inputs — for example smoothness assumptions or information on the analytic properties of the spectral function [55, 56, 57, 58, 59, 60, 61, 62, 63, 64, 65]. At high enough temperatures that quark-gluon plasma becomes weakly coupled, a complementary analytical approach based upon resummed hard-thermal-loop perturbation theory becomes available [66, 67, 68, 69]. These calculations have the advantage that analytical continuation from Euclidean to Minkowski space does not introduce additional uncertainties, but it remains unclear to what extent they can treat a strongly coupled quark-gluon plasma. In broad terms, all these calculations support the qualitative

picture behind the original suggestion of Matsui and Satz that color screening in the quark-gluon plasma is an efficient mechanism for quarkonium dissociation. In addition, these studies support the picture of a sequential dissociation pattern [17], in which loosely bound, large, quarkonia such as the Ψ' and χ_c cease to exist close to T_c, the temperature of the crossover between hadronic matter and quark-gluon plasma, whereas more tightly bound, smaller, states dissociate only at significantly higher temperatures. In particular, J/Ψ mesons continue to exist for a range of temperatures above the QCD phase transition and dissociate only above a temperature that lies between $1.5\,T_c$ and $2.5\,T_c$ [17]. The observation of bound-state-specific quarkonia suppression patterns could thus provide detailed information about the temperature attained in heavy ion collisions.

On the experimental side, there are by now data from the NA50 and NA60 experiments at the CERN SPS and from the PHENIX experiment at RHIC demonstrating that the production of J/Ψ mesons is suppressed in ultra-relativistic nucleus-nucleus collisions compared to proton-proton or proton-nucleus collisions at the same center of mass energy [70, 71, 72]. However, due to lack of statistics and resolution, an experimental characterization of other charmonium states (Ψ', χ_c, ...) has not yet been possible at RHIC, and bottomonium states have not yet been characterized in any nucleus-nucleus collisions. Moreover, the observed yield of J/Ψ mesons is expected to receive significant decay contributions from Ψ' and χ_c, meaning that the observed suppression of J/Ψ mesons may originate only in the suppression of the larger Ψ' and χ_c states [17], or may indicate a suppression in the number of primary J/Ψ mesons themselves in addition. Thus, at present an experimental test of the sequential quarkonium suppression pattern is not in hand. It is expected that the LHC heavy ion program will furnish such a test, since two LHC experiments [73, 74, 75] have demonstrated capabilities for discriminating between the different states of the charmonium and bottomonium families.

From the existing data in ultra-relativistic heavy ion collisions and their phenomenological interpretation, it has become clear that an unambiguous characterization of color screening effects in the quarkonium systems requires good experimental

and theoretical control of several confounding factors. These include in particular control over the spatio-temporal evolution of the medium, control over the time scale and mechanism of quarkonium formation, as well as control over the effects of quarkonium propagation through the medium. We now comment on these three sources of uncertainty in more detail:

First, there is ample evidence by now that the systems produced in ultra-relativistic heavy ion collisions display effects of position-momentum correlated motion (a.k.a. flow), which are as important as the effects of random thermal motion [76, 77, 78, 79]. Moreover, the energy density achieved in these collisions drops rapidly with time as the matter expands and falls apart after approximately 10 fm/c. As a consequence, the modeling of quarkonium formation in heavy ion collisions cannot be limited to a description of heavy quark bound states in a heat bath at constant temperature (which is the information accessible in *ab initio* calculations in lattice-regularized QCD). The effects of a rapid dynamical evolution during which the relevant degrees of freedom in the medium change from partonic to hadronic must be taken into account.

Second, regarding the formation process, the conversion of a heavy quark pair produced in a hard collision into a bound quarkonium state is not fully understood, even in the absence of a medium. There are different production models, which all have known limitations and for which a systematic calculation scheme remains to be fully established (for a short review of these issues, see [80]). The need for further clarification of the vacuum case has even led to suggestions that nuclear matter could serve as a filter to distinguish between different production mechanisms [81, 82]. However, it has also been pointed out that there may be a novel quarkonium production mechanism operating only in ultra-relativistic heavy ion collisions at RHIC and at the LHC [83, 84, 85]: charm quarks may be so abundant in these collisions that c and $\bar{c}$ quarks produced separately in different primary hard scattering interactions may find each other and combine, contributing significantly to charmonium production at soft and intermediate transverse momentum. To a lesser extent, this mechanism may also contribute to the production of Upsilon mesons. Identifying and characterizing such a novel formation process is of considerable interest, since recombination is likely to

be quadratically sensitive to the phase space density of charm and thus to properties of the produced matter. On the other hand, if realized in nature recombination also implies that quarkonium spectra at soft and intermediate transverse momenta are determined predominantly during the late hadronization stage and cannot be viewed as probes which test color screening in the quark gluon plasma. This would indicate that the high transverse momentum regime (say above 5-8 GeV) of quarkonium spectra, which should not be significantly affected by recombination, is better suited for tests of the fundamental color screening effects predicted by QCD. However, the sensitivity of high transverse momentum spectra to properties of the medium remains to be established. In particular, quarkonium formation or dissociation proceeds on a time scale comparable to the size of the bound state in its rest frame, meaning that quark-antiquark pairs with very high transverse velocity may escape the finite-sized droplet of hot matter produced in a heavy ion collision before they have time to form a meson, meaning in turn that screening effects cease to play a role in quarkonium production above some very high transverse momentum [86]. At lower transverse momenta, where screening does play a role, one must nevertheless understand for how long quarkonium is exposed to the medium and how readily it dissociates if moving relative to that medium. For quarkonium at high transverse momentum, the time of exposure to the medium depends on the geometry of the collision region, which determines the in-medium path length, and it depends on the propagation velocity. The results contained in this chapter give novel input to modeling this process by demonstrating that the real part of the finite temperature quarkonium dispersion relation can differ significantly from the vacuum one, and can imply a limiting quarkonium propagation velocity which is much smaller than c, the velocity of light in vacuum. Our results indicate that at temperatures close to but below that at which a given quarkonium state dissociates, these mesons move through a strongly coupled quark-gluon plasma at a velocity that is much smaller than c even if they have arbitrarily high transverse momentum. Certainly this means that the formation time arguments of [86] will need rethinking before they can be applied quantitatively.

Third, we turn to the question of how the relative motion of quarkonium with

43

respect to the local rest frame of the medium affects quarkonium production. As discussed above, the standard vacuum relation between the momentum of a quarkonium state and its velocity can be altered in the presence of a medium and this effect may be phenomenologically relevant. In addition, it is expected that a finite relative velocity between the medium and the bound state enhances the probability of dissociation [31]. In a recent strong coupling calculation of hot $\mathcal{N} = 4$ supersymmetric QCD, three of us have have shown [10, 11] that the screening length L_s for a heavy quark-antiquark pair decreases with increasing velocity as $L_s(v, T) \sim L_s(0, T)/\sqrt{\gamma}$, with $\gamma = 1/\sqrt{1 - v^2}$ the Lorentz boost factor. This suggests that a quarkonium state that is bound at $v = 0$ at a given temperature could dissociate above some transverse momentum due to the increased screening, providing a significant additional source of quarkonium suppression at finite transverse momentum. The present work started from the motivation to establish how this velocity scaling manifests itself in a description of mesons at finite temperature, rather than via drawing inferences from a calculation of the screening length that characterizes the quark-antiquark potential. This motivation is analogous to that behind going from lattice QCD calculations of the static potential in QCD to calculations of the Minkowski space meson spectral function. We shall do our calculation in a different strongly coupled gauge theory plasma, in which we are able to do this investigation for mesons with nonzero velocity. We shall see that the critical velocity for the dissociation of quarkonium inferred from the velocity scaling of the screening length also appears as a limiting velocity for high-momentum quarkonium propagation in the hot non-abelian plasma.

Finally, the characterization of color screening also depends on the experimental and theoretical ability to separate its effects on quarkonium production from effects arising during the late time hadronic phase of the heavy ion collision. In particular, it has been noted early on that significant charmonium suppression may also occur in confined hadronic matter [87, 88, 89]. However, it has been argued on the basis of model estimates for the hadronic J/Ψ dissociation cross section [90, 91, 92] that dissociation in a hadronic heat bath is much less efficient than in a partonic one. The operational procedure for separating such hadronic phase effects is to measure them

separately in proton-nucleus collisions [93], and to establish then to what extent the number of J/Ψ mesons produced in nucleus-nucleus collisions drops below the yield extrapolated from proton-nucleus collisions [70, 71, 72, 94].

The above discussion highlights the extent to which an understanding of quarkonium production in heavy ion collisions relies on theoretical modeling as the bridge between experimental observations and the underlying properties of hot QCD matter. This task involves multiple steps. It is of obvious interest to validate or constrain by first principle calculations as many steps as possible, even in a simplified theoretical setting. The present work is one of a number of recent developments [95] that explore to what extent techniques from string theory, in particular the AdS/CFT correspondence, can contribute to understanding processes in hot QCD by specifying how these processes manifest themselves in a large class of hot strongly coupled non-abelian gauge theories. Although it is not known how to extend the AdS/CFT correspondence to QCD, there are several motivations for turning to this technique. First, there are a growing number of explicit examples which indicate that a large class of thermal non-abelian field theories with gravity duals share commonalities such that their properties in the thermal sector are either universal at strong coupling, i.e. independent of the microscopic dynamics encoded in the particular quantum field theory under study, or their properties are related to each other by simple scaling laws e.g. depending on the number of elementary degrees of freedom. This supports the working hypothesis that by learning something about a large class of strongly coupled thermal non-abelian quantum field theories, one can gain guidance towards understanding the thermal sector of QCD. Second, the AdS/CFT correspondence allows for a technically rather simple formulation of problems involving real-time dynamics. This is very difficult in finite temperature lattice-regularized calculations, which exploit the imaginary time formalism. In particular, this is the reason why so far lattice QCD calculations treat only static quark-antiquark pairs in the plasma, and why the only nonperturbative calculation of the velocity dependence of quarkonium dissociation exploits the AdS/CFT correspondence. Third, data from experiments at RHIC pertaining to many aspects of the matter produced in heavy ion collisions indicate

that this matter is strongly coupled. Since the AdS/CFT correspondence provides a mapping of difficult nonperturbative calculations in a quantum field theory with strong coupling onto relatively simple, semi-classical calculations in a gravity dual, it constitutes a novel — and often the only — technique for addressing dynamical questions about hot strongly coupled non-abelian matter, questions that are being raised directly by experimental results on QCD matter coming from RHIC.

We have focused in this Section on the larger context for our results. In Section 2, which is an introduction in a more narrow sense, we review the past results which serve as an immediate motivation for our work, in particular the screening length that characterizes the potential between a static quark and antiquark in a moving plasma wind. Adding fundamental quarks with finite mass m_q, and hence mesons, into $\mathcal{N} = 4$ SYM theory requires adding a D7-brane in the dual gravity theory, as we review in Section 3. The fluctuations of the D7-brane are the mesons, as we review for the case of zero temperature in Section 3. In Section 4 we set up the analysis of the mesons at nonzero temperature, casting the action for the D7-brane fluctuations in a particularly geometric form, written entirely in terms of curvature invariants. Parts of the derivation are explained in more detail in Appendix A. With all the groundwork in place, in Section 5 we derive the meson dispersion relations. In addition to obtaining them numerically without taking any limits as has been done previously [37], we are able to calculate them analytically in three limits: first, upon taking the low temperature limit at fixed k; second, upon taking the low temperature limit at fixed kT; and third, using insights from the first two calculations, at large k for any temperature. At large k we find

$$\omega = v_0 k + a + \frac{b}{k} + \dots \tag{2.1}$$

where v_0 is independent of meson quantum numbers, depending only on T/m_q. v_0 turns out to be given by the local speed of light at the "tip of the D7-brane", namely the place in the higher dimensional gravity dual theory where the D7-brane comes closest to the black hole [37]. We compute a and b in terms of meson quantum

46

numbers and T/m_q. Our result for the limiting velocity v_0 for mesons at a given temperature T can be inverted, obtaining $T_{\text{diss}}(v)$, the temperature above which no mesons with velocity v are found. We find that up to few percent corrections, our result can be summarized by

$$T_{\text{diss}}(v) = (1 - v^2)^{1/4} T_{\text{diss}} , \qquad (2.2)$$

where T_{diss} is the temperature at which zero-velocity mesons dissociate, obtained in previous work and introduced in Section 3. As we discuss in Section 2, our results obtained by direct calculation of meson dispersion relations confirm inferences reached (in two different ways) from the analysis of the screened potential between a static quark and antiquark in a hot plasma wind. In Section 6, we close with a discussion of potential implications of these dispersion relations for quarkonia in QCD as well as a look at open questions. The dispersion relations that we calculate in this chapter describe how mesons propagate and so affect a class of observables, but determining whether quarkonium meson formation from a precursor quark-antiquark pair is suppressed by screening is a more dynamical question that can at present be addressed only by combining our calculation and the more heuristic results of [11].

2.2 From screening in a hot wind to moving mesons

In the present work, we shall use the AdS/CFT correspondence to study the propagation of mesonic excitations moving through a strongly coupled hot quark-gluon plasma. In this Section, however, we introduce what we have learned from the simpler calculation of the potential between a test quark-antiquark pair moving through such a medium. This will allow us to pose the questions that we shall address in the present chapter.

As discussed in the previous chapter at nonzero temperature, the potential takes

47

the form [29, 30, 46]

$$V(L,T) \approx \sqrt{\lambda} \tilde{f}(L) \qquad L < L_c$$
$$\approx \lambda^0 g(L) \qquad L > L_c \,. \qquad (2.3)$$

In (2.3), at $L_c = 0.24/T$ there is a change of dominance between different saddle points and the slope of the potential changes discontinuously. When $L < L_c$, the potential is determined as at zero temperature by the area of a string world sheet bounded by the worldlines of the quark and antiquark, but now the world sheet hangs down into a different five-dimensional spacetime: introducing nonzero temperature in the gauge theory is dual to introducing a black hole horizon in the five-dimensional spacetime. When $L \ll L_c$, $\tilde{f}(L)$ reduces to its zero temperature behavior (1.10). When $L \gg L_c$, $g(L)$ has the behavior [96]

$$g(L) \propto c_1 - c_2 e^{-m_{\mathrm{gap}} L} \,, \qquad (2.4)$$

with c_1, c_2 and m_{gap} constants all of which are proportional to T. This large-L potential arises from two disjoint strings, each separately extending downward from the quark or antiquark all the way to the black hole horizon, exchanging supergravity modes the lightest of which has a mass given by $m_{\mathrm{gap}} = 2.34 \, \pi T$. (There are somewhat lighter modes with nonzero R-charge, but these are not relevant here [97].) It is physically intuitive to interpret L_c as the screening length L_s of the plasma since at L_c the qualitative behavior of the potential changes. Similar criteria are used in the definition of screening length in QCD [54], although in QCD there is no sharply defined length scale at which screening sets in. Lattice calculations of the static potential between a heavy quark and antiquark in QCD indicate a screening length $L_s \sim 0.5/T$ in hot QCD with two flavors of light quarks [15] and $L_s \sim 0.7/T$ in hot QCD with no dynamical quarks [51]. The fact that there *is* a sharply defined L_c in (2.3) is an artifact of the limit in which we are working.[1]

---

[1]The theoretical advantage of using $1/m_{\mathrm{gap}}$ to define a screening length as advocated in [96] is that it can be precisely defined in $\mathcal{N} = 4$ SYM theory at finite λ and N_c, as well as in QCD,

In [10, 11], the authors studied the velocity scaling of the screening length L_s in $\mathcal{N} = 4$ super-Yang-Mills theory and found that[2]

$$L_s(v, \theta, T) = \frac{f(v, \theta)}{\pi T} \left(1 - v^2\right)^{1/4} , \qquad (2.5)$$

where θ is the angle between the orientation of the quark-antiquark dipole and the velocity of the moving thermal medium in the rest frame of the dipole. $f(v, \theta)$ is only weakly dependent on both of its arguments. That is, it is close to constant. So, to a good approximation we can write

$$L_s(v, T) \approx L_s(0, T)(1 - v^2)^{1/4} \propto \frac{1}{T}(1 - v^2)^{1/4} . \qquad (2.6)$$

This result, also obtained in [12, 13, 7] and further explored in [98, 34, 99], has proved robust in the sense that it applies in various strongly coupled plasmas other than $\mathcal{N} = 4$ SYM [98, 34, 99]. The velocity dependence of the screening length (2.6) suggests that in a theory containing dynamical heavy quarks and meson bound states (which $\mathcal{N} = 4$ SYM does not) the dissociation temperature $T_{\text{diss}}(v)$, defined as the temperature above which mesons with a given velocity do not exist, should scale with velocity as [10]

$$T_{\text{diss}}(v) \sim T_{\text{diss}}(v = 0)(1 - v^2)^{1/4} , \qquad (2.7)$$

since $T_{\text{diss}}(v)$ should be the temperature at which the screening length $L_s(v)$ is comparable to the size of the meson bound state. The scaling (2.7) then indicates that slower mesons can exist up to higher temperatures than faster ones. In this chapter,

---

as it characterizes the behavior of the static potential in the $L \to \infty$ limit. The disadvantage of this proposal from a phenomenological point of view is that quarkonia are not sensitive to the potential at distances much larger than their size. For questions relevant to the stability of bound states, therefore, the length scale determined by the static potential that is phenomenologically most important is that at which the potential flattens. Although this length is not defined sharply in QCD, it is apparent in lattice calculations and can be defined operationally for practical purposes [51, 15]. This L_s seems most analogous to L_c in (2.3), and we shall therefore continue to refer to $L_s \equiv L_c$ as the screening length, as in the original literature [29, 30, 46]. Note that L_c is larger than $1/m_{\text{gap}}$ by a purely numerical factor $\simeq 1.8$.

[2]In [10, 11] L_s was defined using a slightly different quantity than L_c in (2.3), such that $L_s = 0.28/T$ for a quark-antiquark at rest. For technical reasons, this other definition was more easily generalizable to nonzero velocity.

we shall replace the inference that takes us from the calculated result (2.6) to the conclusion (2.7) by a calculation of the properties of mesons themselves, specifically their dispersion relations. We shall reproduce (2.7) in this more nuanced setting, finding few percent corrections to the basic scaling result inferred previously.

Before beginning our analysis, let us first note a curious feature regarding the quark potential observed in [10, 11]. There one introduces a probe brane near the boundary of the AdS$_5$ black hole geometry with open strings ending on it corresponding to fundamental "test quarks" of mass $m_q \gg \sqrt{\lambda}T$. It was found that for any given quark mass m_q, there exists a maximal velocity v_c given by

$$v_c^2 = 1 - \frac{\lambda^2 T^4}{16 m_q^4} \, , \qquad (2.8)$$

beyond which there is no $\mathcal{O}(\sqrt{\lambda})$ potential between the pair for any value of their separation larger than their Compton wavelength, i.e. for any distance at which a potential can be defined. This result can be interpreted as saying that for any given T and m_q, it is impossible to obtain bound states beyond (2.8), i.e. as indicating that there is a velocity bound (a "speed limit") for the mesons. One can also turn (2.8) around and infer that for any large m_q and v close to 1, the dissociation temperature is given by

$$T_{\text{diss}} = \frac{2 m_q}{\sqrt{\lambda}} (1 - v^2)^{\frac{1}{4}} \, , \qquad (2.9)$$

which is consistent with (2.7). Note that the above argument is at best heuristic since $\mathcal{N} = 4$ SYM itself does not contain dynamical quarks and thus genuine mesons do not exist. In the present chapter, however, we shall see by deriving them from meson dispersion relations that (2.8) and (2.9) are precisely correct in the limit of large quark mass once we introduce fundamentals, and hence mesons, into the theory. We shall also find that the more dynamical, albeit heuristic, interpretation of (2.8) as a velocity beyond which a quark and antiquark do not feel a potential that can bind them remains of value.

2.3 D3/D7-brane construction of mesons

In this Section we review the gravity dual description of strongly coupled $\mathcal{N} = 4$ SYM theory with gauge group $SU(N)$ coupled to $N_f \ll N$ $\mathcal{N} = 2$ hypermultiplets in the fundamental representation of $SU(N)$, introduced in [100] and studied in [101, 43, 102, 103, 44, 104, 105, 36, 38, 37, 106, 107, 108]. We will first describe the theory at zero temperature and then turn to nonzero temperature. We will work in the limit $N \to \infty$, $\lambda = g_{YM}^2 N \to \infty$ and N_f finite (in fact $N_f = 1$). In the deconfined strongly coupled plasma that this theory describes, heavy quark mesons exist below a dissociation temperature that, for mesons at rest, is given by $T_{\mathrm{diss}} = 2.166 \, m_q / \sqrt{\lambda}$ [43, 36, 38, 37]. In Section 5 we shall calculate the dispersion relations for these mesons, namely the meson spectrum at nonzero momentum k and in so doing determine $T_{diss}(v)$ directly, rather than by inference as described in Section 2.

2.3.1 Zero temperature

Consider a stack of N coincident D3-branes and N_f coincident D7-branes in 9+1-dimensional Minkowski space, which we represent by the array

$$
\begin{array}{lllllllllll}
\text{D3:} & 0 & 1 & 2 & 3 & \cdot & \cdot & \cdot & \cdot & \cdot & \cdot \\
\text{D7:} & 0 & 1 & 2 & 3 & 4 & 5 & 6 & 7 & \cdot & \cdot
\end{array}
\tag{2.10}
$$

which denotes in which of the 9+1 dimensions the D3- and D7-branes are extended, and in which they occupy only points. The D3-branes sit at the origin of the 89-plane, with L denoting the distance between the D3- and the D7-branes in the 89-plane. Without loss of generality (due to rotational symmetry in 89-plane), we can take the D7-branes to be at $x_8 = L$, $x_9 = 0$. This is a stable configuration and preserves one quarter of the total number of supersymmetries, meaning that it describes an $\mathcal{N} = 2$ supersymmetric gauge theory as we now sketch [100].

The open string sector of the system contains 3-3 strings, both of whose ends lie on one of the N D3-branes, 7-7 strings ending on N_f D7-branes, and 3-7 and 7-3

51

strings stretching between D3- and D7-branes. In the low energy limit

$$\alpha' \to 0, \qquad \frac{L}{2\pi\alpha'} = \text{finite}, \qquad\qquad (2.11)$$

all the stringy modes decouple except for: (i) the lightest modes of the 3-3 strings, which give rise to an $SU(N)$ $\mathcal{N} = 4$ SYM theory in 3+1-dimensional Minkowski space; (ii) the lightest modes of the 3-7 and 7-3 strings, which give rise to N_f hypermultiplets in the $\mathcal{N} = 2$ gauge theory transforming under the fundamental representation of $SU(N)$. The whole theory thus has $\mathcal{N} = 2$ supersymmetry. We will call N_f hypermultiplets quarks below even though they contain both fermions and bosons. The mass of the quarks is given by

$$m_q = \frac{L}{2\pi\alpha'} \,, \qquad\qquad (2.12)$$

where $1/(2\pi\alpha')$ is the tension of the strings.

In the limit

$$N \to \infty, \qquad N_f = \text{finite}, \qquad \lambda = g_{YM}^2 N \gg 1 \,, \qquad\qquad (2.13)$$

the above gauge theory has a gravity description [100] in terms of D7-branes in the near-horizon geometry of the D3-branes, which is $AdS_5 \times S_5$ with a metric

$$\begin{aligned}
ds^2 &= \frac{r^2}{R^2}\left(-dt^2 + dx_1^2 + dx_2^2 + dx_3^2\right) + \frac{R^2}{r^2}dr^2 + R^2 d\Omega_5^2 \\
&= \frac{r^2}{R^2}\left(-dt^2 + dx_1^2 + dx_2^2 + dx_3^2\right) + \frac{R^2}{r^2}\sum_{i=4}^{9} dx_i^2 \,, \qquad\qquad (2.14)
\end{aligned}$$

where $r^2 = \sum_{i=4}^{9} x_i^2$ and $d\Omega_5^2$ is the metric on a 5-sphere. R is the curvature radius of AdS and is related to the Yang-Mills theory 't Hooft coupling by

$$\frac{R^2}{\alpha'} = \sqrt{\lambda} \,. \qquad\qquad (2.15)$$

The string coupling constant g_s is related to the gauge theory parameters by

$$4\pi g_s = g_{YM}^2 = \frac{\lambda}{N} \, , \qquad (2.16)$$

where g_{YM}^2 is defined according to standard field theory conventions and is twice as large as the Yang-Mills gauge coupling defined according to standard string theory conventions. In this zero temperature setting, the embedding of the D7-branes in the $AdS_5 \times S_5$ geometry (2.14) can be read directly from (2.10). The D7-brane worldvolumes fill the (t, x_i) coordinates, with $i = 1, \ldots, 7$, and are located at the point $x_8 = L$, $x_9 = 0$ in the 89-plane. Since N_f remains finite in the large N limit, the gravitational back-reaction of the D7-branes on the spacetime of the D3-branes (2.14) may be neglected.

The dictionary between the gauge theory and its dual gravity description can thus be summarized as follows. On the gauge theory side we have two sectors: excitations involving adjoint degrees of freedom only and excitations involving the fundamentals. The first type of excitations correspond to closed strings in $AdS_5 \times S_5$ as in the standard AdS/CFT story. The second type is described by open strings ending on the D7-branes[3]. In particular, the low-lying (in a sense that we shall define later) meson spectrum of the gauge theory can be described by fluctuations of $x_{8,9}$ and gauge fields on D7-branes. We shall focus on the fluctuations of $x_{8,9}$ on the D7-brane (equivalently, the fluctuations of the position of the D7-brane in the (x_8, x_9) plane) which describe scalar mesons. There are also gauge fields localized within the D7-brane, and their fluctuations describe vector mesons. The description of the vector mesons is expected to be similar to that of the scalar mesons. We shall limit our presentation entirely to the scalar mesons. We shall take $N_f = 1$, meaning that the gauge theory is specified by the parameters N, λ and m_q which are related to their counterparts in the dual gravity theory by (2.15), (2.16) and (2.12). We see that the $N \rightarrow \infty$ limit corresponds to $g_s \rightarrow 0$, making the string theory weakly coupled. Considering the theory with the parameter λ taken to ∞ corresponds to

---

[3]We will not consider baryons in this chapter.

taking the string tension to infinity. These limits justify the use of the classical gravity approximation in which we consider strings moving in a background spacetime.

For later generalization to finite temperature, it is convenient to describe the D7-brane in a coordinate system which makes the symmetries of its embedding more manifest. We split the $\mathbb{R}^6$ factor in the last term of (2.14) into $\mathbb{R}^4 \times \mathbb{R}^2$ (i.e. parts longitudinal and transverse to the D7-brane) and express them in terms of polar coordinates respectively. More explicitly,

$$r^2 = \rho^2 + y^2, \qquad \rho^2 = x_4^2 + x_5^2 + x_6^2 + x_7^2, \qquad y^2 = x_8^2 + x_9^2,$$

$$x_8 = y\cos\phi, \qquad x_9 = y\sin\phi . \qquad (2.17)$$

The metric (2.14) then becomes

$$ds^2 = \frac{\rho^2 + y^2}{R^2} \left(-dt^2 + d\vec{x}^2\right) + \frac{R^2}{\rho^2 + y^2} \left(d\rho^2 + \rho^2 d\Omega_3^2 + dy^2 + y^2 d\phi^2\right) . \qquad (2.18)$$

The D7-brane now covers $(t, \vec{x}) = (t, x_1, x_2, x_3, \rho, \Omega_3)$ and sits at $y = L$ and $\phi = 0$. Note that in the radial direction the D7-brane extends from $\rho = 0$, at which the size of the three-sphere Ω_3 becomes zero, to $\rho = \infty$. The point $\rho = 0$ corresponds to $r = L$.

We now briefly describe how to find the low-lying meson spectrum described by the fluctuations of $x_{8,9}$. The action of the D7-brane is given by the Dirac-Born-Infeld action

$$S_{D7} = -\mu_7 \int d^8\xi \sqrt{-\det\tilde{h}_{ij}} , \qquad (2.19)$$

where the ξ^i (with $i = 0, 1, \ldots, 7$) denote the worldvolume coordinates of the D7 brane and $\tilde{h}_{ij}$ is the induced metric in the worldvolume

$$\tilde{h}_{ij} = G_{\mu\nu}(X)\frac{\partial X^\mu}{\partial \xi^i}\frac{\partial X^\nu}{\partial \xi^j} . \qquad (2.20)$$

The value of the D7-brane tension, $\mu_7 = (2\pi)^{-6}g_s^{-1}\alpha'^{-4}$, will play no role in our considerations. The spacetime metric $G_{\mu\nu}$ is given by (2.18) and $X^\mu(\xi)$ describe the

embedding of the D7-brane, where μ runs through all spacetime coordinates. The action (2.19) is invariant under the coordinate transformations $\xi \to \xi'(\xi)$. We can use this freedom to set $\xi^i = (t, \vec{x}, \rho, \Omega_3)$, and the embedding described below equation (2.18) then corresponds to the following solution to the equations of motion of (2.19):

$$y(\xi) = L, \quad \phi(\xi) = 0 \qquad \text{or} \qquad x_8(\xi) = L, \quad x_9(\xi) = 0 . \tag{2.21}$$

To find the meson spectrum corresponding to the fluctuations of the brane position, we let

$$x_8 = L + 2\pi\alpha'\psi_1(\xi) , \qquad x_9 = 0 + 2\pi\alpha'\psi_2(\xi), \tag{2.22}$$

and expand the action (2.19) to quadratic order in $\psi_{1,2}$, obtaining

$$S_{D7} \simeq \mu_7 \int d^8\xi \, \rho^3 \left(-1 - \frac{1}{2}(2\pi\alpha'R)^2 \frac{h^{ij}}{\rho^2 + L^2}(\partial_i\psi_1\partial_j\psi_1 + \partial_i\psi_2\partial_j\psi_2) \right) . \tag{2.23}$$

In (2.23), h_{ij} denotes the induced metric on the D7-brane for the embedding (2.21) in the absence of any fluctuations, i.e.

$$ds^2 = h_{ij}d\xi^i d\xi^j = \frac{\rho^2 + L^2}{R^2}\left(-dt^2 + d\vec{x}^2 \right) + \frac{R^2}{\rho^2 + L^2}\left(d\rho^2 + \rho^2 d\Omega_3^2 \right) . \tag{2.24}$$

Note that when $L = 0$, the above metric reduces to $AdS_5 \times S^3$, reflecting the fact that in the massless quark limit the Yang-Mills theory is conformally invariant in the large N/N_f limit.

The equation of motion following from (2.23) is

$$\frac{R^4}{(\rho^2 + L^2)^2}\partial_\alpha\partial^\alpha\psi + \frac{1}{\rho^3}\frac{\partial}{\partial\rho}\left(\rho^3 \frac{\partial}{\partial\rho}\psi \right) + \frac{1}{\rho^2}\nabla^2\psi = 0 , \tag{2.25}$$

where ψ denotes either ψ_1 or ψ_2, where $\alpha = 0 \dots 3$, and where ∇^2 denotes the Laplacian operator on the unit S^3. Eq. (2.25) can be solved exactly and normalizable solutions have a discrete spectrum. It was found in [101] that the four dimensional

mass spectrum is given by

$$m_{nl} = \frac{4\pi m_q}{\sqrt{\lambda}} \sqrt{(n+l+1)(n+l+2)}, \qquad n = 0, 1, \ldots, \quad l = 0, 1, \ldots, \qquad (2.26)$$

with degeneracy $(\ell + 1)^2$, where l is the angular momentum on S^3. The $(\ell + 1)^2$ degeneracy is understood in the field theory as arising because the scalar mesons are in the $(\ell/2, \ell/2)$ representation of a global $SU(2) \times SU(2)$ symmetry corresponding to rotations in the S^3 in the dual gravity theory [101].

The mass scale appearing in (2.26) can also be deduced without calculation via a scaling argument. Letting

$$t \to \frac{R^2}{L}t, \qquad \vec{x} \to \frac{R^2}{L}\vec{x}, \qquad \rho \to L\rho, \qquad (2.27)$$

the metric (2.24) can be solely expressed in terms of dimensionless quantities:

$$\frac{ds^2}{R^2} = (\rho^2 + 1)\left(-dt^2 + d\vec{x}^2\right) + \frac{1}{\rho^2 + 1}\left(d\rho^2 + \rho^2 d\Omega_3^2\right) . \qquad (2.28)$$

Thus, the mass scale for the mesonic fluctuations must be

$$M \equiv \frac{L}{R^2} = \frac{2\pi m_q}{\sqrt{\lambda}} , \qquad (2.29)$$

as is indeed apparent in the explicit result (2.26). We see that the mesons are very tightly bound in the large λ limit with a mass M that is parametrically smaller than the rest mass of a separated quark and antiquark, $2m_q$. This means that the binding energy is $\approx -2m_q$. From this fact and the Coulomb potential (1.10), one can also estimate that the size of the bound states is parametrically of order $\sim \frac{1}{M} \sim \frac{\sqrt{\lambda}}{m_q}$.

Finally, we can now explain the sense in which our analysis is limited to low-lying mesons. We are only analyzing those scalar mesons whose mass is of order M. There are other, stringy, excitations in the theory with meson quantum numbers whose masses are of order $L/(R\sqrt{\alpha'}) \sim M\lambda^{1/4} \sim m_q/\lambda^{1/4}$ and of order $L/\alpha' \sim M\lambda^{1/2} \sim m_q$ [101]. They are parametrically heavier than the mesons we analyze, and can be

56

neglected in the large λ limit even though those with masses $\sim m_q/\lambda^{1/4}$ are also tightly bound, since their masses are also parametrically small compared to m_q. In Section 5, we shall see again in a different way that our analysis of the dispersion relations for the mesons with masses $\sim m_q/\sqrt{\lambda}$ that we focus on is controlled by the smallness of $1/\lambda^{1/4}$.

2.3.2 Nonzero Temperature

We now put the Yang-Mills theory at nonzero temperature, in which case the AdS_5 part of the metric (2.14) is replaced by the metric of an AdS Schwarzschild black hole[4]

$$ds^2 = -f(r)dt^2 + \frac{r^2}{R^2}d\vec{x}^2 + \frac{1}{f(r)}dr^2 + R^2 d\Omega_5^2, \tag{2.30}$$

$$f(r) \equiv \frac{r^2}{R^2}\left(1 - \frac{r_0^4}{r^4}\right). \tag{2.31}$$

The temperature of the gauge theory is equal to the Hawking temperature of the black hole, which is

$$T = \frac{r_0}{\pi R^2}. \tag{2.32}$$

This is the one addition at nonzero temperature to the dictionary that relates the parameters of the (now hot) gauge theory to those of its dual gravity description.

At nonzero temperature, the embedding of the D7-brane is modified because the D7-brane now feels a gravitational attraction due to the presence of the black hole. To find the embedding, it is convenient to use coordinates which are analogous to those in (2.18). For this purpose, we introduce a new radial coordinate u defined by

$$\frac{dr^2}{f(r)} = \frac{R^2 du^2}{u^2}, \quad \text{i.e.} \quad u^2 = \frac{1}{2}\left(r^2 + \sqrt{r^4 - r_0^4}\right), \tag{2.33}$$

---

[4]Note the notation used in this chapter is slightly different to that of Chapter 1,3 and 4.

in terms of which (2.30) can then be written as

$$ds^2 = -fdt^2 + \frac{r^2}{R^2}d\vec{x}^2 + \frac{R^2}{u^2}(du^2 + u^2 d\Omega_5^2) \tag{2.34}$$

$$= -fdt^2 + \frac{r^2}{R^2}d\vec{x}^2 + \frac{R^2}{u^2}\left(d\rho^2 + \rho^2 d\Omega_3^2 + dy^2 + y^2 d\phi^2\right) . \tag{2.35}$$

As in (2.18), we have split the last term of (2.34) in terms of polar coordinates on $\mathbb{R}^4 \times \mathbb{R}^2$, with

$$u^2 = y^2 + \rho^2 . \tag{2.36}$$

In (2.34) and (2.35), f and r should now be considered as functions of u,

$$r^2 = u^2 + \frac{r_0^4}{4u^2}, \qquad f(u) = \frac{(u^4 - r_0^4/4)^2}{u^2 R^2(u^4 + r_0^4/4)} . \tag{2.37}$$

In terms of u, the horizon is now at $u_0 = \frac{r_0}{\sqrt{2}}$.

The D7-brane again covers $\xi^i = (t, \vec{x}, \rho, \Omega_3)$ and its embedding $y(\xi), \phi(\xi)$ in the (y, ϕ) plane will again be determined by extremizing the Dirac-Born-Infeld action (2.19). Because of the rotational symmetry in the ϕ direction, we can choose $\phi(\xi) = 0$. Because of the translational symmetry in the $(t, \vec{x})$ directions and the rotational symmetry in S^3, y can depend on ρ only. Thus, the embedding is fully specified by a single function $y(\rho)$. The induced metric on the D7-brane worldvolume can be written in terms of this function as

$$h_{ij}d\xi^i d\xi^j = -f(u)dt^2 + \frac{r^2}{R^2}d\vec{x}^2 + \frac{R^2}{u^2}\left((1 + y'(\rho)^2)d\rho^2 + \rho^2 d\Omega_3^2\right) , \tag{2.38}$$

where u in (2.36) and hence $f(u)$ are functions of ρ and $y(\rho)$. Substituting (2.38) into (2.19), one finds

$$S_{D7} \propto \int d\rho \frac{\rho^3}{u(\rho)^8}\left(16\left(\frac{u(\rho)}{r_0}\right)^8 - 1\right)\sqrt{1 + y'(\rho)^2} , \tag{2.39}$$

which leads to the equation of motion

$$\frac{y''}{1+y'^2} + \frac{3y'}{\rho} + \frac{8r_0^8}{u^2}\frac{(\rho y' - y)}{16u^8 - r_0^8} = 0 \qquad (2.40)$$

for $y(\rho)$, where $u^2(\rho) = \rho^2 + y^2(\rho)$.

To solve (2.40) one imposes the boundary condition that $y \to L$ as $\rho \to \infty$, and that the induced metric (2.38) is non-singular everywhere. L determines the bare quark mass as in (2.12). It is convenient to introduce a parameter

$$\epsilon_\infty \equiv \frac{u_0^2}{L^2} = \frac{r_0^2}{2L^2} = \frac{\lambda T^2}{8m_q^2} = \frac{\pi^2 T^2}{2M^2} \,, \qquad (2.41)$$

where we have used (2.32) and (2.29). Because $\mathcal{N} = 4$ SYM is scale invariant before introducing the massive fundamentals, meaning that all dimensionful quantities must be proportional to appropriate powers of T, when we introduce the fundamentals the only way in which the quark mass m_q can enter is through the dimensionless ratio m_q/T. Scale invariance alone does not require that this ratio be accompanied by a $\sqrt{\lambda}$, but it is easy to see that, after rescaling to dimensionless variables as in (2.27), the only combination of parameters that enters (2.40) is ϵ_∞. The small ϵ_∞ regime can equally well be thought of as a low temperature regime or a heavy quark regime. In the remainder of this section, we shall imagine m_q as fixed and describe the physics as a function of varying T, i.e. varying horizon radius r_0.

The equation of motion (2.40) that specifies the D7-brane embedding can be solved numerically. Upon so doing, one finds that there are three types of solutions with different topology [43, 36, 37]:

- Minkowski embeddings: The D7-brane extends all the way to $\rho = 0$ with $y(0) > u_0 = \frac{r_0}{\sqrt{2}}$ (see e.g. the upper three curves in Fig. 2-1). In order for the solution to be regular one needs $y'(0) = 0$. This gives rise to a one-parameter family of solutions parameterized by $y(0)$. The topology of the brane is $\mathbb{R}^{1,7}$.

- Critical embedding: The D7-brane just touches the horizon, i.e. $y(0) = u_0$ (see e.g. the middle curve in Fig. 2-1). The worldvolume metric is singular at the
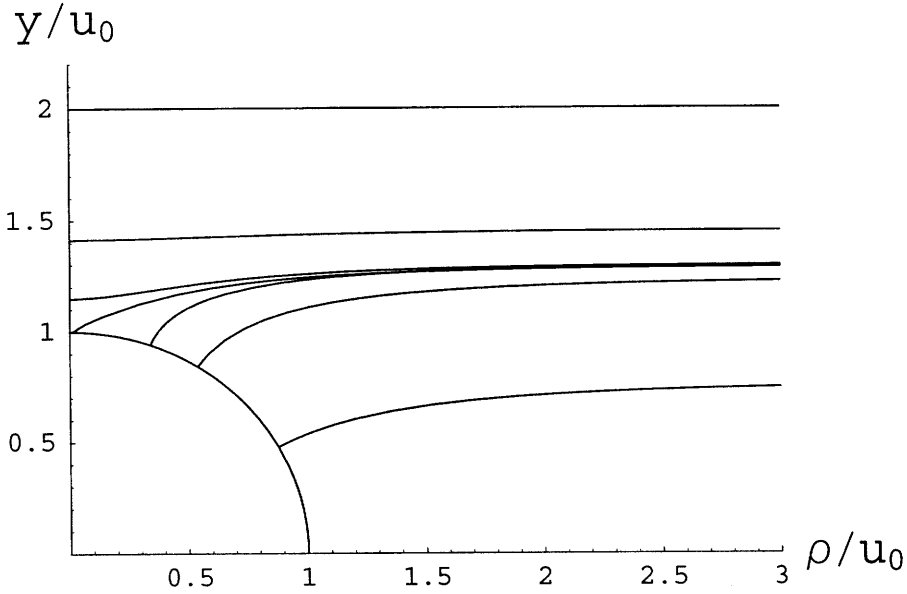
Figure 2-1: Some possible D7-brane embeddings $y(\rho)$. The quark mass to temperature ratio is determined by $y(\infty) = L$. Specifically, $\sqrt{8}m_q/(T\sqrt{\lambda}) = y(\infty)/u_0 \equiv 1/\sqrt{\epsilon_\infty}$. The top three curves are Minkowski embeddings, with $y(\rho)$ extending from $\rho = 0$ to $\rho = \infty$. The bottom three curves are black hole embeddings, in which the D7-brane begins at the black hole horizon at $y^2 + \rho^2 = u_0$. The middle curve is the critical embedding. The seven curves, ordered from top to bottom as they occur in the left part of the figure, are drawn for temperatures specified by $\epsilon_\infty = 0.249, 0.471, 0.5865,$ 0.5948, 0.5863, 0.647 and 1.656. Note that the $\epsilon_\infty = 0.5863$ black hole embedding crosses both the $\epsilon_\infty = 0.5948$ critical embedding and the $\epsilon_\infty = 0.5865$ Minkowski embedding.

point where the D7-brane touches the horizon.

- Black hole embeddings: The D7-brane ends on the horizon $u_0 = r_0/\sqrt{2}$ at some $\rho > 0$ (see e.g. the lower three curves in Fig. 2-1). The topology of the D7-brane is then $\mathbb{R}^{1,4} \times S^3$.

It turns out [38, 37] that Minkowski embeddings that begin at $\rho = 0$ with y close to $r_0/\sqrt{2}$, just above the critical embedding, can cross the critical embedding, ending up at $\rho \to \infty$ with $y(\infty)$ just below that for the critical embedding. Similarly, embeddings that begin just below the critical embedding can end up just above it. Furthermore, those embeddings that begin even closer to the critical embedding can cross it more than once. This means that there is a range of values around the critical $\epsilon_\infty^c = 0.5948$ for which there are three or more embeddings for each value

60

of ϵ_∞. At low temperatures (precisely, for $\epsilon_\infty < 0.5834$) this does not occur: there is only a single Minkowski embedding for each value of ϵ_∞. At high temperatures (precisely, for $\epsilon_\infty > 0.5955$) there is only a single black hole embedding per value of ϵ_∞. In the intermediate range of temperatures $0.5834 < \epsilon_\infty < 0.5955$, one needs to compare the free energy of each of the three or more different D7-brane embeddings that have the same value of ϵ_∞ to determine which is favored. One finds that there is a first order phase transition at a temperature T_c at which $\epsilon_\infty = 0.5863$, where the favored embedding jumps discontinuously from a Minkowski embedding to a black hole embedding as a function of increasing temperature [38, 37].[5]

As we shall study in detail in Section 4, fluctuations about a Minkowski embedding describe a discrete meson spectrum with a mass gap of order $O(M)$. In contrast, fluctuations about a black hole embedding yield a continuous spectrum [38, 37]. A natural interpretation of the first order transition is that $T_c = T_{\text{diss}}$, the temperature above which the mesons dissociate [38, 37]. It is interesting, and quite unlike what is expected in QCD, that all the mesons described by the zero temperature spectrum (2.26) dissociate at the same temperature. This is presumably related to the fact that the mesons are so tightly bound, again unlike in QCD. We shall therefore focus on the velocity-dependence of the meson spectrum at nonzero temperature — in other words, the meson dispersion relations first studied in [37]. As we have explained in Section 1, the velocity-dependence is currently inaccessible to lattice QCD calculations. Hence, even qualitative results are sorely needed. Furthermore, inferences drawn from a previous calculation of the potential between a moving quark-antiquark pair lead to a velocity-scaling (2.7) of T_{diss} that has a simple physical interpretation, which suggests that it could be applicable in varied theories [10]. We shall see this velocity dependence emerge from the meson dispersion relations in Section 5.

It is interesting to return to the qualitative estimate of T_{diss} obtained from the static quark-antiquark potential in Section 2, and see how it compares to the $T_{\text{diss}} = T_c$ obtained from the analysis of the mesons themselves. Equating the size of a

---

[5]The critical embedding occurs at an $\epsilon_\infty = 0.5948$ which is greater than the ϵ_∞ at which the first order phase transition occurs, meaning that at $\epsilon_\infty = 0.5948$ there is a black hole embedding that has a lower free energy than the critical embedding.
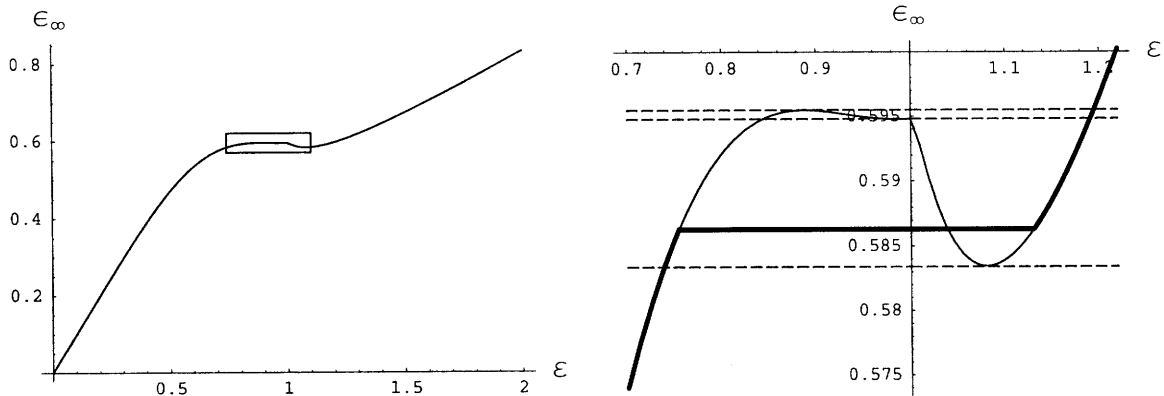
Figure 2-2: ϵ_∞ (determined by the embedding y at infinity) versus ε (determined either by $y(0)$, for Minkowski embeddings with $\varepsilon < 1$, or by where the embedding intersects the horizon, for $\varepsilon > 1$). The right panel zooms in on the vicinity of the critical embedding at $\varepsilon = 1$. The stable embeddings and the first order phase transition are indicated by the thick curve; the metastable embeddings are indicated by the thin curves.

meson with binding energy $2m_q$, determined by the zero-temperature potential (1.10), with the screening length $L_s = L_c = 0.24/T$, determined by the potential (2.3) at nonzero temperature, yields the estimate that T_{diss} should be $\sim 2.1m_q/\sqrt{\lambda}$. This is in surprisingly good agreement with $T_{\text{diss}} = \sqrt{8\epsilon_\infty}\, m_q/\sqrt{\lambda} = 2.166\, m_q/\sqrt{\lambda}$ for $\epsilon_\infty = 0.5863$.

In subsequent sections, we shall derive the dispersion relations for mesons at $T < T_{\text{diss}}$. We close this section by introducing some new notation that simplifies the analysis of the Minkowski embedding of the D7-brane, whose fluctuations we shall be treating. We first introduce parameters

$$L_0 \equiv y(0) \,, \qquad \varepsilon \equiv \frac{u_0^2}{L_0^2} = \frac{r_0^2}{2L_0^2} \,. \qquad (2.42)$$

For Minkowski embeddings, ε takes value in the range $[0, 1]$, with $\varepsilon = 0$ corresponding to zero temperature, and $\varepsilon = 1$ to the critical embedding. Although ϵ_∞ that we introduced earlier has the advantage of being directly related to the fundamental parameters of the theory according to (2.41), the new parameter has the advantage that there is only one embedding for each value of ε. And, ε will turn out to be convenient for analyzing the equations of motion (2.40) and the fluctuations on D7-

branes. When $\epsilon_\infty \ll 1$, $\varepsilon \approx \epsilon_\infty$. A full analytic relation between ε and ϵ_∞ is not known, but given an ε one can readily find the corresponding ϵ_∞ numerically. For example, at $T = T_c$, $\varepsilon = 0.756$ and $\epsilon_\infty = 0.586$ while for the critical embedding, $\varepsilon = 1$ and $\epsilon_\infty = \epsilon_\infty^c = 0.5948$. We depict the relation between ϵ_∞ and ε in Fig. 2-2. In order to make this figure, for the black hole embeddings we have defined $\varepsilon = 1/\sin^2\theta$ where θ is the angle in the (y, ρ) plane of Fig. 2-1 at the point at which the black hole embedding $y(\rho)$ intersects the black hole horizon $y^2 + \rho^2 = u_0^2$. That is, $1 < \varepsilon < \infty$ parametrizes black hole embeddings which begin at different points along the black hole horizon. The seven embeddings in Fig. 2-1 have $\varepsilon = 0.25$, 0.5, 0.756, 1.00, 1.13, 1.41 and 4.35, from top to bottom as they are ordered on the left, i.e. at the tip of the D7-brane at $y = 0$ for the Minkowski embeddings and at the horizon for the black hole embeddings.

Finally, it will also prove convenient to introduce dimensionless coordinates by a rescaling according to

$$t \longrightarrow \frac{R^2}{L_0}t, \qquad x_i \longrightarrow \frac{R^2}{L_0}x_i, \qquad \rho \longrightarrow L_0\rho, \qquad y \longrightarrow L_0 y, \qquad (2.43)$$

after which the spacetime metric becomes

$$\frac{ds^2}{R^2} = G_{\mu\nu}dx^\mu dx^\nu = -f(u)dt^2 + r(u)^2 d\vec{x}^2 + \frac{1}{u^2}\left(d\rho^2 + \rho^2 d\Omega_3^2 + dy^2 + y^2 d\phi^2\right) \quad (2.44)$$

and the induced metric becomes

$$\frac{ds_{D7}^2}{R^2} = h_{ij}d\xi^i d\xi^j = -f(u)dt^2 + r^2 d\vec{x}^2 + \frac{1}{u^2}\left((1 + y'(\rho)^2)d\rho^2 + \rho^2 d\Omega_3^2\right) \quad (2.45)$$

with

$$u^2 = y^2 + \rho^2, \qquad f(u) = \frac{(u^4 - \varepsilon^2)^2}{u^2(u^4 + \varepsilon^2)}, \qquad r^2(u) = u^2 + \frac{\varepsilon^2}{u^2}, \qquad (2.46)$$

where both $G_{\mu\nu}$ and h_{ij} are now dimensionless. The equation of motion for $y(\rho)$

becomes

$$\frac{y''}{1 + y'^2} + 3\frac{y'}{\rho} + \frac{8}{u^2}\left(\frac{\rho y' - y}{\varepsilon^{-4}u^8 - 1}\right) = 0, \qquad (2.47)$$

with the boundary conditions

$$y(0) = 1, \qquad y'(0) = 0 . \qquad (2.48)$$

This form of the equations of motion that determine the embedding $y(\rho)$ will be useful in subsequent sections.

2.4 Meson Fluctuations at Nonzero Temperature

In this section we derive linearized equations of motion that describe the small fluctuations of the D7-brane position. A version of these equations have been derived and solved numerically by various authors (see e.g. [43, 102, 38, 37]). Here we will rederive the equations in a different form by choosing the worldvolume fields parameterizing the fluctuations in a more geometric way. The new approach gives a nice geometric interpretation for the embedding and small fluctuations. It also simplifies the equations dramatically, which will enable us to extract analytic information for the meson dispersion relations in the next section. We present the main ideas and results in this Section but we leave technical details to Appendix A. In that Appendix, we shall also present a general discussion of the fluctuations of a brane embedded in any curved spacetime.

The action for small perturbations of the D7-brane location can be obtained by inserting

$$X^\mu(\xi) = X_0^\mu(\xi^i) + \delta X^\mu(\xi^i) \qquad (2.49)$$

into the D-brane action (2.19) and (2.20), where $X_0^\mu(\xi)$ denotes the background solution that describes the embedding in the absence of fluctuations, and δX^μ describes small fluctuations transverse to the brane. For the D7-brane under consideration, in

the coordinates used in (2.44) the general expression (2.49) becomes

$$y(\xi) = y_0(\rho) + \delta y(\xi), \qquad \phi(\xi) = \delta\phi(\xi) \qquad (2.50)$$

with $y_0(\rho)$ the embedding solution obtained by solving (2.47). The choice of the worldvolume fields $\delta y, \delta\phi$ is clearly far from unique. Any two independent functions of δy and $\delta\phi$ will also do. (This freedom corresponds to the freedom to choose different coordinates for the 10-dimensional space within which the D7-brane is embedded.) In fact, it is awkward to use δy and $\delta\phi$ as worldvolume fields since they are differences in coordinates and thus do not transform nicely under coordinate changes. Using them obscures the geometric interpretation of the equations. Below we will adopt a coordinate system which makes the geometric interpretation manifest. Since our discussion is rather general, not specific to the particular system under consideration, we will describe it initially using general language.

Consider a point $X_0(\xi)$ on the brane. The tangent space at X_0 perpendicular to the D7-brane is a two-dimensional subspace V_0 spanned by unit vectors n_1^μ, n_2^μ which are orthogonal to the branes, i.e.

$$n_1^\mu \;\propto\; \left(\frac{\partial}{\partial y}\right)^\mu - y_0'(\rho)\left(\frac{\partial}{\partial \rho}\right)^\mu \qquad (2.51)$$

$$n_2^\mu \;\propto\; \left(\frac{\partial}{\partial \phi}\right)^\mu . \qquad (2.52)$$

Any vector η^μ in V_0 can be written as

$$\eta^\mu = \chi_1 n_1^\mu + \chi_2 n_2^\mu . \qquad (2.53)$$

We can then establish a map from (χ_1, χ_2) to small perturbations δX^μ in (2.49) by shooting out geodesics of unit affine parameter from X_0 with tangent η^μ. Such a map should be one-to-one for χ_1, χ_2 sufficiently small. Clearly χ_1 and χ_2 behave like scalars under coordinate changes and we will use them as the worldvolume fields parameterizing small fluctuations of the position of the brane. By solving the geodesic

equation, δX^μ can be expressed in terms of $\chi_{1,2}$ as

$$\delta X^\mu = \eta^\mu - \frac{1}{2}\Gamma^\mu_{\alpha\beta}\eta^\alpha\eta^\beta + \dots , \qquad (2.54)$$

where $\Gamma^\mu_{\alpha\beta}$ are the Christoffel symbols of the 10-dimensional metric. Note that the choice of $\chi_{1,2}$ is not unique. There is in fact an $SO(2)$ "gauge" symmetry under which $\chi_{1,2}$ transform as a vector, since one can make different choices of basis vectors n_1, n_2 that are related by a local $SO(2)$ transformation.

We now insert (2.54) and (2.49) into the Dirac-Born-Infeld action (2.19) and, after some algebra discussed further in Appendix A, we find that the equations of motion satisfied by X_0 (i.e. which determine the embedding in the absence of fluctuations) can be written as

$$K_s = 0, \qquad (2.55)$$

and the quadratic action for small fluctuations $\chi_{1,2}$ about X_0 takes the form

$$S_{D7} = \mu_7 R^8 \int d^8\xi \sqrt{-\det h_{ij}} \left(-\frac{1}{2}D_i\chi_s D^i\chi_s - \frac{1}{2}\chi_s\chi_t \left(-K_{sij}K_t^{ij} + R_{sijt}h^{ij} \right) \right) ,$$

$$(2.56)$$

where $s, t = 1, 2$ and where we have defined the following quantities:

$$h_{ij} = G_{\mu\nu}\partial_i X_0^\mu \partial_j X_0^\nu , \qquad R_{sijt} = n_s^\alpha n_t^\beta \partial_i X_0^\mu \partial_j X_0^\nu R_{\alpha\mu\nu\beta} , \qquad (2.57)$$

$$K_{sij} = \partial_i X_0^\mu \partial_j X_0^\nu \nabla_\mu n_{s\nu} , \qquad K_s = K_{sij}h^{ij} , \qquad (2.58)$$

$$D_i\chi_s = \partial_i\chi_s + U_{ist}\chi_t , \qquad U_{ist} = n_{s\nu}\partial_i X_0^\mu \nabla_\mu n_t^\nu . \qquad (2.59)$$

Note that h_{ij} is the induced metric on the brane and i, j are raised by h^{ij}. $R_{\alpha\mu\nu\beta}$ is the Riemann tensor for the 10-dimensional spacetime. K_{sij} is the extrinsic curvature of the brane along the direction n_s^μ. U_{ist} (which is antisymmetric in s, t) is an $SO(2)$ connection for the $SO(2)$ gauge symmetry and D_i is the corresponding covariant derivative. We see that the embedding equations of motion (2.55) have a very simple geometric interpretation as requiring that the trace of the extrinsic curvature in each

66

orthogonal direction has to vanish, which is what we expect since this is equivalent to the statement that the volume of the D7-brane is extremal.

The symmetries of the D7-brane embedding that we are analyzing allow us to further simplify the action (2.56). Because n_2^μ in (2.52) is proportional to a Killing vector and is hypersurface orthogonal, U_{i12} and K_{2ij} vanish identically. (See Appendix A for a proof, and for the definition of hypersurface orthogonal.) With $K_2 = 0$ satisfied as an identity, the remaining equation of motion specifying the embedding, namely $K_1 = 0$, is then equivalent to the equation of motion for y that we derived in Section 3, namely Eq. (2.47). After some further algebra (see Appendix A) we find that the action (2.56) for small fluctuations reduces to

$$S_{D7} = \mu_7 R^8 \int d^8\xi \sqrt{-\det h_{ij}} \left(-\frac{1}{2}(\partial\chi_1)^2 - \frac{1}{2}(\partial\chi_2)^2 - \frac{1}{2}m_1^2\chi_1^2 - \frac{1}{2}m_2^2\chi_2^2 \right) \quad (2.60)$$

with

$$\begin{aligned}
m_1^2 &= R_{11} + R_{2112} + 2R_{22} + {}^{(8)}R - R \,, \\
m_2^2 &= -R_{22} - R_{2112} \,,
\end{aligned} \quad (2.61)$$

where we have defined

$$\begin{aligned}
R_{2112} &= n_2^\mu n_1^\nu n_1^\sigma n_2^\tau R_{\mu\nu\sigma\tau} \,, \\
R_{11} &= n_1^\nu n_1^\sigma R_{\nu\sigma} \,, \\
R_{22} &= n_2^\nu n_2^\sigma R_{\nu\sigma} \,,
\end{aligned} \quad (2.62)$$

and where R is the Ricci scalar for the 10-dimensional spacetime while ${}^{(8)}R$ is the Ricci scalar for the induced metric h_{ij} on the D7 brane. The background metric h_{ij} is given by (2.44). The "masses" m_1^2 and m_2^2 are nontrivial functions of ρ. Since the worldvolume metric is regular for Minkowski embeddings, they are well defined for $\rho \in [0,\infty)$.

Our result in the form (2.56) is very general, applicable to the embedding of any
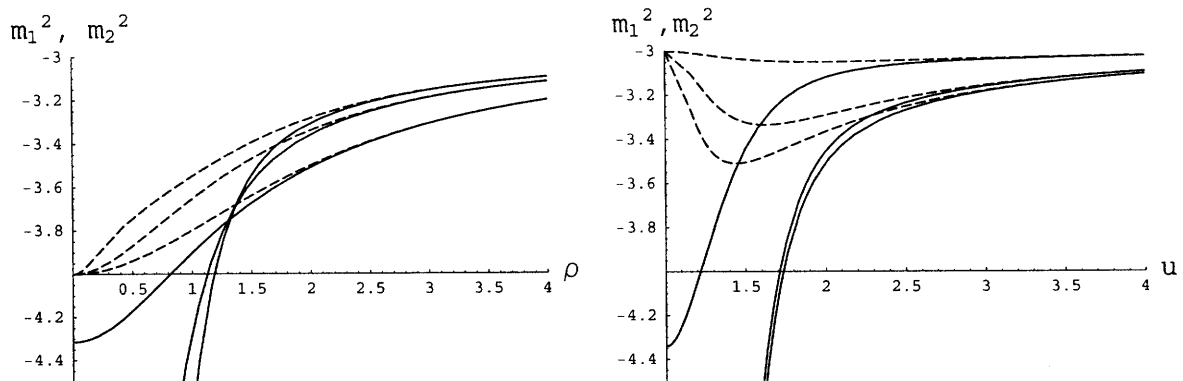
Figure 2-3: The squared "masses" of the two orthonormal geometric modes of the D7-brane fluctuations for Minkowski embeddings (left panel) and black hole embeddings (right panel). In each figure, m_1^2 (m_2^2) is plotted as a solid (dashed) line for three values of ϵ_∞. The Minkowski embeddings have $\epsilon_\infty = 0.587$, 0.471 and 0.249 (top to bottom) and the black hole embeddings have $\epsilon_\infty = 1.656$, 0.647 and 0.586 (again top to bottom, this time with temperature increasing from top to bottom.) The Minkowski embedding is plotted as a function of ρ and the black hole embedding as a function of u with the horizon on the left at $u = 1$.

codimension-two branes in any spacetime geometry. For example, we can apply it to the embedding of D7-branes at zero temperature given by (2.21) and learn that the meson fluctuations at zero temperature are described by (2.60) with

$$m_1^2 = m_2^2 = -\frac{3\rho^2 + 4}{1 + \rho^2} \qquad (2.63)$$

and with h_{ij} in (2.60) given by (2.24). It is also straightforward to check that equations of motion derived from (2.60) with (2.63) and h_{ij} given by (2.24) are equivalent to (2.25). At zero temperature, (2.23) and (2.24) are already simple enough and the formalism we have described here does not gain us further advantage. However, at nonzero temperature the equations of motion obtained from (2.60) yield both technical and conceptual simplification. In Section 5 we shall use the formalism that we have developed to obtain the dispersion relations at large momentum analytically.

Before turning to the dispersion relations, we plot the "masses" m_1^2 and m_2^2 for various D7-brane embeddings at nonzero temperature in Fig. 2-3. Using a numerical solution for $y(\rho)$, it is straightforward to evaluate (2.61), obtaining the masses in the

figure. For the black hole embeddings, the D7-brane begins at the black hole horizon at $u = 1$ rather than at $\rho = 0$, see Fig. 2-1, making it more convenient to plot the masses as a function of u rather than ρ. We can infer several important features from the masses plotted in Fig. 2-3. As $\rho \to \infty$, both m_1^2 and m_2^2 approach -3 for all the embeddings. This implies that χ_1 and χ_2 couple to boundary operators of dimension 3, as shown in [106] by explicit construction of the operators in the boundary theory which map onto χ_1 and χ_2. As $\varepsilon \to 1$ from below for the Minkowski embeddings (from above for the black hole embeddings), the behavior of m_1^2 at the tip of the D7-brane at $\rho = 0$ (at $u = 1$) becomes singular, diverging to minus infinity. This is a reflection of the curvature divergence at the tip of the critical embedding at $\rho = 0$ ($u = 1$).

We have referred to m_1^2 and m_2^2 as "masses" in quotes because the equations of motion obtained by straightforward variation of the action (2.60) in which they arise yields

$$\frac{1}{\sqrt{-h}}\partial_i(\sqrt{-h}h^{ij}\partial_j\chi_s) - m_s^2\chi_s = 0, \quad s = 1, 2 \qquad (2.64)$$

with $h \equiv \det h_{ij}$, which is a Klein-Gordon equation in a curved spacetime with spatially varying "masses". If we could cast the equations of motion in such a way that they take the form of a Schrödinger equation with some potential, this would make it possible to infer qualitative implications for the nature of the meson spectrum immediately via physical intuition, which is not possible to do by inspection of the curves in Fig. 2-3. To achieve this, we recast the equations of motion as follows. We introduce a "tortoise coordinate" z defined by

$$dz^2 = \frac{1}{u^2 f(u)}\left(1 + y_0'(\rho)^2\right)d\rho^2 , \qquad (2.65)$$

in terms of which the induced metric on the brane takes the simple form

$$\frac{ds_{D7}^2}{R^2} = f(-dt^2 + dz^2) + r^2(u)d\vec{x}^2 + \frac{\rho^2}{u^2}d\Omega_3^2 . \qquad (2.66)$$

(We choose the additive constant in the definition of z so that $z = 0$ at $\rho = 0$.) Then,
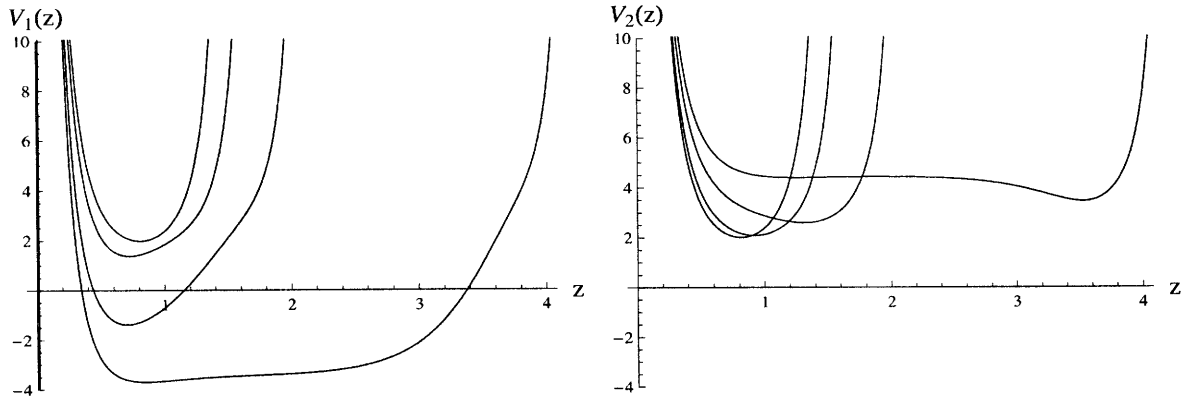
Figure 2-4: Potentials $V_s(z)$ for Minkowski embeddings at various temperatures, all with $k = \ell = 0$. The left (right) panel is for $s = 1$ ($s = 2$). In each panel, the potentials are drawn for ϵ_∞ = 0.249, 0.471, 0.586 and 0.5948, with the potential widening as the critical embedding is approached, i.e. as ϵ_∞ is increased. The $\epsilon_\infty = 0.586$ potential is that for the Minkowski embedding at the first order transition; the widest potential shown describes the fluctuations of a metastable Minkowski embedding very close to the critical embedding. The potential becomes infinitely wide as the critical embedding is approached, but it does so only logarithmically in $\epsilon_\infty^c - \epsilon_\infty$. Note that the tip of the D7-brane is at $z = 0$, on the left side of the figure, whereas $\rho = \infty$ has been mapped to a finite value of the tortoise coordinate $z = z_{\text{max}}$, corresponding to the "wall" on the right side of each of the potentials in the figure.

we seek solutions to the equations of motion (2.64) that separate according to the ansatz

$$\chi_s = \frac{\psi_s(z)}{Z}\, e^{-i\omega t + i\vec{k}\cdot\vec{x}}\, Y_{\ell m \tilde{m}}(\Omega_3) \tag{2.67}$$

with

$$Z \equiv \left(\frac{\sqrt{-h}}{f}\right)^{\frac{1}{2}} = \left(\frac{r\rho}{u}\right)^{\frac{3}{2}} . \tag{2.68}$$

Such a solution is the wave function for a scalar meson of type $s = 1$ or $s = 2$ with energy ω and wave vector $\vec{k}$ (note the plane wave form for the dependence on (3+1)-dimensional Minkowski space coordinates) and with quantum numbers ℓ, m and $\tilde{m}$ specifying the angular momentum spherical harmonic on the "internal" three-sphere. (Rotation symmetry of the three-sphere guarantees that the quantum numbers m and $\tilde{m}$ will not appear in any equations.) The $\psi_s(z)$ that we must solve for are the wave functions of the meson states in the fifth dimension.

The reasons for the introduction of the tortoise coordinate z and the ansatz (2.67)

for the form of the solution become apparent when we discover that the equations of motion (2.64) now take the Schrödinger form

$$-\frac{\partial^2}{\partial z^2}\psi_s + V_s(k, z)\psi_s = \omega^2\psi_s \ , \tag{2.69}$$

with potentials for each value of $k = |\vec{k}|$ and for each of the two scalar mesons labelled by $s = 1, 2$ given by

$$V_s(k, z) = \frac{Z''}{Z} + fm_s^2 + \frac{fk^2}{r^2} + \frac{l(l+2)fu^2}{\rho^2} \ . \tag{2.70}$$

Here, the prime denotes differentiation with respect to z. Recall that $u^2 = \rho^2 + y_0^2(\rho)$ and it should be understood that ρ, u, and y_0 are all functions of the tortoise coordinate z. In Figs. 2.4 and 2-5, we provide plots of $V_s(z)$ with $k = \ell = 0$ for $s = 1, 2$ and for Minkowski (Fig. 2.4)) and black hole (Fig. 2-5) embeddings at various temperatures. With the tortoise coordinate z defined as we have described, in a Minkowski embedding z extends from $z = 0$, which corresponds to the tip of the D7-brane, to

$$z = z_{\max} \equiv \int_0^\infty \frac{d\rho}{u}\sqrt{\frac{1 + y_0'(\rho)^2}{f(u)}} \ , \tag{2.71}$$

which corresponds to $\rho = \infty$. Here, $u(\rho)$ and $f(u)$ are given in (2.46). This defines the width of the potentials for the Minkowski embeddings shown in Fig. 2.4, which get wider and wider as the critical embedding is approached.

If we used the same tortoise coordinate for the black hole embeddings, the lower limit of the integral (2.71) is then the ρ at which $y(\rho)$ intersects the horizon and $f(u)$ vanishes, making the integral divergent. This means that $\rho = \infty$ is mapped onto $z = \infty$ for black hole embeddings. It is more convenient to define z_{bh} by first choosing the integration constant such that $\rho = \infty$ corresponds to $z_{bh} = 0$, and then multiplying by -1. This is the tortoise coordinate that we have used in Fig. 2-5

The qualitative implications for the meson spectrum can be inferred immediately from Figs. 2.4 and 2-5, since we have intuition for solutions of the Schrödinger equation. We can see immediately that the Minkowski embeddings all have a discrete

71
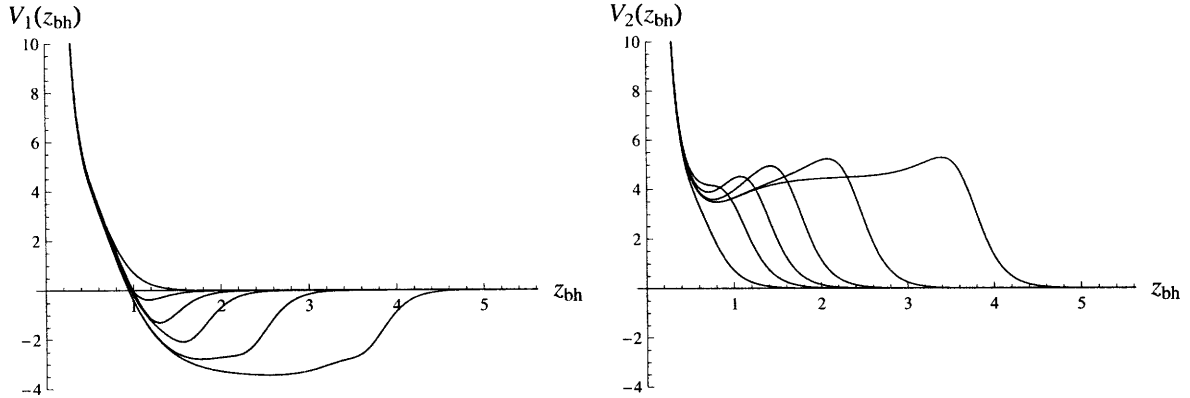
Figure 2-5: Potentials $V_s(z_{bh})$ for black hole embeddings at various temperatures, all with $k = \ell = 0$. The left (right) panel is for $s = 1$ ($s = 2$). In each panel, the potentials are drawn for $\epsilon_\infty = 3584., 0.647, 0.586, 0.586, 0.5940$ and 0.5948, from narrower to wider, with the potential widening as the critical embedding is approached from the right along the curve in Fig. 2-2. Note that z_{bh} is defined such that the horizon is at $z_{bh} = \infty$, and $\rho = \infty$ is at $z_{bh} = 0$. The narrower (wider) of the two potentials with $\epsilon_\infty = 0.586$ is that for the stable (unstable) black hole embedding: at this ϵ_∞, there is a first order transition (see Fig. 2-2) between the stable Minkowski embedding (whose potential is found in Fig. 2.4) and the stable black hole embedding. The potentials at $\epsilon_\infty = 0.5940$ and 0.5948 describe fluctuations of metastable black hole embeddings, with the latter being a black hole embedding very close to the critical embedding.

spectrum of meson excitations, while the fluctuations of the black hole embeddings all have continuous spectra. This justifies the identification of the first order phase transition from Minkowski to black hole embeddings that we described in Section 3 as the transition at which mesons dissociate.

Other phenomena that are discussed quantitatively in [37, 38, 106] can be inferred qualitatively directly from the potentials in Figs. 2.4 and 2-5. For example we see from the left panel in Fig. 2-5 that, in addition to the continuous spectrum characteristic of all black hole embeddings, those embeddings that are close to the critical embedding will have discrete bound states for the ψ_1 fluctuations. These bound states will always have negative mass-squared, representing an instability. This instability arises only in a regime of temperatures at which the black hole embeddings already have a higher free energy than the stable Minkowski embedding, that is, at temperatures below the first order transition [37]. They therefore represent an instability of the branch of the spectrum that was already metastable. Similarly, the left panel of Fig. 2.4 shows

72

that Minkowski embeddings close to the critical embedding also have negative mass-squared bound states; again, this instability only occurs for embeddings that were already only metastable [37]. We see from the right panel of Fig. 2-5 that resonances may also occur in the ψ_2 channel for the black hole embedding. They are interpreted as quasi-normal modes; close to the transition these resonances become more well defined and may be interpreted as quasi-particle meson excitations [38, 106].

2.5 Dispersion relations

We have now laid the groundwork needed to evaluate the dispersion relations for the ψ_1 and ψ_2 scalar mesons, corresponding in the gravity dual to fluctuations of the position of the D7 brane. These fluctuations are governed by (2.69), which are Schrödinger equations with the potentials $V_1(k, z)$ or $V_2(k, z)$ given by (2.70) and (2.61) and depicted in Fig. 2.4. The eigenvalues of these Schrödinger equations are ω^2 for the mesons. So, it is now a straightforward numerical task to find the square root of the eigenvalues of the Schrödinger equation with, say, potential $V_1(k, z)$, at a sequence of values of k. At $k = 0$, this will reproduce the results that we reviewed in Section 3.2. As we increase k, we map out the dispersion relation ω of each of the ψ_1 mesons. In Fig. 2-8 in Section 2.5.3 below, we show the dispersion relations for the ground state ψ_1 meson at several values of the temperature. Such dispersion relations have also been obtained numerically in [37]. In order to more fully understand the dispersion equations, and their implications, we shall focus first on analytic results. The potentials are complicated enough that we do not have analytic solutions for the general case. We shall show, however, that in the low temperature and/or the large-k limit, the equations simplify sufficiently that we can find the dispersion relations analytically. It is the large-k limit that is of interest to us, but it is very helpful to begin first at low temperatures, before then analyzing the dispersion relations in the large-k limit at any temperature below the dissociation temperature.

Readers who are only interested in the final results can proceed directly to Section 2.5.4, where we summarize and discuss our central results for the dispersion

relations.

2.5.1 Low temperature

At low temperature, $\varepsilon \ll 1$, the D7-branes are far from the horizon of the black hole. In this regime, we can expand various quantities that occur in the potentials (2.70) as power series in ε^2. We shall then be able to determine the dispersion relations analytically to order ε^2 in two limits: (i) $\varepsilon \to 0$ at fixed k, meaning in particular that $\varepsilon k \to 0$; and (ii) $\varepsilon \to 0$ at fixed, large, εk, meaning that $k \to \infty$ as $\varepsilon \to 0$.

We begin by seeing how the equation (2.47) that determines the embedding $y(\rho)$ in the absence of fluctuations simplifies at small ε. Expanding $y(\rho)$ as a power series in ε, one immediately finds that $y(\rho)$ is modified only at order ε^4, i.e.

$$y(\rho) = 1 + \mathcal{O}(\varepsilon^4) \ , \tag{2.72}$$

which in turn implies that

$$\epsilon_\infty = \varepsilon \left(1 + \mathcal{O}(\varepsilon^4)\right) \ . \tag{2.73}$$

Thus, if we work only to order ε^2, we can treat the embedding as being $y(\rho) = 1$, as at zero temperature, and can neglect the difference between ε and ϵ_∞ (which is to say the difference between $y(0)$ and $y(\infty)$). From (2.46), then,

$$u^2 = 1 + \rho^2 + \mathcal{O}(\varepsilon^4), \qquad f(u) \approx u^2 \left(1 - \frac{3\varepsilon^2}{u^4} + \mathcal{O}(\varepsilon^4)\right) \ . \tag{2.74}$$

By expanding the curvature invariants in (2.61) to order ε^2, we find that

$$m_1^2 = m_2^2 = -\frac{4 + 3\rho^2}{1 + \rho^2} + \mathcal{O}(\varepsilon^4) \ , \tag{2.75}$$

meaning that to order ε^2 the mass terms occurring in (2.47) are as in (2.63) at zero temperature. Next, we expand the tortoise coordinate (2.65), finding

$$z = \tan^{-1}\rho + \varepsilon^2 g(\rho) + \mathcal{O}(\varepsilon^4), \quad \text{with} \ \ g(\rho) = \frac{3}{16}\left(3\tan^{-1}\rho + \frac{\rho(5 + 3\rho^2)}{(1 + \rho^2)^2}\right) \ . \tag{2.76}$$

We can then invert (2.76) to obtain ρ in terms of z:

$$\rho = \tan z - \varepsilon^2 \frac{g(\tan z)}{\cos^2 z} + \ldots . \qquad (2.77)$$

Using these equations, we find that the potential (2.70) is given to order $O(\varepsilon^2)$ by

$$V(z) = k^2 + V^0(z) - 4\varepsilon^2 k^2 \cos^4 z + \varepsilon^2 h(z) + O(\varepsilon^4, \varepsilon^4 k^2), \qquad (2.78)$$

where

$$V^0(z) \equiv \frac{4\alpha_\ell}{\sin^2 2z} - 1, \quad \text{with} \quad \alpha_\ell \equiv \frac{3}{4} + \ell(\ell+2) \qquad (2.79)$$

is the potential at zero temperature, and

$$h(z) = \frac{3\alpha_\ell \left(\sin^2(2z) + 6z \cot(2z) - 3 \right)}{2\sin^2(2z)} + \frac{9}{4} \sin^2(2z) . \qquad (2.80)$$

We shall not use the explicit form of $h(z)$ in the following.

Low temperature at fixed k

At zero temperature ($\varepsilon = 0$), solving the Schrödinger equation (2.69) with potential $V^0(z)$ yields the eigenvalues (and hence the dispersion relations)

$$\omega^2 - k^2 = m_{n\ell}^2, \qquad n = 1, 2, \ldots , \quad l = 0, 1, \ldots , \qquad (2.81)$$

with $m_{n\ell}$ given by (2.26) (after restoring its dimensions). If we work in the limit $\varepsilon \to 0$ with k fixed, then both the $O(\varepsilon^2)$ and the $O(\varepsilon^2 k^2)$ terms that describe the effects of nonzero but small temperature in the potential (2.79) can be treated using quantum mechanical perturbation theory. To first order in ε^2, the dispersion relation becomes

$$\omega^2 = v_{n\ell}^2 k^2 + m_{n\ell}^2 + \varepsilon^2 b_{n\ell} + O(\varepsilon^4) \qquad (2.82)$$

with

$$
\begin{aligned}
v_{n\ell}^2 &= 1 - a_{n\ell}\,\varepsilon^2 \ , \\
a_{n\ell} &= 4\langle n,\ell|\cos^4 z|n,\ell\rangle \ , \\
b_{n\ell} &= \langle n,\ell|h(z)|n,\ell\rangle \ ,
\end{aligned}
\tag{2.83}
$$

where $|n,\ell\rangle$ are the eigenfunctions of the Hamiltonian with the unperturbed potential V^0 of (2.79), with wave functions

$$
\psi_{n\ell}^0(z) = \Gamma\left(\ell + \frac{3}{2}\right) 2^{1+\ell} \sqrt{\frac{n\left(n + \ell + \frac{3}{2}\right)}{\pi\Gamma\left(n + 2\ell + 3\right)}}\,(\sin z)^{\frac{3}{2}+\ell}\, C_n^{(\ell+\frac{3}{2})}(\cos z) \ .
\tag{2.84}
$$

Using the recursion relations for the generalized Gegenbauer polynomials $C_n^{(\alpha)}$ [109], $a_{n\ell}$ can be evaluated analytically, yielding

$$
a_{n\ell} = 2 - \frac{(n + 2l + 1)(n + 2l + 2)}{4(n + l + 1/2)(n + l + 3/2)} - \frac{(n + 1)(n + 2)}{4(n + l + 3/2)(n + l + 5/2)} \ .
\tag{2.85}
$$

So, for the ground state with $n = \ell = 0$, $a_{00} = 18/15$. $b_{n\ell}$ can be computed numerically, but we will not do so here. The dispersion relation (2.82) is valid for $\varepsilon^2 \ll 1$ and $\varepsilon^2 k^2 \ll 1$, meaning that at small ε it is valid for $k \ll 1/\varepsilon$. No matter how small ε is, the perturbation theory breaks down for $k \sim \frac{1}{\varepsilon}$ and (2.82) does not apply. In other words, the low temperature $\varepsilon \to 0$ limit and the high meson momentum $k \to \infty$ limits do not commute. Even though (2.82) cannot be used to determine the meson velocity at large k, it is suggestive. We shall see below that in the large-k limit, the meson velocity is indeed $1 - \mathcal{O}(\varepsilon^2)$, but the coefficient of ε^2 is not given by (2.85).

Low temperature at fixed, large, εk

To explore the behavior of the dispersion relations in the large-k limit, we now consider the following scaling limit

$$
\varepsilon \to 0, \qquad k \to \infty, \qquad \text{with} \qquad \Lambda^2 = k^2\varepsilon^2 = \text{finite}.
\tag{2.86}
$$

76
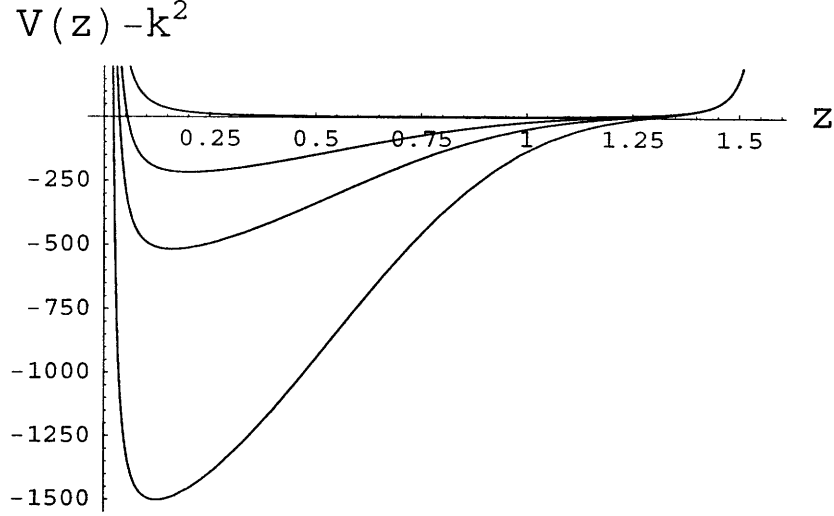
Figure 2-6: The potential (2.87) with $\varepsilon = 0.756$ and $k = 5$, 20 and 100. We see that as $\Lambda = \varepsilon^2 k^2$ increases, the minimum of the potential moves towards $z = 0$, the potential deepens, and the curvature around the minimum increases.

In this limit, the potential (2.70) again greatly simplifies and, consistent with (2.78), becomes

$$V(z) = k^2 + \frac{4\alpha_\ell}{\sin^2 2z} - 1 - 4\Lambda^2 \cos^4 z \; . \tag{2.87}$$

This potential is valid in the limit (2.86) for any value of Λ, small or large. If Λ is small, the dispersion relation can be determined using perturbation theory as before, yielding (2.82) without the $\varepsilon^2 b_{n\ell}$ term. In order to analyze the large-k regime, we now consider $\Lambda \gg 1$, and seek to evaluate the dispersion relation as an expansion in $1/\Lambda$. For this purpose, we notice that as $\Lambda \to \infty$ the potential (2.87) develops a minimum at

$$z_0 = \left(\frac{\alpha_\ell}{8\Lambda^2}\right)^{\frac{1}{4}} \to 0 \quad \text{for} \quad \Lambda \to \infty \; , \tag{2.88}$$

as depicted in Fig. 2-6. The curvature about the minimum is $V''(z_0) \propto \Lambda^2$. Thus, if we imagine watching how the wave function changes as we take the large-Λ limit, we will see the wave function getting more and more tightly localized around the point $z = z_0$ which gets closer and closer to $z = 0$. That is, the wave function will be localized around the tip of the brane $z = 0$. This motivates us to expand the

potential around $z = 0$, getting

$$V(z) - k^2 + 1 = \alpha_l \left(\frac{1}{z^2} + \frac{4}{3} + \frac{16z^2}{15} + \dots \right) - 4\Lambda^2 \left(1 - 2z^2 + \frac{5z^4}{3} + \dots \right) . \quad (2.89)$$

If we now introduce a new variable $\xi = \Lambda^{\frac{1}{2}} z$, the Schrödinger equation (2.69) becomes

$$\left(-\partial_\xi^2 + \frac{\alpha_\ell}{\xi^2} + \frac{1}{4}\Omega^2\xi^2 \right) \psi + \tilde{V}\psi = E\psi \quad (2.90)$$

where

$$\Omega^2 = 32, \qquad E = \frac{1}{\Lambda}(\omega^2 - k^2 + 4\Lambda^2) , \quad (2.91)$$

and $\tilde{V}$ contains only terms that are higher order in $1/\Lambda$:

$$\tilde{V} = \frac{1}{\Lambda} \left(\frac{4\alpha_\ell}{3} - 1 - \frac{20}{3}\xi^4 \right) + \mathcal{O}(1/\Lambda^2) . \quad (2.92)$$

Thus to leading order in the large Λ limit, we can drop the $\tilde{V}$ term in (2.90). Upon so doing, and using the expression (2.79) for α_ℓ, the equation (2.90) becomes that of a harmonic oscillator in 4 dimensions with mass $\frac{1}{2}$ and frequency Ω. This quantum mechanics problem can be solved exactly, with wave functions given by

$$\psi_{nl} = \xi^{3/2+\ell} L_\nu^{(\ell+1)} \left(\frac{\Omega}{2}\xi^2 \right) e^{-\frac{\Omega}{4}\xi^2} , \quad (2.93)$$

up to a normalization constant, and with eigenvalues given by

$$E_n = \Omega(n + 2), \quad n = 0, 1, \dots \quad (2.94)$$

In (2.93), $L_\nu^{(\alpha)}$ is the generalized Laguerre polynomial of order

$$\nu = \frac{n - \ell}{2} . \quad (2.95)$$

The allowed values of ℓ are determined by the requirement that ν must be a non-negative integer. The degeneracy of n-th energy level is $\frac{(n+3)!}{3!n!}$. Higher order correc-

78

tions in $1/\Lambda$ can then be obtained using perturbation theory. For example, with the next order correction included, the degeneracy among states with different ℓ and the same n is lifted and the eigenvalues are given by

$$E_{n\ell} = \Omega(n + 2) + \frac{c_{n\ell}}{\Lambda} + \mathcal{O}(1/\Lambda^2) \qquad (2.96)$$

with

$$c_{n\ell} = -\frac{5}{4}(n + 2)^2 + \frac{7}{4}\ell(\ell + 2) \ . \qquad (2.97)$$

Thus, in the small-ε limit with Λ fixed and large, we find using (2.91) that the dispersion relation becomes

$$\omega_{n\ell}^2 = (1 - 4\varepsilon^2)k^2 + 4\sqrt{2}(n + 2)k\varepsilon + c_{n\ell} + O(1/k) \ . \qquad (2.98)$$

Notice that $c_{n\ell}$ is negative for the ground state, and indeed for any n at sufficiently small ℓ. We learn from this calculation that in the large-k limit, at low temperatures mesons move with a velocity given to order ε^2 by $v = \sqrt{1 - 4\varepsilon^2} = 1 - 2\varepsilon^2$. Recalling that to the order we are working $\epsilon_\infty = \varepsilon$, this result can be expressed in terms of T, m_q and λ using (2.41). In the next subsection, we shall obtain the meson velocity at large k for any ε .

2.5.2 Large-k dispersion relation at generic temperature

The technique of the previous subsection can be generalized to analyze the dispersion relation in the large-k limit at a generic temperature below the dissociation temperature. For general $\varepsilon < 1$, one again observes that the potential has a sharper and sharper minimum near the tip of the brane $z = 0$ as k becomes larger and larger. Thus, in the large k limit, we only need to solve the Schrödinger equation near $z = 0$.

To find the potential $V(z)$ as a power series in z near $z = 0$, we need to know the

solution $y(\rho)$ of (2.47) near the tip of the brane at $\rho = 0$:

$$y = 1 + \frac{\rho^2}{\varepsilon^{-4} - 1} + \frac{\varepsilon^4(5 + 5\varepsilon^4 - 3\varepsilon^8)}{3(\varepsilon^4 - 1)^3}\rho^4 + \mathcal{O}(\rho^4) \ . \qquad (2.99)$$

At small ρ, using the expansion of y in (2.99), we find the tortoise coordinate z has the expansion

$$z = \frac{\sqrt{1 + \varepsilon^2}}{1 - \varepsilon^2}\rho + \mathcal{O}(\rho^3). \qquad (2.100)$$

Using (2.99) and (2.100) in (2.70), after some algebra we find

$$V_s(z) = k^2 \left(v_0^2 + \frac{1}{4}\Omega^2\varepsilon^2 z^2 + \beta_\ell z^4 + \dots \right) + \frac{\alpha_\ell}{z^2} + \gamma_{s\ell} + \mathcal{O}(z^2) \ , \qquad (2.101)$$

where

$$v_0 = \frac{1 - \varepsilon^2}{1 + \varepsilon^2}, \qquad (2.102)$$

$$\Omega^2 = \frac{32(1 - \varepsilon^2)^2(1 + \varepsilon^4)}{(1 + \varepsilon^2)^5} \ , \qquad (2.103)$$

$$\beta_\ell = -\Omega^2\varepsilon^2\frac{5 - 36\varepsilon^2 + 28\varepsilon^4 - 36\varepsilon^6 + 5\varepsilon^8}{24(1 + \varepsilon^2)^3} \ , \qquad (2.104)$$

$$\gamma_{1\ell} = \frac{\ell(\ell + 2)\left(\frac{4}{3} + 4\varepsilon^2 + \frac{4}{3}\varepsilon^4 + 4\varepsilon^6 + \frac{4}{3}\varepsilon^8\right) - 56\varepsilon^4}{(1 + \varepsilon^2)^3} \ , \qquad (2.105)$$

$$\gamma_{2\ell} = \gamma_{1\ell} + \frac{80\varepsilon^4}{(1 + \varepsilon^2)^3} \ , \qquad (2.106)$$

and where α_ℓ is given by (2.79). We can understand why the leading difference between the potentials V_1 and V_2 for the mesons ψ_1 and ψ_2 arises in this approximation in the constant terms $\gamma_{1\ell}$ and $\gamma_{2\ell}$ as follows. We see from (2.70) that the difference between V_1 and V_2 comes only from m_1^2 and m_2^2, which do not enter multiplied by k^2 and so cannot affect v_0, Ω^2 or β_ℓ. Furthermore, m_1^2 and m_2^2 are curvature invariants, see (2.61), and must therefore be smooth as $\rho \to 0$ because for Minkowski embeddings the D7 brane is smooth at $\rho = 0$. This means that m_1^2 and m_2^2 cannot affect the coefficient of $1/z^2$ in (2.101).

We can now obtain the dispersion relations from the Schrödinger equations with potentials (2.101) as we did in the previous subsection. After making the rescaling $z = k^{-1/2}\xi$, the Schrödinger equation (2.69) takes exactly the form (2.90), with

$$E = \frac{1}{k}(\omega^2 - v_0^2 k^2) , \qquad (2.107)$$

where Ω and v_0 are given by (2.102) and (2.103) respectively, and where $\tilde{V}_s(z)$ contains only terms that are subleading in the $1/k$ expansion, and is given by

$$\tilde{V}_s(z) = \frac{1}{k}\left(\gamma_{s\ell} + \beta_\ell \xi^4\right) + \mathcal{O}(k^{-2}) . \qquad (2.108)$$

Thus, we find the large-k dispersion relation

$$\omega_s^2 = k^2 v_0^2 + k\Omega\varepsilon(n+2) + d_{sn\ell} + \mathcal{O}(1/k) \qquad (2.109)$$

with

$$d_{1n\ell} = \frac{1}{(1+\varepsilon^2)^3}\left[\frac{4}{3}\ell(\ell+2)\left(1 + 3\varepsilon^2 + \varepsilon^4 + 3\varepsilon^6 + \varepsilon^8\right)\right.$$
$$\left. -\left(\frac{5}{4} - 9\varepsilon^2 + 7\varepsilon^4 - 9\varepsilon^6 + \frac{5}{4}\varepsilon^8\right)(n+2)^2 - 56\varepsilon^4\right] \qquad (2.110)$$

and

$$d_{2n\ell} = d_{1n\ell} + \frac{80\varepsilon^4}{(1+\varepsilon^2)^3} . \qquad (2.111)$$

Restoring dimensionful quantities in the dispersion relation (2.109), i.e. undoing (2.43), means multiplying the k and constant terms by L_0/R^2 and L_0^2/R^4, respectively.

We can easily obtain an explicit expression for the wave functions themselves if we neglect the β_ℓ, $\gamma_{s\ell}$ and higher order terms, as the potential (2.101) is then that in the radial wave equation for a four-dimensional harmonic oscillator. To this order, the wave functions are given up to a normalization constant by

$$\psi = z^{3/2+\ell} L_\nu^{(\ell+1)}\left(\frac{1}{2}\Omega\varepsilon k z^2\right)\exp\left(-\frac{1}{4}\Omega\varepsilon k z^2\right) , \qquad (2.112)$$

81

where, as before, $\nu = (n - \ell)/2$ is the order of the generalized Laguerre polynomial $L_\nu^{(\ell+1)}$.

The dispersion relations (2.109) are the central result of Section 5. We shall analyze (2.109) and discuss its consequences at length in Sections 5.4 and 6. First, however, we close this more technical discussion with a few remarks related to the approximation that we have used to obtain the large-k dispersion relations:

1. The wave function is localized at the tip of the brane, near $\rho = 0$ which is the fixed point of the $SO(4)$ symmetry at which the S^3 shrinks to zero size and the fluctuations are fluctuations in R^4. This is the reason why we find a four-dimensional harmonic oscillator.

2. Our approximation is valid for wave functions that are tightly localized near $z = 0$. Evidently, this approximation must break down for mesons with high enough n, whose wave functions explore more of the potential. More precisely, if we increase n and ℓ while keeping ν fixed and small, the wave functions are peaked at $z_0 \sim \left(\frac{n}{k\Omega\varepsilon}\right)^{\frac{1}{2}}$ with a width $\frac{1}{(k\Omega\varepsilon)^{\frac{1}{2}}}$. Or, if we increase n and ν while keeping ℓ fixed and small, the wave functions become wider, with ν oscillations over a range of z from near zero to near $z_0 \sim \left(\frac{n}{k\Omega\varepsilon}\right)^{\frac{1}{2}}$ and hence a wavelength $\sim \frac{1}{(nk\Omega\varepsilon)^{\frac{1}{2}}}$. In either case, our approximation must break down for $n \sim k$, since for n this large z_0 is no longer small and the wave function is no longer localized near $z = 0$.

3. We must ask at what k (or, at what ω) stringy effects that we have neglected throughout may become important in the dispersion relations for the mesons that we have analyzed. We can answer this question by comparing the length scale over which the meson wave functions that we have computed varies to the string length scale $\alpha'^{\frac{1}{2}}$. Considering first the case where ν is small, we see from (2.66) that the proper distance between the maximum of the wave function at $z = z_0$ and the tip of the brane at $z = 0$ is

$$l_0 \sim \sqrt{f(0)}\, R\, z_0 \sim \frac{1 - \varepsilon^2}{\sqrt{1 + \varepsilon^2}}\, R \left(\frac{4n}{k\Omega\varepsilon}\right)^{\frac{1}{2}} \qquad (2.113)$$

and the width of the wave function is

$$\delta l \sim \frac{1 - \varepsilon^2}{\sqrt{1 + \varepsilon^2}} R \left(\frac{1}{k\Omega\varepsilon} \right)^{\frac{1}{2}} . \qquad (2.114)$$

Stringy effects can be neglected as long as $\delta l \gg \alpha'^{\frac{1}{2}}$, meaning

$$k < \mathcal{O}(\lambda^{\frac{1}{4}} M) , \qquad (2.115)$$

where in the last expression we have restored the dimensions of k using (2.29) and (2.43). (Since $\omega = v_0 k$ at at large k, this parametric criterion is the same for ω as for k.) If ν is large, the wavelength of the wave function should be compared to $\alpha'^{\frac{1}{2}}$ meaning that δl is reduced by a factor $\sim 1/\sqrt{\nu}$ and stringy effects can be neglected only as long as

$$k < \mathcal{O}(\lambda^{\frac{1}{4}} M/\nu) . \qquad (2.116)$$

We can conclude from either (2.115) or (2.116) that we are justified in using the dispersion relation that we have derived in the $k \to \infty$ limit, as long as we take the $\lambda \to \infty$ limit first.[6]

4. Notice that as $\varepsilon \to 1$ (i.e. approaching the critical embedding), both v_0 and Ω vanish. Our approximation will therefore break down at the critical embedding. (One way to see this is to note that in the leading terms in (2.101) we will then have zero times infinity, meaning that it is no longer obvious that these *are* the leading terms.) However, the first order phase transition occurs at $\varepsilon = 0.756$, long before this happens.
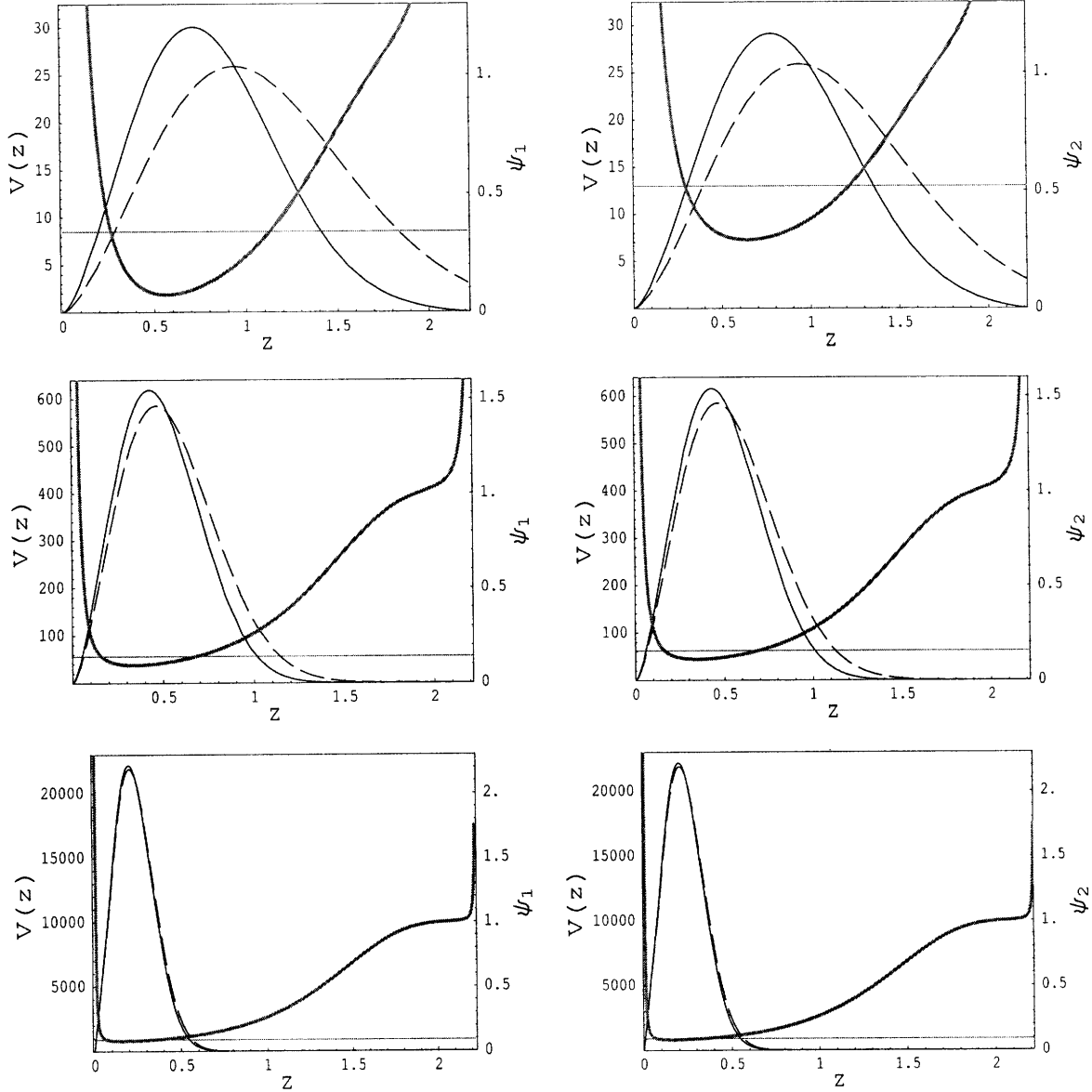
Figure 2-7: Potential and ground state wave function for ψ_1 (left three panels) and ψ_2 (right three panels) for k given by 5, 20 and 100 (top to bottom). All plots have $\varepsilon = 0.756$, corresponding to the Minkowski embedding at the dissociation transition. $V(z)$ and the ground state ($n = \ell = 0$) solutions to the Schrödinger equation in the potentials V are both shown as solid lines, and the ground state energies are indicated by the horizontal (red) lines. The dashed lines show the approximation (2.112) to the wave functions.

2.5.3 Numerical results

We can also obtain the meson wave functions and dispersion relations numerically, without making either a small ε or a large-k approximation. In this subsection we

---

[6]Recall that although the mesons that we have focused on have masses of order $M \sim m_q/\sqrt{\lambda}$, there are also higher-lying stringy mesonic excitations with masses of order $M\lambda^{\frac{1}{4}} \sim m_q/\lambda^{\frac{1}{4}}$. Requiring $\lambda^{1/4}$ to be large is what justifies our neglect of these stringy mesonic excitations, just as it justifies our neglect of stringy corrections to the dispersion relations of the low-lying mesons. Note

plot a few examples of such results, and compare them to the analytic expressions that we have derived above upon making the large-k approximation.

In Fig. 2-7 we plot the potentials (2.70) and ground state wave functions for those potentials that we have obtained numerically for three values of k. Note the changing vertical scale in the plots of V; as k increases, V deepens. We see that as k increases and the potential deepens, the wave function gets more and more localized near $z = 0$ and, correspondingly, the expression (2.112) for the wave function that we have derived in the large-k limit using the fact that the wave function becomes localized becomes a better and better approximation to the exact wave function.

In Fig. 2-8 we show dispersion relations obtained numerically for the ground state ψ_1 meson at several values of the temperature. At each k, we solve the Schrödinger equation to find the ground state (using the shooting method) and from the eigenvalue we obtain ω^2 and hence a point on the dispersion relation. By doing this at many k's, we obtain the curves plotted. We also overlay the linear approximation to the large-k dispersion relations that we shall discuss in Sect. 2.5.4. In Fig. 2-9, we plot the corresponding group velocities.

2.5.4 Summary, limiting velocity and dissociation temperature

In this Section we restate our central result for the dispersion relation and then discuss its implications vis à vis a limiting velocity for mesons at a given temperature as well as a limiting temperature below which mesons with a given velocity are found, and above which they are not.

In Section 5.2, we have derived the large-k approximation to the meson dispersion relations at any temperature below the dissociation transition. We have checked this result against numerical solutions valid at any k in Section 5.3. We begin by restating

---

also that the latter becomes important at an ω of order the mass of the former.
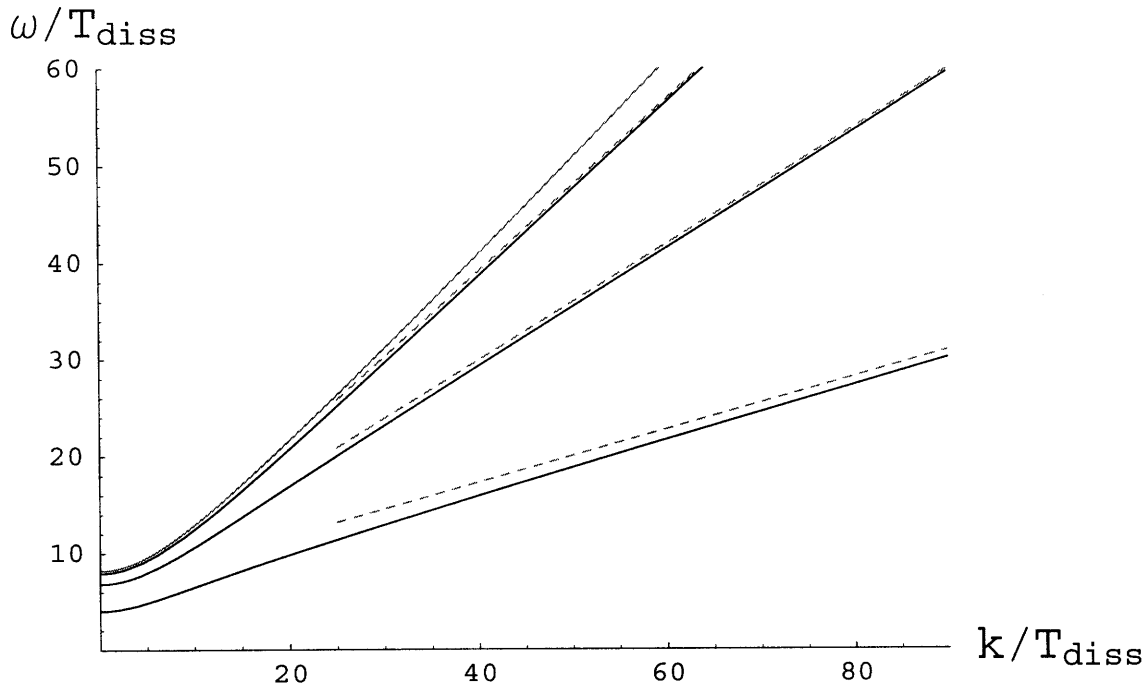
Figure 2-8: Dispersion relations for the ground state ψ_1 meson with $n = \ell = 0$ at various values of ε (i.e. at various temperatures). The top (red) curve is the zero temperature dispersion relation $\omega = \sqrt{k^2 + m^2}$ with m given by (2.26) and with a group velocity that approaches 1 at large k, as required in vacuum by Lorentz invariance. The next three solid (black) curves are the dispersion relations for $\varepsilon = 0.25$, 0.5 and 0.756, top to bottom, the latter corresponding to the Minkowski embedding at the temperature T_{diss} at which the first order phase transition occurs. The dashed (red) lines are the large-k approximation discussed in Section 2.5.4, given by $\omega(k) = v_0 k + \Omega \varepsilon L_0/(v_0 R^2)$ with Ω specified by (2.124). We see that the dispersion relations approach their large-k linear behavior from below. The limiting velocity v_0 decreases with increasing temperature. Had we plotted dispersion relations for $0.756 < \varepsilon < 1$ corresponding to metastable Minkowski embeddings with $T > T_{\text{diss}}$, we would have seen $v_0 \to 0$ as $\varepsilon \to 1$, approaching the critical embedding.

the analytic result (2.109):

$$\omega^2 = v_0^2 k^2 + \Omega \varepsilon (n + 2) \frac{L_0}{R^2} k + d_{sn\ell} \frac{L_0^2}{R^4} , + \mathcal{O}(1/k) \qquad (2.117)$$

where

$$v_0 = \frac{1 - \varepsilon^2}{1 + \varepsilon^2} , \quad \Omega^2 = \frac{32(1 - \varepsilon^2)^2(1 + \varepsilon^4)}{(1 + \varepsilon^2)^5} . \qquad (2.118)$$

86
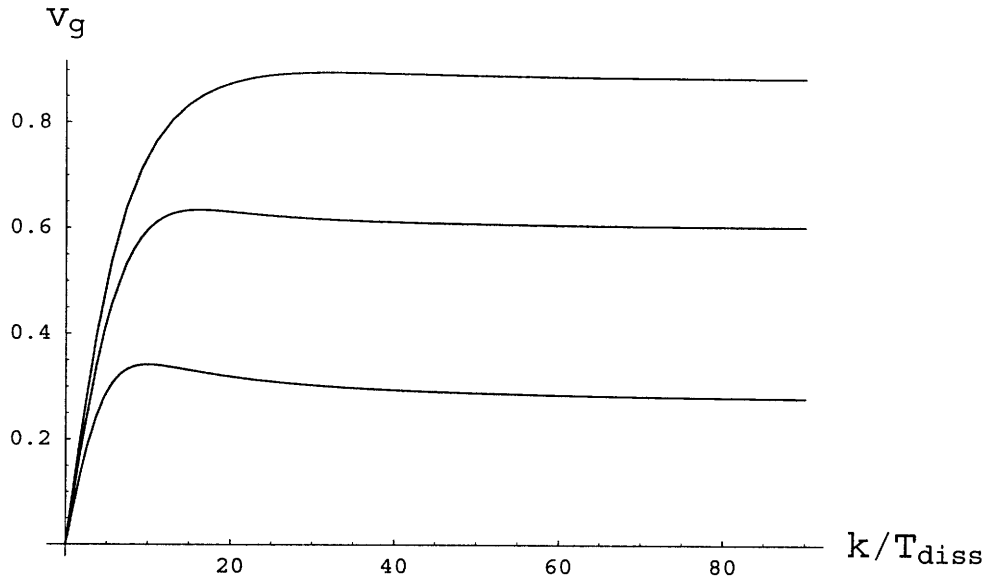
Figure 2-9: Group velocities $v_g = d\omega/dk$ for the dispersion relations from Fig. 2-8, with $\varepsilon = 0.25$, 0.5 and 0.756 (top to bottom). We see that the group velocity approaches its large-k value v_0 from above. And, we see v_0 decreasing with increasing temperature. (Again, v_0 would approach zero if we included the metastable Minkowski embeddings with $T > T_{\text{diss}}$.)

The constant term $d_{sn\ell}$ (which depends on whether we are discussing the ψ_1 or ψ_2 mesons — $s = 1$ or $s = 2$ — and on the quantum numbers n and ℓ) was given in (2.110) and (2.111). In writing the dispersion relation (2.117) we have restored dimensions by undoing the rescaling (2.43). The dimensionful quantity that we had scaled out and have now restored can be written as

$$\frac{L_0}{R^2} = \left(\frac{2\pi m_q}{\sqrt{\lambda}}\right)\sqrt{\frac{\epsilon_\infty}{\varepsilon}}, \qquad (2.119)$$

where we have used (2.32), (2.41) and (2.42). The first factor in (2.119) is a (dimensionful) constant. The quantity $\epsilon_\infty/\varepsilon$ appearing in the second, dimensionless, factor is weakly temperature dependent: it can be read from Fig. 2-2, and is not constant to the degree that the curve in this plot is not a straight line (in the relevant regime $0 < \varepsilon < 0.756$, as $\varepsilon = 0.756$ corresponds to $T = T_{\text{diss}}$.) Although using dimensionless variables obtained via scaling by the temperature-dependent L_0/R^2 was very convenient in deriving all our results, in plotting the dispersion relation and group velocity

87

in Figs. 2-8 and 2-9 we have instead plotted ω and k in units of $T_{\text{diss}} = 2.166\, m_q/\sqrt{\lambda}$, which is a relevant, constant, physical, quantity comparable in magnitude to L_0/R^2. In the remainder of this section, we shall analyze (2.117).

In the large-k limit, the asymptotic value of the group velocity $d\omega/dk$ is given by v_0. This velocity decreases with increasing temperature, and vanishes as $\varepsilon \to 1$ on the critical embedding that separates Minkowski and black hole embeddings in Figs. 2-1 and 2-2. At the temperature at which the first order dissociation transition occurs, $\varepsilon = 0.756$ and $v_0 = 0.273$.

There is a natural explanation within the dual gravity theory for how the asymptotic velocity v_0 can arise. Using (2.46), it is easy to show that v_0 in (2.118) can also be written as

$$v_0^2 = \frac{f(\rho = 0)}{r^2(\rho = 0)} \, , \tag{2.120}$$

which we see from (2.44) is precisely the local speed of light at the tip of the D7-brane. (The local speed of light is 1 at $u = \infty$, and decreases with decreasing u, decreasing to v_0 at the tip of the D7-brane where $\rho = 0$ and $u = y = 1$.) Since we have seen that in the large-k limit the wave function of the meson fluctuations becomes more and more localized closer and closer to the tip of the D7-brane, this makes it natural that v_0 emerges as the asymptotic velocity for mesons with large k.

In the low temperature (equivalently, heavy quark) limit, we find (either directly from (2.118) or, initially, in (2.98) in Section 5.1) that

$$v_0^2 \approx 1 - 4\varepsilon^2 \, . \tag{2.121}$$

Since $\epsilon_\infty \approx \varepsilon$ at small ε, using (2.41) we have

$$v_0^2 \approx 1 - \frac{\lambda^2 T^4}{16 m_q^4} \, , \tag{2.122}$$

which is precisely the critical velocity (2.8) obtained in [11] from the screening calculation as the velocity above which the potential between two moving quarks of mass m_q cannot be defined. This is the first of two quantitative comparisons that we will be

able to make between our present results for meson propagation and results obtained previously via the screening calculation. We see from Fig. 2-10 that (2.121) works very well where $T \ll m_q/\sqrt{\lambda}$, which is where it was derived (both here and in [10]).
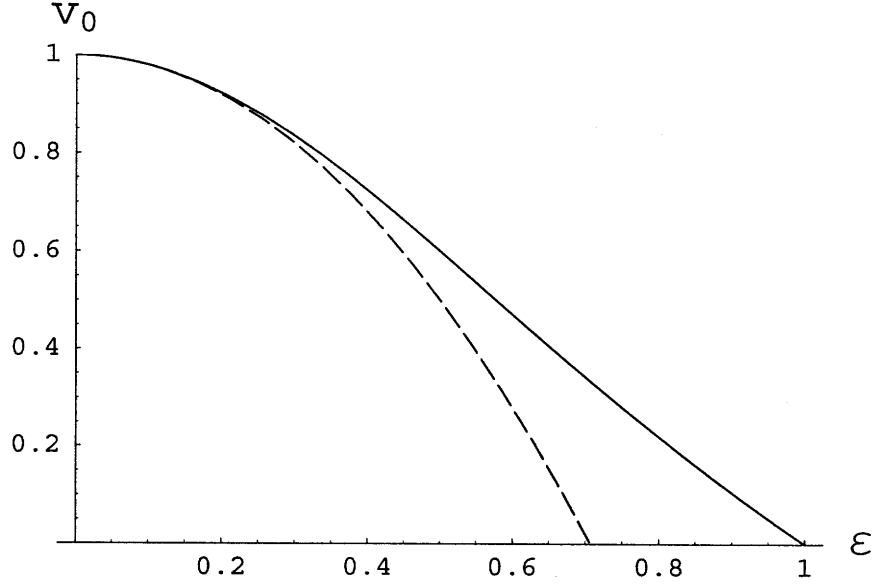
Figure 2-10: The asymptotic velocity v_0 from (2.118) as a function of ε. The low temperature approximation (2.121) is plotted as a dashed line. Recall that the dissociation transition occurs at $\varepsilon = 0.756$.

In order to analyze (2.117) beyond the k^2 term, it is instructive to rewrite it as a large-k approximation to the dispersion relation ω itself rather than to ω^2, yielding

$$\omega(k) = v_0 k + \frac{\Omega \varepsilon (n+2) L_0}{2 v_0 R^2} + \frac{4 d_{sn\ell} v_0^2 - \Omega^2 \varepsilon^2 (n+2)^2}{8 v_0^3} \frac{L_0^2}{R^4} \frac{1}{k} + \mathcal{O}(1/k^2) , \quad (2.123)$$

in the form we discussed in Section 1. We see that the term linear in k in (2.117) yields a constant shift in the meson energies in (2.123). Whereas v_0 is independent of s, n and ℓ, the constant term in (2.123) results in evenly spaced dispersion relations for mesons with differing n quantum number, separated by

$$\frac{\Omega \varepsilon L_0}{2 v_0 R^2} = \left(\frac{2 \pi m_q}{\sqrt{\lambda}} \right) \sqrt{\frac{8 \epsilon_\infty \varepsilon (1 + \varepsilon^4)}{(1 + \varepsilon^2)^3}} , \quad (2.124)$$

which we plot in Fig. 2-11.

If we neglect the $\mathcal{O}(1/k)$ and higher order terms in (2.123), the dispersion relations
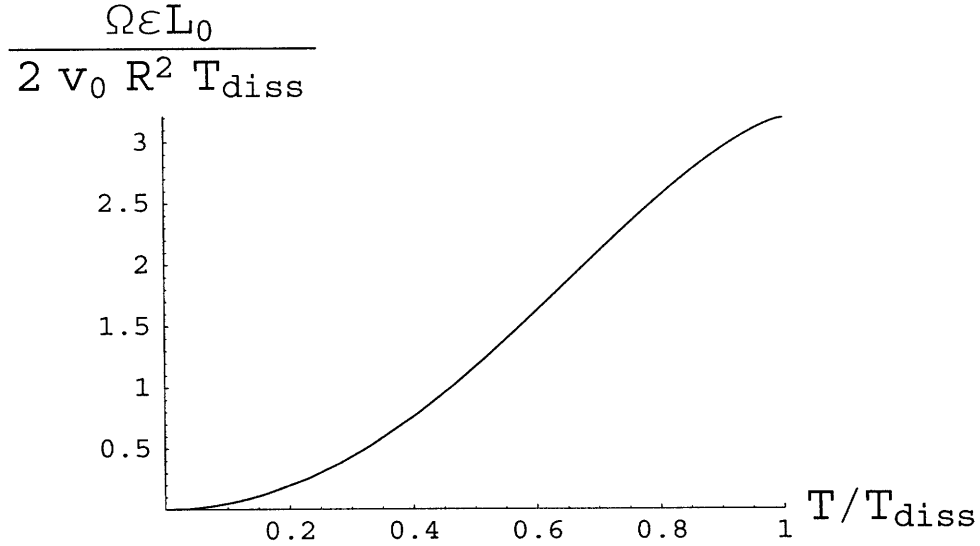
$$\frac{\Omega \varepsilon L_0}{2\, v_0\, R^2\, T_{\rm diss}}$$

Figure 2-11: The k-independent spacing $\Omega \varepsilon L_0 / 2 v_0 R^2$ between the dispersion relations for any two mesons whose n quantum numbers differ by 1, in units of $T_{\rm diss}$. See (2.124).

are the same for mesons ψ_1 and ψ_2 and are independent of ℓ. These degeneracies are broken at order $\mathcal{O}(1/k)$, where $d_{sn\ell}$ first appears. We find that the coefficient of $1/k$ in $\omega(k)$ of (2.123) is typically negative: it is negative at all $\varepsilon < 1$ if $\ell = 0$ for any n; it can become positive only if ε, n and ℓ are all large enough. When this coefficient is negative, it means that $\omega(k)$ approaches its large-k asymptotic behavior (which is a straight line with slope v_0 offset by the constant term in (2.123)) from below. This means that $d^2\omega/dk^2 < 0$ at large k and means that the group velocity $v = d\omega/dk$ approaches v_0 from above at large k, as shown in Fig. 2-9. However, at $k = 0$ the group velocity vanishes and $d^2\omega/dk^2 > 0$. (We have shown this analytically at small ε in Section 5.1, see (2.82), and our numerical results as in Section 5.3 indicate that this is so at all ε.) So, as a function of increasing k, the group velocity begins at zero, increases to some maximum value that is greater than v_0, and then decreases to v_0 as $k \to \infty$ as depicted in Fig. 2-9.[7] Although v_0 is not the maximum possible group velocity, it appears that the maximal velocity exceeds v_0 only by a small margin. For

---

[7]This behavior is not inconsistent with our identification of v_0 with the local speed of light at the tip of the brane: it is only for $k \to \infty$ that the meson wave function is squeezed down to the tip of the brane; at finite k, the wave function is peaked where the local speed of light exceeds v_0.
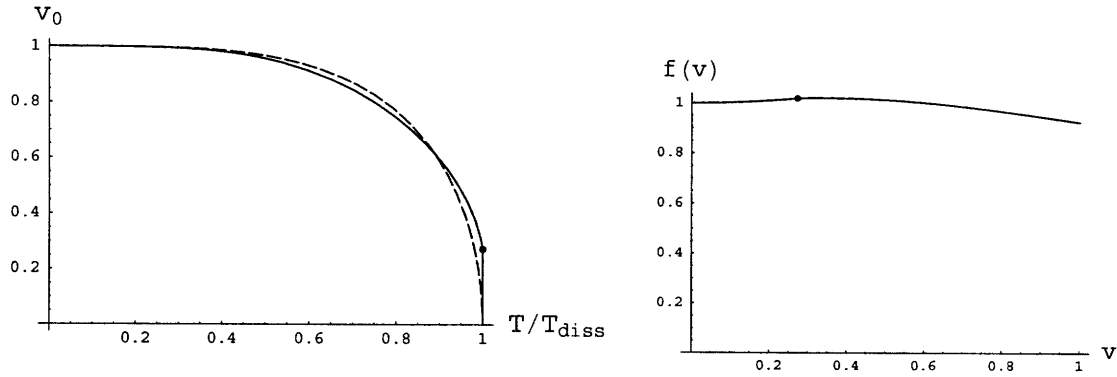
Figure 2-12: Left panel: The solid curve is the limiting velocity v_0 as a function of T/T_{diss}, where T_{diss} is the temperature of the dissociation transition at zero velocity. The dissociation transition occurs at the dot, where $v_0 \approx 0.273$. The dashed curve is the approximation obtained by setting $f(v) = 1$ in (2.125). Right panel: $f(v)$, the ratio of the solid and dashed curves in the left panel at a given v. We see that $f(v)$ is within a few percent of 1 at all velocities.

example, for the ground state ψ_1 meson whose dispersion relations are given in Figs. 2-8 and 2-9, we find that $v_0 = 0.882$, 0.6, and 0.273 for $\varepsilon = 0.25$, 0.5, and 0.756 whereas the maximal velocities are 0.896, 0.634 and 0.342, respectively. We shall therefore simplify the following discussion by taking the maximal possible meson velocity at a given temperature to be the limiting velocity v_0, neglecting the slight imprecision that this introduces.

We now wish to compare our results for the limiting meson velocity v_0 at a given temperature to the result (2.7) inferred (qualitatively) from the analysis of screening in a hot wind in [11]. We must first convert $v_0(\varepsilon)$ into $v_0(T)$, meaning that we must convert from ε to ϵ_∞ as discussed in and around Fig. 2-2. The result is the solid curve in the left panel of Fig. 2-12, where we have plotted v_0 versus T/T_{diss}. We have derived this curve as a limiting meson velocity at a given temperature. However, it can just as well be read (by asking where it cuts horizontal lines rather than vertical ones) as giving $T_{\text{diss}}(v)$, the temperature below which mesons with a given velocity v are found and above which no mesons with that velocity exist. We see that $T_{\text{diss}}(v) \to 0$ for $v \to 1$, the regime where v_0 is given by (2.122) and $T_{\text{diss}}(v)$ is therefore given by (2.9). In order to compare our result for $T_{\text{diss}}(v)$ at all velocities to (2.7), we parameterize

our result as

$$T_{\text{diss}}(v) = f(v)(1 - v^2)^{1/4} T_{\text{diss}}(0) \ . \tag{2.125}$$

In the left panel of Fig. 2-12 we compare our result (the solid curve) to (2.125) with $f(v)$ set to 1, which is of course (2.7). In the right panel, we plot $f(v)$. We see that this function is close to 1 at all velocities, varying between 1.021 at its maximum and 0.924 at $v = 1$. The weakness of the dependence of $f(v)$ on v is a measure of the robustness with which the simple scaling (2.7) describes our result for the meson dissociation temperature at all velocities.

2.6   Discussion and Open Questions

We have used the AdS/CFT correspondence to compute the dispersion relation $\omega(k)$ for the heavy "quarkonium" mesons that exist as stable bound states in the strongly coupled plasma of $\mathcal{N} = 4$ SYM to which heavy fundamental quarks with mass m_q have been added. In Section 4 we have introduced a new, and more geometrical, method of analyzing these mesons that has allowed us, in Section 5, to obtain the dispersion relations at large-k analytically in the form (2.123), which we can summarize as in Section 1 by writing

$$\omega(k) = v_0 k + a + \frac{b}{k} + \dots \ . \tag{2.126}$$

We have computed a and b explicitly and analytically in Section 5, but at present we have no argument that the behavior of these coefficients, which depend on the meson quantum numbers, could teach us lessons that generalize beyond the particular theory in which we have computed them. On the other hand, the limiting large-k meson velocity v_0 seems to encode much physics that may generalize to meson bound states in other strongly coupled gauge theory plasmas.

- Our explicit result is

$$v_0 = \frac{1 - \varepsilon^2}{1 + \varepsilon^2} \ , \tag{2.127}$$

where ε is related to $\epsilon_\infty = \lambda T^2/(8m_q^2)$ as in Fig. 2-2. We see that v_0 depends

92

on the temperature (in the combination $\sqrt{\lambda}T/m_q$) but not on the meson quantum numbers. We see in Figs. 2-8 and 2-9 that v_0 decreases with increasing temperature, becoming much less than 1 as the temperature approaches T_{diss}, the temperature at which mesons at rest dissociate. We see in these figures that the coefficient b in (2.126) can be negative, meaning that the group velocity approaches its large-k value v_0 from above. Thus, v_0 is the limiting meson velocity at large k, but the maximal velocity occurs at finite k and is slightly larger than v_0. We describe this quantitatively in Section 5, but it is a small effect and in this discussion we shall ignore the distinction between v_0 and the maximal velocity.

- We find that v_0, which in the gauge theory is the limiting velocity of the mesons that they attain at large k, also has a nice interpretation in the dual gravity theory. It is precisely the local velocity of light at the "tip" of the D7-brane, namely where the D7-brane reaches closest to the black hole. This is physically sensible because we have shown that the D7-brane fluctuations — i.e. the mesons in the dual gravity theory — are localized at the D7-brane tip in the large-k limit.

- At low temperatures or, equivalently, for heavy quarks we find

$$v_0 \approx 1 - \frac{\lambda^2 T^4}{32 m_q^4} \, . \tag{2.128}$$

This is precisely, i.e. even including the numerical factor, the criterion for meson dissociation inferred from a completely different starting point in [11]. The logic there was that the screening length that characterizes the potential between a quark and antiquark moving with $v > v_0$ is shorter than the quark Compton wavelength, meaning that if a quark and antiquark moving with $v > v_0$ are separated by more than a Compton wavelength, to leading order in $\sqrt{\lambda}$ they feel no attractive force. By inference, no mesons should exist with $v > v_0$. We now see this result emerging by direct calculation of meson dispersion relations,

rather than by inference.

- We have a result for $v_0(T)$, the limiting velocity beyond which there are no meson bound states, at all $T < T_{\text{diss}}$ not just at low temperatures, see Fig. 2-12. We can just as well read this as determining a temperature $T_{\text{diss}}(v)$ above which no meson bound states with velocity v exist. We find that up to few percent corrections, see Fig. 2-12, this is given by

$$T_{\text{diss}}(v) = (1 - v^2)^{1/4}T_{\text{diss}} \ . \tag{2.129}$$

Once again, this is a result that was previously inferred from analysis of the velocity dependence of the screening length characterizing the potential between a quark and antiquark moving through the plasma [10]. We have now derived this result and the (few percent) corrections to it for the mesons whose dispersion relations we have explicitly constructed. We should also note that it is a slight abuse of terminology to call $T_{\text{diss}}(v)$ at $v > 0$ a "dissociation" temperature: although it *is* a temperature above which no mesons with velocity v exist, if we imagine heating the plasma through $T_{\text{diss}}(v)$ we have not shown that any mesons present therein dissociate — they may simply slow down. The question of what happens in this hypothetical context is a dynamical one that cannot be answered just from the dispersion relations we have analyzed.

- As we discussed in Section 2, the result (2.129) can be read as saying that no mesons with velocity v exist when the energy density of the strongly coupled plasma exceeds $\rho_{\text{diss}}(v)$ where, up to small corrections,

$$\rho_{\text{diss}}(v) = (1 - v^2)\rho_{\text{diss}} \ , \tag{2.130}$$

with ρ_{diss} the energy density at which mesons at rest dissociate. Correspondingly, the low temperature result (2.128) can be written as

$$1 - v_0 = \text{constant}\frac{\rho}{\rho_{\text{diss}}} \ , \tag{2.131}$$

94

valid when $\rho \ll \rho_{\text{diss}}$ and v_0 is close to 1. Thinking as in [34], we can ask whether the same result holds in other theories. It will be interesting to address this question in $(3 + 1)$-dimensional gauge theories that are in various senses more QCD-like than $\mathcal{N} = 4$ SYM. At present, however, we have only investigated the $(p + 1)$-dimensional gauge theories described by N Dp-branes [110] into which fundamental quarks, and hence mesons, have been introduced by embedding a Dq-brane [111, 105, 36, 37]. The Dp-branes fill coordinates $0, 1, \ldots, p$. The Dq-brane fills the first $d+1$ of these coordinates $0, 1, \ldots, d$, where d may be less than or equal to p, as well as $q - d$ of the remaining $9 - p$ coordinates. In Appendix B, we sketch an investigation of those theories for which $p - d + q - d = 4$. (The case that we have analyzed throughout the rest of this chapter is $p = d = 3$, $q = 7$.) These theories are not conformal for $p \neq 3$, as their coupling constant λ has dimension $p - 3$. It is convenient to introduce a dimensionless $\lambda_{\text{eff}} \equiv \lambda T^{p-3}$. We have not repeated our entire construction for the Dp-Dq-brane theories. However, we expect that the wave functions for large-k mesons will again be localized at the tip of the Dq-brane, and therefore expect that in these theories v_0 will again be given by the local velocity of light at this location. We compute this velocity in Appendix B. Assuming that this is indeed the limiting meson velocity, we find

$$v_0 = \left(\frac{1 - \varepsilon^{(7-p)/2}}{1 + \varepsilon^{(7-p)/2}} \right) , \qquad (2.132)$$

where ε is given at small T/m_q by

$$\varepsilon \approx \epsilon_\infty \propto \left(\frac{T}{m_q} \right)^2 \lambda_{\text{eff}}^{2/(5-p)} = \frac{\lambda^{2/(5-p)} T^{4/(5-p)}}{m_q^2} . \qquad (2.133)$$

(Relating ε to ϵ_∞ beyond the small T/m_q limit requires solving the embedding equation given in Appendix B.) In these theories, the energy density of the plasma depends on parameters according to [110]

$$\rho \propto N^2 T^{p+1} \lambda_{\text{eff}}^{(p-3)/(5-p)} = N^2 \lambda^{(p-3)/(5-p)} T^{(14-2p)/(5-p)} , \qquad (2.134)$$

95

and zero-velocity mesons dissociate at some energy density ρ_{diss} corresponding to $\varepsilon = \varepsilon_{\text{diss}}$ where $\varepsilon_{\text{diss}} = \mathcal{O}(1)$. From these results we notice that at small ε

$$\varepsilon^{(7-p)/2} \propto \frac{\lambda^{(7-p)/(5-p)} T^{(14-2p)/(5-p)}}{m_q^{7-p}} \propto \frac{\rho}{\rho_{\text{diss}}} \ , \tag{2.135}$$

meaning that the velocity v_0 of (2.132) can be written in the form (2.131) for all values of p! In Appendix B, we describe the verification that (2.129) also holds, but only when phrased as in (2.130) in terms of energy density rather than temperature.

Emboldened by these successes, we advocate investigating the consequences that follow from hypothesizing that Υ and J/Ψ mesons in the strongly coupled quark-gluon plasma of QCD propagate with a dispersion relation (2.126) with v_0 dropping dramatically as the temperature approaches T_{diss} from below, and with no bound states with velocity v possible if $T > T_{\text{diss}}(v)$ given by (2.129). In applying (2.129) to QCD, it is important to scale $T_{\text{diss}}(v)$ relative to the T_{diss} for Υ and J/Ψ mesons in QCD itself. The result $T_{\text{diss}} = 2.166 m_q/\sqrt{\lambda}$ for the mesons that we have analyzed is surely affected by the fact that they are deeply bound and so should not be used as a guide to quarkonia in QCD. For example, it seems to overestimate T_{diss} for J/Ψ mesons by a factor of 2 or 3. However, as argued in [10, 11] and as we have discussed above, the velocity scaling (2.129) may transcend the detailed meson physics in any one theory and apply to mesonic bound states in any strongly coupled plasma. The successful comparison of our detailed results to this simple scaling form supports this conjecture.

As we have explained at length in Section 1, meson propagation is only one piece of the physics that must be treated in order to understand quarkonium suppression in heavy ion collisions. Introducing the dispersion relation and limiting velocity that we have found into such a treatment is something we leave to the future, instead making only a few qualitative remarks.

First, from the dispersion relations alone we *cannot* conclude that if a quark-antiquark pair is produced (from an initial hard scattering) with a velocity $v > v_0(T)$,

with $v_0(T)$ the limiting meson velocity in the plasma of temperature T in which the quark-antiquark pair finds itself, then the quark-antiquark pair do not bind into a meson. The reason that we cannot make this inference is that the dispersion relations describe stable mesons with arbitrarily large momentum k, making it a logical possibility that a high velocity quark-antiquark pair with arbitrarily high momentum interacts with the medium in some way such as to slow down and lose energy while conserving its momentum, and thus in some way dresses itself into a meson with arbitrarily high momentum k, and velocity v_0. That is, since the dispersion relations describe the propagation of mesons with arbitrarily large momentum, by themselves they do not require that quarkonium production is suppressed when the precursor quark-antiquark pair has velocity $v > v_0(T)$. Excluding this possibility, allowed by the kinematics, requires some consideration of the dynamics. The heuristic argument of [11] provides guidance: the precursor quark-antiquark pair with $v > v_0(T)$ do not attract each other and so even though it is kinematically allowed by the meson dispersion relations for them to slow down and form a meson, instead they will propagate independently through the medium. Thus, the p_T-dependent quarkonium suppression pattern proposed in [10], with the production of quarkonium states with T_{diss} higher than the temperature reached in a given heavy ion collision experiment nevertheless becoming suppressed above a threshold transverse momentum at which a quark-antiquark pair with that transverse momentum has velocity $v_0(T)$, rests upon the dynamical argument of [11]. It is natural that analyzing quarkonium suppression requires consideration of both the precursor quark-antiquark pair and the putative meson, and only the latter is described by the meson dispersion relation. It is then nice to discover that the limiting meson velocity $v_0(T)$ agrees precisely with the velocity at which quark-antiquark pairs can no longer feel a force at order $\sqrt{\lambda}$.

The argument of the previous paragraph is rather heuristic, and would be hard to confirm directly from a string theory calculation. Indeed it would be quite disappointing if the weakened interactions between quark-antiquark pairs at high velocity did not directly imprint itself on the meson bound states studied in this chapter. In Chapter 3 we will fix this discrepancy, and in so doing strengthen the argument

above. This will be done by first finding a mechanism for these mesons to decay and then studying the *momentum* dependence of the resulting widths. As we have mentioned the mesons we have analyzed at $T < T_{\mathrm{diss}}$ are stable, with zero width. The dispersion relations that we have found have no imaginary part. This is certainly an artifact of the large number of colors N and large coupling λ limits that we have taken throughout. Processes in which one meson decays into two mesons are suppressed by $1/N$. And, thermal fluctuations which unbind a meson whose binding energy is $2m_q$ are suppressed by the Boltzmann factor

$$\exp(-2m_q/T) = \exp(-0.92\sqrt{\lambda}T_{\mathrm{diss}}/T) \,, \qquad (2.136)$$

which at some fixed T/T_{diss} is nonperturbative in an expansion about infinite λ. In Chapter 3 we will show how to calculate such a contribution to the widths, we will be particularly interested in the momentum dependence of the widths.

We will find that as the meson approaches its limiting velocity $v_0(T)$ its width grows quadratically with momentum. We will see that this growth is related to the existence of a limiting velocity. So in hindsight it is not necessary to make dynamical arguments about the formation of a meson from a quark-antiquark pair in order to predict increased suppression at high p_T, however such dynamical considerations are still important and may lead to further suppression. It is pleasing to note that both suppression mechanisms have a related origin.

We have just argued that the very large-k region of the meson dispersion relation is unlikely to be populated in heavy ion collisions. But, whether or not such large-k modes are excited, it is clear from Fig. 2-8 that at temperatures near to T_{diss} mesons at any k move much more slowly than they would if they propagated with their vacuum dispersion relation. There are several in-principle-observable signatures of the slow velocity of quarkonium mesons. First, it increases the separation in space long after the collision between those mesons that are produced at the surface of the fireball moving outwards, and hence escape into vacuum promptly, and those which are produced in the center of the plasma and hence move more slowly than if they had

their vacuum dispersion relation. An increase in the typical separation of identical mesons because of this slow velocity effect will shift the onset of Bose-Einstein enhancement in the two particle momentum correlation to a lower relative momentum. This simple idea underlies a technique widely used in heavy ion physics and often referred to as Hanbury-Brown Twiss (HBT) two-particle interferometry, in which identical two-particle momentum correlations are used to determine spatio-temporal characteristics of the collision region. For a review, see Ref. [112]. Quarkonium HBT interferometry would thus in principle be able to find signatures of a depressed meson velocity. Second, non-identical two-particle correlation functions are sensitive to whether one particle species A is emitted from the medium on average before or after another particle species B. Such a difference in average emission times could result, for instance, if the maximal velocities in the dispersion relations for A and B differ because of their different mass. The analysis of the effect of a difference in average emission times on non-identical two-particle correlation functions can be found in [113]. In principle, this provides a second way of finding signatures of a depressed velocity for those mesons for which the plasma reaches temperatures close to their dissociation temperature.

Of course for mesons with a nonzero width, their slow velocity has a further consequence in the context of heavy ion collisions: because they move more slowly, they spend a longer time in the medium giving the absorptive imaginary part more time to effect the dissociation of the meson than would otherwise be the case.

Our discussion in this Section has highlighted different avenues of further investigation opened up by our analysis of meson dispersion relations in a strongly coupled gauge theory plasma. The first is the investigation of the phenomenological consequences for J/Ψ and Υ suppression in heavy ion collisions of a dispersion relation of the form (2.126) with (2.129). Second, we could gain significant confidence in the application of the lessons we have learned to QCD by repeating our analysis for heavy quark mesons in the plasma of other strongly coupled gauge theories, in particular those with a controlled degree of nonconformality.

Finally as emphasized here in the next Chapter of this thesis we will answer some questions/speculations raised here by studying the width of the mesons in this system at finite λ. Most importantly we will demonstrate that their lifetime becomes smaller at larger momentum consistent with the discussion of this section.

Chapter 3

Properties of mesons II - width

3.1 Introduction

A heavy quarkonium bound state, like J/ψ or Υ, which finds itself in the quark-gluon plasma (QGP), becomes increasingly unstable and eventually dissociates at sufficiently high temperatures. On the one hand this can be attributed to the weakening attraction between a heavy quark and anti-quark in the bound state due to color screening of the medium [14]. On the other hand the bound state can be broken up from collisions with the deconfined quarks and gluons in the medium [90]. Given that the QGP at RHIC and LHC is likely strongly coupled, understanding such medium effects on the propagation and dissociation of heavy quarkonia presents nontrivial theoretical challenges which must be confronted in order to interpret experimental data on quarkonium suppression.

Interesting insights have recently been made into this problem from strongly coupled model gauge theories using the AdS/CFT correspondence. AdS/CFT-based methods are powerful at attacking questions of dynamical origin, such as how the motion of quarkonia relative to the medium affects their various properties. The simplest example of the correspondence is provided by the duality between $\mathcal{N} = 4$ $SU(N_c)$ super Yang-Mills (SYM) theory and string theory in $AdS_5 \times S_5$ [18, 19, 20, 21]. As described in Chapter 1, based on a calculation of the potential between a pair of heavy external quark and antiquark moving in the strongly coupled hot $\mathcal{N} = 4$ plasma,

it has been argued in [10, 11] (see also [12, 13]) that the dissociation temperature T_{diss} of a heavy quarkonium *decreases* with their velocity v relative to the medium as $T_{\text{diss}}(v) \approx (1 - v^2)^{\frac{1}{4}} T_{\text{diss}}(v = 0)$. Such a velocity scaling, which can be heuristically understood as due to increased screening from the boosted medium, could provide a significant additional source of quarkonium suppression at nonzero transverse momentum in heavy ion collisions [10, 11].

Rather than drawing inferences from the heavy quark potential, it is also possible to directly study the propagation of mesons in a strongly coupled plasma. While $\mathcal{N} = 4$ SYM theory itself does not contain dynamical mesons, one can obtain a closely related theory which does contain mesons by adding to it $N_f \ll N_c$ fundamental "quarks", which corresponds to adding some D7-branes to $AdS_5 \times S_5$ in the gravity picture [100]. We saw in Chapter 2 that meson dispersion relations are dramatically modified by the plasma and in particular, there exists a limiting velocity $v_c(T) < 1$, which decreases with increasing temperature. The existence of a subluminal limiting velocity is consistent with the velocity-enhanced screening obtained from the heavy quark potential, as when $v > v_c(T)$ the quark and anti-quark are completely screened and no bound states are possible.

For a more complete understanding of the dissociation of mesons one needs to study their widths. We will be particularly interested in the momentum dependence of the widths. This has not been possible within the classical gravity approximation developed so far. In this approximation, the mesons are stable (i.e. they have zero width) for T smaller than a dissociation temperature T_{diss}, but completely disappear for $T > T_{\text{diss}}$ [101, 43, 102, 38, 37]. The approximation also has another important drawback: the densities of quarks and antiquarks are identically zero for a range of temperatures and chemical potentials [42] even though they should obey the standard thermal distribution.

In this chapter, we discuss a novel tunneling effect on the string worldsheet which gives rise to nonzero quark densities and meson widths for $T < T_{\text{diss}}$. This enables us to calculate explicitly the momentum dependence of the width of a meson in a strongly coupled QGP. We find that the width increases quadratically with momentum at large

momentum. These non-perturbative effects also have important implications for the phase structure of the theory obtained in the classical gravity limit.

3.2 Setup

Recall that at finite temperature, $\mathcal{N} = 4$ SYM theory can be described by a string theory in the spacetime of a black hole in AdS$_5 \times S_5$, whose metric can be written as

$$ds^2 = -fdt^2 + \frac{1}{f}dr^2 + \frac{r^2}{R^2}d\vec{x}^2 + R^2 d\Omega_5^2 \tag{3.1}$$

where $f = \frac{r^2}{R^2}\left(1 - \frac{r_0^4}{r^4}\right)$, $\vec{x} = (x_1, x_2, x_3)$. $d\Omega_5^2$ is the metric on a unit five-sphere S_5 which can be written as

$$d\Omega_5^2 = d\theta^2 + \sin^2\theta d\Omega_3^2 + \cos^2\theta d\phi^2, \quad \theta \in \left[0, \frac{\pi}{2}\right] \tag{3.2}$$

with $d\Omega_3^2$ the metric for a three-sphere S_3. The string coupling g_s is related to the Yang-Mills coupling g_{YM} by $g_s = 4\pi g_{YM}^2$ and the curvature radius R is related to the 't Hooft coupling $\lambda = g_{YM}^2 N_c$ by $\frac{R^2}{\alpha'} = \sqrt{\lambda}$. The perturbative g_s and α' expansions in the bulk string theory are related to the $1/N_c$ and $\frac{1}{\sqrt{\lambda}}$ expansions in the Yang-Mills theory respectively. The temperature T of the YM theory is given by the Hawking temperature of the black hole, $T = \frac{r_0}{\pi R^2}$. Adding N_f fundamental "quarks" can be described in the dual string theory by adding N_f D7-branes in (3.1) [100]. A fundamental "quark" in the YM theory can be described by an open string with one end on the D7-branes and the other end on the black hole. Open strings with both ends on the D7-branes can be considered as "bound states" of a quark and antiquark, thus describing meson-type excitations in the YM theory.

We now briefly outline the standard procedure for obtaining the meson spectrum [101, 43, 102], which was obtained in more detail in the previous chapter. We will take $N_f = 1$, $N_c \to \infty$, and λ large but finite throughout the chapter. The D7-brane can be chosen to lie along the directions $\xi^\alpha = (t, \vec{x}, \Omega_3, \theta)$ and using the symmetries of the problem the embedding in the two remaining transverse directions
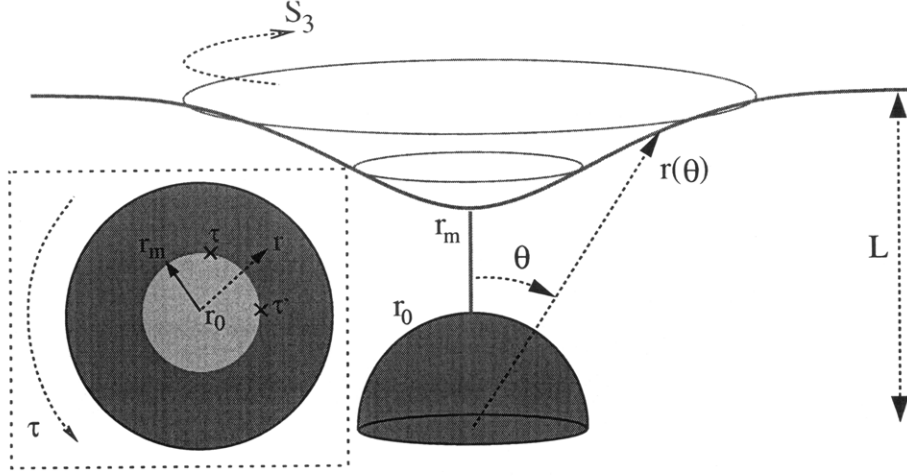
Figure 3-1: An embedding of the D7 brane (green) in the $AdS_5 \times S_5$ black hole geometry for $T < T_{\text{diss}}$ which lies entirely outside the black hole. Inset: the Euclidean $r - \tau$ plane at $\theta = 0$ showing a world-sheet instanton (red) connecting the tip of D7 brane $r = r_m$ to the horizon at the center of the disk $r = r_0$.

can be taken as $\phi(\xi^\alpha) = 0$ and $r(\xi^\alpha) = r(\theta)$. At the lowest order in the α' expansion, $r(\theta)$ can be determined by extremizing the Dirac-Born-Infeld (DBI) action of the D7-brane with the boundary condition $r(\theta) \cos \theta|_{\theta \to \frac{\pi}{2}} \to L$, where L is related to the mass m_q of a quark in the Yang-Mills theory as $m_q = \frac{L}{2\pi\alpha'}$. For T smaller than some T_{diss}, $r(\theta)$ has the form shown in Fig. 3-1. The brane is closest to the black hole at $\theta = 0$, where there lies a 4-dimensional subspace spanned by $(t, \vec{x})$ since here the S_3 in (3.2) shrinks to a point. Denoting $r_m \equiv r(\theta = 0) > r_0$, the shortest open string connecting the D7-brane to the horizon has a mass in the YM theory

$$m_q^{(T)} = \frac{r_m - r_0}{2\pi\alpha'} = \sqrt{\lambda} T \frac{\Lambda_m - 1}{2}, \qquad \Lambda_m = \frac{r_m}{r_0} \tag{3.3}$$

Note that Λ_m is a dimensionless number of $O(\lambda^0)$ determined by the ratio L/r_0, and $m_q^{(T)}$ can be interpreted as the effective mass of a quark at temperature T.

The mesons corresponding to massless fluctuations on the D7-brane can be found by solving the linearized equations resulting from expanding the DBI action around the embedding. For example, the quadratic action for the fluctuation $\chi^\phi(\xi^\alpha)$ of the

location of D7-brane in the ϕ direction can be written as

$$S_{DBI}[\chi^\phi] = -\frac{\mu_7}{2} \int d^8\xi \sqrt{-g}\, G_{\phi\phi}\, g^{\alpha\beta} \partial_\alpha \chi^\phi \partial_\beta \chi^\phi \qquad (3.4)$$

where $\mu_7 = \frac{1}{(2\pi)^7 g_s \alpha'^4}$ is the tension of the D7-brane, $G_{\phi\phi} = R^2 \cos^2\theta$, and $g_{\alpha\beta}$ denotes the induced metric on the D7-brane. Writing $\chi^\phi = e^{-i\omega t + i\vec{k}\cdot\vec{x}} Y_l(\Omega_3)\psi(\theta)$, the equation of motion for ψ can be written as

$$\hat{H}(\vec{k},l)\psi(\theta) = \omega^2 \psi(\theta) \qquad (3.5)$$

where $\hat{H}(\vec{k},l)$ is a second order differential operator in θ and Y_l are spherical harmonics on the S_3. For a given $\vec{k}, l$, $\hat{H}(\vec{k},l)$ has only discrete eigenvalues ω_n^2 labeled by an integer n, giving rise to dispersion relations $\omega = \omega_n(\vec{k},l)$, all of which have zero width. In particular, the meson masses are of order $M = \frac{2\sqrt{2}L}{R^2} = \frac{4\sqrt{2}\pi m_q}{\sqrt{\lambda}}$. Since M is parametrically smaller than m_q in $\sqrt{\lambda}$, the mesons have a large binding energy, given by $2m_q^{(T)}$. There exists a temperature $T_{\text{diss}} = 0.122M$, beyond which the D7 brane falls into the black hole and mesons cease to exist as well-defined quasi-particles [38, 37].

We stress that the zero-width conclusion only depends on the topology of the embedding in Fig. 3-1. Since mesons can only dissociate by falling into the black hole, when the D7-brane lies above the black hole horizon the mesons are necessarily stable. Given that the brane embedding and the background geometry are smooth, including higher order perturbative corrections in α' should not change the topology of the brane embedding if the distance between the brane and the horizon is parametrically larger than the string scale. This implies that the widths of mesons should remain zero to all orders in the perturbative $\frac{1}{\sqrt{\lambda}}$ expansion.

One can also turn on a quark chemical potential $\mu < m_q^{(T)}$ in the boundary theory by setting $A_t = \mu$, where A_t is the time component of the gauge field on the D7-brane [42, 41, 40, 125]. Since the DBI action and its higher order α' corrections contain only derivatives of A_t, the D7-embedding and the meson spectrum are not modified by turning on the constant mode of A_t. Thus, the meson widths and the net quark density remain zero to all orders in the α' expansion even at a finite chemical

potential [1].

The above conclusions can be further illuminated by simple thermodynamic reasoning. From (3.3), $\beta m_q^{(T)} \propto \sqrt{\lambda}$, the quark (or anti-quark) density, being proportional to $e^{-\beta m_q^{(T)} \pm \beta \mu}$, is then exponentially suppressed in $\sqrt{\lambda}$ for $\mu < m_q^{(T)}$. Similarly, since the binding energy E_{BE} of a meson is $2m_q^{(T)}$, thermal effects which destabilize the mesons are also exponentially suppressed in $\sqrt{\lambda}$. Thus the meson widths and quark densities are not visible in the perturbative expansion in $1/\sqrt{\lambda}$ and can only have non-perturbative origins on the worldsheet.

There are indeed non-perturbative corrections in α' which effectively change the topology of the D7-brane embedding and generate non-vanishing meson widths and quark densities. To see this it is more convenient to analytically continue (3.1) to Euclidean signature with $t \rightarrow -i\tau$. Then the $r - \tau$ plane has the topology of a disk. The angular direction τ has a period given by the inverse temperature β. The center of the disk is located at $r = r_0$. Open strings on the D7-brane are described by worldsheets with the topology of a disk whose boundary lies on the D7-brane. Denoting the worldsheet coordinates as $\rho \in [0, 1]$ and $\sigma \in [0, 2\pi)$, the worldsheets separate into different topological sectors corresponding to the winding number m of the target space disk (r, τ) wrapping around the worldsheet disk (ρ, σ). The DBI action arises from the sector of trivial winding number $m = 0$, in which (ρ, σ) is mapped to a single point on the D7-brane. In all the other (nontrivial) sectors, the string worldsheet is mapped to the region in the $r - \tau$ plane from the location of the D7-brane all the way to the horizon $r = r_0$ (see inset of Fig. 3-1). When analytically continued back to the Lorentzian signature, such a worldsheet describes a tunneling process in which a tiny neck is generated between the D7-brane and the black hole horizon. As a result mesons can leak through the tiny neck into the black hole and dissociate.

---

[1] Above $\mu > m_q^{(T)}$ a new phase, where the D7 brane falls into the horizon, is thermodynamically preferred. This phase exhibits both meson widths and finite quark density [127, 126, 41, 42].

3.3 Calculation of the width

As an illustration, we now calculate the contributions from $m = \pm 1$ sectors to the quark density and the widths of mesons in (3.4). We will only be interested in the lowest order term in the α' expansion. The relevant spacetime effective action for the D7-brane can be obtained from the worldsheet path integral [129]

$$S_E[\chi^\phi] = \int_{\text{disk}} DX \, e^{-I[X] + \oint_{\rho=1} d\sigma \, \mu \frac{d\tau}{d\sigma} - I_B[\chi^\phi]} \tag{3.6}$$

where $X = (\xi_\alpha, r, \phi)$ denotes collectively the worldsheet fields. $I[X]$ is the worldsheet action, which for our purpose can be taken to be the Nambu-Goto action for a string propagating in (3.1)

$$I[X] = \frac{1}{2\pi\alpha'} \int d\sigma d\rho \sqrt{\det h_{ab}} \tag{3.7}$$

with $h_{ab} = G_{MN} \partial_a X^M \partial_b X^N$ the induced metric on the worldsheet and G_{MN} the Euclidean version of the metric (3.1). The second term in the exponential of (3.6) corresponds to turning on $A_\tau = -i\mu$ which gives in the Euclidean theory a nonzero (quark) chemical potential μ in the boundary YM theory. $I_B[\chi^\phi] = \oint_{\rho=1} d\sigma \, \frac{R^2}{2\pi\alpha'} \chi^\phi \partial_\rho \phi$ is the boundary action which couples the worldsheet to $\chi^\phi(\xi_\alpha)$. We have suppressed any dependence on spacetime and world sheet fermions. The integral (3.6) can be evaluated using the saddle point approximation in each topological sector [130, 131], i.e. $S_E = S_{m=0} + S_{m=+1} + S_{m=-1} + \cdots$ with $S_{m=0} = S_{DBI}$.

For $m = \pm 1$, (3.7) has a classical solution given by

$$\tau = \pm \frac{\beta}{2\pi} \sigma, \quad r = \hat{r}(\rho), \quad \theta = 0, \quad \phi = 0, \quad \vec{x} = \vec{x}_0 \tag{3.8}$$

where $\vec{x}_0$ is an arbitrary constant position vector and $\hat{r}(\rho)$ is chosen so that $\hat{r}(1) = r_m$ and $f d\tau^2 + \frac{1}{f} d\hat{r}^2 \propto d\rho^2 + \rho^2 d\sigma^2$. Eq. (3.8) represents the worldsheet of a string connecting the tip of the brane to the horizon with the $\pm$ sign corresponding to opposite orientations. It has a classical action $I_\pm = \beta m_q^{(T)}$ where $m_q^{(T)}$ is the effective quark mass introduced in (3.3). One can readily verify that (3.8) minimizes the action and satisfies the right boundary conditions at the D7-brane. Note that there are only

three bosonic zero modes in (3.8) [2], since it costs energy to move away from $\theta = 0$ and the worldsheet time σ now coincides with τ. With χ^ϕ set to zero, Eq. (3.6) then yields

$$S_{m\pm 1} = e^{-\beta m_q^{(T)}} e^{\pm \mu \beta} \frac{1}{g_s} DV_3 = -n_\pm V_3 \tag{3.9}$$

where the $e^{\pm \mu \beta}$ arises from the second term in the exponential of (3.6), V_3 is the spatial volume from integrating over the three zero modes in (3.8), and the $\frac{1}{g_s}$ factor arises because we are evaluating the disk path integral. D is a real number coming from Gaussian integration around the saddle point (3.8) (including worldsheet fermions) whose sign we will fix from physical requirements. Identifying the Euclidean action with $\beta F(\beta, \mu)$ where $F(\beta, \mu)$ is the free energy, equation (3.9) leads to a net quark *charge* density $-\frac{2D}{g_s} e^{-\beta m_q^{(T)}} \sinh \beta \mu$, which in turn requires that D should be *negative* [3]. It is natural to interpret $S_{m=\pm 1}$ as the contributions from quarks and anti-quarks separately leading to a quark and antiquark *number* density given by $n_\pm = e^{-\beta m_q^{(T)}} e^{\pm \mu \beta} \frac{1}{g_s} (-D)$ from which we obtain the second equality in (3.9). Note that $n_\pm \propto 1/g_s \propto N_c$ since quarks come in an N_c-multiplet.

In our derivation of (3.9) we have assumed the embedding of the D7-brane is given by that determined by the DBI action. This is justified for $\mu < m_q^{(T)}$ since the correction to the DBI action is exponentially small. When $\mu \geq m_q^{(T)}$, the backreactions from instantons become large and the embedding of Fig. 3-1 cannot be trusted.

The nonzero quark densities for nonzero $\mu < m_q^{(T)}$ have important implications for the phase structure of the theory. As discussed in [42] (see also [41]) based on the analysis of the DBI action (which corresponds to $\lambda = \infty$), at low temperature there is a phase transition in chemical potential at which the net quark charge density jumps from zero to a nonzero value. Our results strongly indicate this phase transition is smoothed to a crossover at any finite value of λ.

To find the widths of the mesons described by (3.4), we need to compute (3.6) to

---

[2] In contrast, the $n = 0$ sector has eight zero modes corresponding to all directions on the D7-brane. There are also no fermionic zero modes here.

[3] There are a few other indications that D should be negative. The instanton action also induces a tadpole for the r component of the transverse fluctuations. One finds for D negative the tadpole pulls the brane toward the horizon as required by physical consistency. Also only for D negative, do the meson widths we calculated below have the correct sign.

quadratic order in χ^ϕ. For simplicity, we will restrict to the $l = 0$ mode on the S_3. Near $\theta = 0$, the worldsheet action for ϕ is given by $\frac{R^2}{4\pi\alpha'} \int d\rho d\sigma \, (\partial\phi)^2$, which is free. The path integral is then straightforward to compute and yields for $S_{m=\pm1}$

$$-\frac{R^2 n_\pm}{2\pi\alpha'\beta^2} \int d^3x_0 d\tau d\tau' \left(\chi^\phi(\tau,\vec{x}_0) \tilde{G}_D(\sigma,\sigma') \chi^\phi(\tau',\vec{x}_0) \right)_{\theta=0} \qquad (3.10)$$

where $\tilde{G}_D(\sigma,\sigma') = \lim_{\rho\to1,\rho'\to1} \partial_\rho \partial_{\rho'} G_D(\rho,\sigma;\rho',\sigma')$ with $G_D(\rho,\sigma;\rho',\sigma')$ the Dirichlet propagator for a canonically normalized massless field on the unit disk and $\sigma = \frac{2\pi}{\beta}\tau$. Note that (3.10) only depends on the value of χ^ϕ at the tip of the brane and is nonlocal in the Euclidean time direction.

Treating (3.10) as a small perturbation to (3.4), one can compute the corrections to the Euclidean two-point function of the (meson) operator dual to χ^ϕ in the boundary YM theory, from which the corrections to the Lorentzian retarded function can be found by analytic continuation. One finds that the poles of the retarded function now obtain a nonzero imaginary part, see Appendix ?? for a discussion of the analytic structure of this retarded greens function. Alternatively one can directly obtain the Lorentzian counterpart of (3.10) by analytically continuing the worldsheet disk to Lorentzian signature with $\sigma = i\eta = i2\pi t/\beta$, which gives the part of Rindler spacetime $ds^2 = d\rho^2 - \rho^2 d\eta^2$ with $\rho \leq 1$. The Lorentzian spacetime effective action can be obtained using the Schwinger-Keldysh contour (see Appendix ??), giving the Lorentzian equation of motion [4]

$$\partial_\alpha \left(\sqrt{-g} G_{\phi\phi} \partial^\alpha \chi^\phi \right) = -\frac{R^2 n_\pm \delta(\theta)}{\mu_7 \pi \alpha' \beta^2} \int dt' \, \tilde{G}_R(\eta - \eta') \chi^\phi(t') \qquad (3.11)$$

where $\tilde{G}_R(\eta - \eta') = \lim_{\rho\to1,\rho'\to1} \partial_\rho \partial_{\rho'} G_R(\rho,\eta;\rho',\eta')$ with $G_R(\rho,\eta;\rho',\eta')$ the *retarded* propagator for a massless field in the Rindler spacetime with Dirichlet boundary condition at $\rho = 1$. Fourier transforming (3.11) to momentum space and using

---

[4]Eq. (3.11) can also be obtained directly from the Euclidean action (3.10) using the following general prescription: write down the equation of motion following from the Euclidean action; replace the Euclidean worldsheet time by the Lorentzian worldsheet time and the Euclidean propagator by the corresponding retarded propagator in the Lorentzian signature.

$\int d\eta\, e^{i\nu\eta} \tilde{G}_R(\eta) = i\nu$, one finds that (3.5) is modified to

$$\hat{H}(\vec{k}, l = 0)\psi - \frac{i\omega n_\pm}{4\pi^3 \alpha' \mu_7 A}\delta(\theta)\psi(\theta) = \omega^2 \psi(\theta) \tag{3.12}$$

with $A = \sqrt{-g}(-g^{tt})$. Writing the dispersion relation as $\omega = \omega_n - \frac{i}{2}\Gamma_n$ where n denotes the excitation number, and using first order perturbation theory in $n_\pm$ we find [5]

$$\Gamma_n^{(\pm1)} = \frac{32\pi^3 \sqrt{\lambda}}{N_c m_q^2}|\psi_n(\theta = 0)|^2 n_\pm \tag{3.13}$$

with $\psi_n(\theta = 0)$ eigenfunctions of (3.5) evaluated at the tip of the brane. Recall that $n_\pm$ are thermal densities for quarks and antiquarks and are proportional to N_c.

The ratio

$$\frac{\Gamma_n(k)}{\Gamma_n(0)} = \frac{|\psi_n(\theta = 0; \vec{k})|^2}{|\psi_n(\theta = 0; \vec{k} = 0)|^2} \tag{3.14}$$

can be evaluated numerically and the results are shown in Fig. 3-2. For large k, the asymptotic form of the wave function, found in [124], can be used to show that the width (3.14) scales like k^2 for large k: $\Gamma_n(k)/\Gamma_n(0) = R_n[T/M](k/M)^2 + \mathcal{O}(k)$ for some function $R_n[T/M]$. Furthermore for temperatures $T \ll M$ and $k \gg \frac{M^3}{T^2}$ one finds the closed form expression $\frac{\Gamma_n(k)}{\Gamma_n(0)} \approx \frac{2(4\pi)^4}{(n+2)(n+3/2)}\frac{T^4 k^2}{M^6}$. Fig. 3-2 has the interesting feature that the width is roughly constant for small k, but turns up quadratically around $k/M = 0.52(T_{\text{diss}}/T)^2$, which is roughly the momentum at which the meson approaches its limiting velocity $v_c(T)$. This is consistent with the conclusions based on the velocity dependence of the screened quark potential found in [10]. Note that the width as defined here is in the rest frame of the plasma, so the k^2 behavior at large k should be contrasted with the $1/k$ behavior of a relativistic decay width which comes from the usual time-dilation argument.

The plots here also share some similarities with those in [126] for momentum-dependence of meson widths obtained for $\mu > m_q^{(T)}$ with $\lambda = \infty$ where the relevant D7 brane embedding resembles a long spike reaching down to the horizon.

---

[5]We normalize the eigenfunctions ψ_n of $\hat{H}(\vec{k}, l)$ as $\frac{1}{L^2 R^4}\int_0^{\frac{\pi}{2}} d\theta \sqrt{-g}\, G_{\phi\phi}\,(-g^{tt})\,|\psi_n(\vec{k}, l; \theta)|^2 = 1$ so that ψ_n is dimensionless and has a smooth zero temperature limit. It depends on ratios of T, M and k but not explicitly on λ.
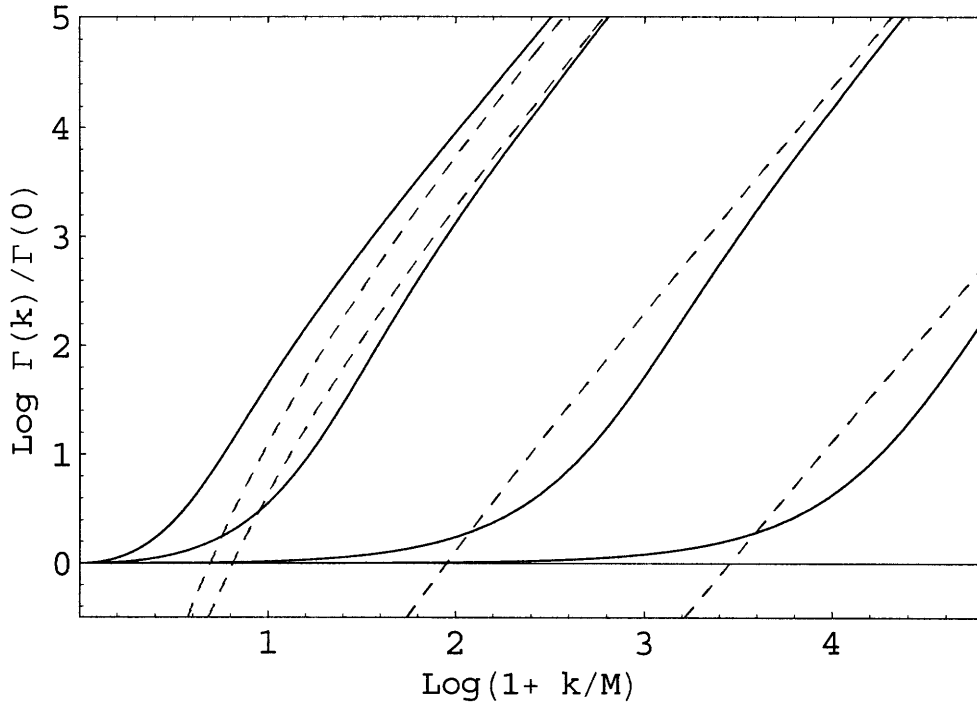
Figure 3-2: The behavior of the width as a function of k for $T/T_{\text{diss}} = .99, .71, .3, .13$ from left to right. The dashed lines are analytic results for large momenta.
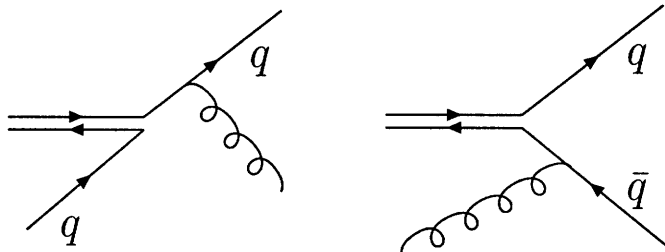
Figure 3-3: *Schematic* diagrams of the relevant thermal processes contributing to the meson width. For large λ the first process is dominant, coming from the single instanton sector.

3.4 Discussion

Our result (3.13) has a very simple physical interpretation as shown in the left plot of Fig. 3-3, in which a meson breaks apart by colliding with a quark (or anti-quark) in the thermal bath. There are also processes corresponding to a meson breaking up by colliding with gluons in the thermal bath, shown in the right plot of Fig. 3-3. For such a process to happen the gluon should have an energy above the binding energy of the meson. The density of such gluons is thus suppressed by $e^{-2\beta m_q^{(T)}}$ and should

be described by an instanton and anti-instanton so that the resulting worldsheet has trivial topology. We expect that contributions from such processes are also controlled by the value of the meson wave function at the tip of the brane, and possibly have similar growth with momentum.

Our method should be generic to any theory with a holographic dual. While the precise value of the width is clearly model dependent, it is conceivable that the momentum dependence may apply in a wider context including QCD. In particular, our result highlights the contributions to quarkonium suppression from the collisions with medium quarks and gluons in the large transverse momentum region in heavy ion collisions.

Consider the effect of such a momentum scaling on J/ψ with $M \approx 3\text{GeV}$. The dissociation temperature from the gravity set-up is $T_{\text{diss}} = 0.122M \approx 370\text{MeV}$ in fairly good agreement with lattice data [58, 59, 62, 64] for QCD $T_{diss} \approx 2.1T_c$ for $T_c = 170\text{MeV}$ [42]. If we take the RHIC temperature of $T = 250\text{MeV}$ (this corresponds to the second curve from the left in Fig. 2) then a moving J/Ψ's width will increase by a factor of 2(10) at a momentum $k = 6(13)\text{GeV}$. When the width of a meson approaches the spacing between different meson states, the meson can no longer be considered as a well-defined quasi-particle. The momentum scaling thus implies a maximal momentum beyond which the meson no longer exists. As an illustration, suppose the width for the J/ψ in the QGP at zero momentum is about 200 MeV (which is not known) then one expects a maximal momentum around 7 GeV.

Finally, we expect the worldsheet instantons found here to have many other applications to various aspects of flavor physics in AdS/CFT.

Chapter 4

Small quark density analysis of the D3/D7 model

4.1 Introduction

In this chapter we are interested in understanding the phase structure of a large N_c gauge theory coupled to a small number N_f fundamental quarks at strong coupling from gravity. More precisely, we consider $\mathcal{N} = 4$ SYM theory with a gauge group $SU(N_c)$ coupled to N_f ($\mathcal{N} = 2$) hypermultiplets in the fundamental representation of $SU(N_c)$, which in the limit of $N_c \gg N_f$ and strong 't Hooft coupling can be described in terms of N_f probe D7-branes in the AdS$_5 \times S_5$ geometry [100][1]. Comparing to QCD, the system has the following distinct features:

1. $N_c \gg N_f$, while in QCD $N_c \sim N_f$.

2. There are both fermionic and *bosonic* "quarks", which are charged under a $U(1)_B$ baryon number symmetry.

3. The beta-function for gauge coupling is zero to leading order in N_f/N_c. The scale of the system is set by the quark mass m_q.

---

[1]See [108] for a review of the system.

Despite many important differences from QCD, the system appears to be rather interesting in its own right and provides a nice laboratory for studying strongly coupled quark-gluon systems under extreme conditions. At zero baryon density and finite temperature it has been used to model heavy quark mesons in QCD [132, 106, 127, 128, 133, 134, 124]. At finite baryon density and zero temperatures some novel dynamical features were recently found in [135, 136, 137, 138].

The phase diagram of the system at finite temperature T and baryon chemical potential[2] μ_q can be worked out by studying possible configurations of D7-branes in the background geometry (which is a black hole in $AdS_5 \times S_5$) and has been studied by various authors in [36, 39, 40, 41, 42, 43, 44, 45] [3]. The results can be summarized as follows (see Fig. 4-1):

1. There is a transition curve in the $\mu_q - T$ plane which intersects with the horizontal axis at $\mu_q = m_q$ with m_q the bare quark mass, and with the vertical axis at some temperature $T = T_d$. Except for a small region near the vertical axis, the transition curve is given by

$$\mu_q = m_q^{(T)}(T) \tag{4.1}$$

where $m_q^{(T)}$ is the effective quark mass at finite temperature (it decreases with temperature). In particular, the transition is second order [41] along the horizontal axis $(T = 0)$ and first order along the vertical axis $(\mu_q = 0)$ [36]. The transition along the vertical axis at $T = T_d$ has been interpreted as a dissociation transition for mesons [36, 38, 37].

2. The region inside the curve in the $\mu_q - T$ plane is described by a D7-brane embedding which lies entirely outside the black hole (Minkowski-type embedding), while the region outside the curve is described by a configuration in which

---

[2]In this chapter we will use the terms baryon charge density and quark charge density interchangeably without a factor $1/N_c$ between them. In other words we take the $U(1)_B$ charge of a quark (anti-quark) to be 1(-1).

[3]For related studies of the same system see [125, 139, 140] and for related studies of a confining theory see [141, 141]

part of the D7-branes falls into the black hole (black hole-type embedding). In terms of the boundary gauge theory, the baryon number density is zero inside the curve and becomes nonzero outside (except along the vertical axis μ_q where the baryon density is always zero.)
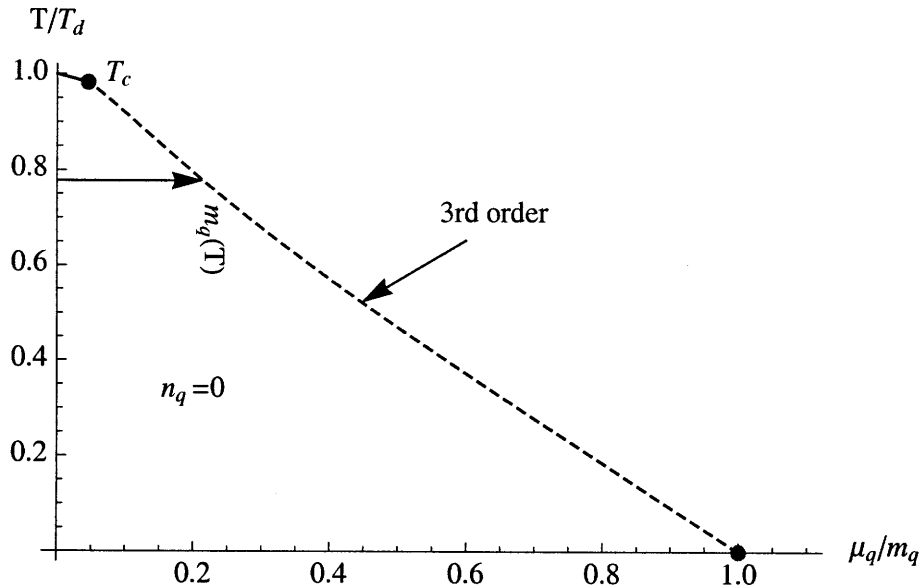
Figure 4-1: The phase diagram in the $\mu_q - T$ plane. The dashed line indicates a continuous transition. The transition line lies exactly on the curve $m_q^{(T)}$ until a critical temperature T_c very close (but not equal) to the dissociation temperature T_d.

In this chapter we improve on the above description and show that the transition along the curve (4.1) is a *continuous* (3rd order) phase transition which connects to a first order line (near the vertical axis) through a tricritical point whose location we identify precisely, see Fig .4-1.

While our conclusions of a continuous phase transition along (4.1) are consistent with the analysis of [40] who noted a phase transition along the $m_q^{(T)}$ line at zero density they are different from a later discussion in [42] where a first order transition was noted. In [42] the relation between charge density and temperature was studied numerically near the transition line and a very small discontinuity in density was noticed, due to a change in dominance between a Minkowski type embedding with zero density and a black hole embedding. It appears to us that the discontinuity likely has to do with the numerical accuracy of their calculation. We do not find a discon-

tinuity in charge density along the transition line (see equation (4.2) below)[4]. More importantly, we have identified a clear physical reason for the phase transition, which indicates that it should not be considered as an exchange of dominance between different embedding solutions, which was behind the reasoning of the conclusion in [42]. As observed in [143], for Minkowski type embedding at finite temperature, there are worldsheet instanton corrections to the leading order Dirac-Born-Infeld (DBI) action for the D7-branes. While for a Minkowski type embedding, particle excitations on the D7-branes are not sensitive to the value of the chemical potential, the worldsheet instantons which correspond to semi-classical strings stretched between D7-branes and the black hole do. In particular, when the baryon chemical potential exceeds the value (4.1), the instanton actions exponentially dominate over the DBI action in the large 't Hooft coupling limit and induce an instability. The consequence of the instability is that instantons "condense" and generate a genuine neck between the D7-branes and the black hole. Thus beyond (4.1) the Minkowski-type embedding cannot exist and should be replaced by a black hole type embedding.[5] The transition also has a simple interpretation in the gauge theory. As discussed in [143], the instantons can be interpreted in the boundary gauge theory as thermal medium quarks. When μ_q exceeds the value of (4.1), the quarks have negative free energies and will condense and generate a finite charge density, although it is not clear whether it is fermionic quarks or bosonic quarks which are condensing.

More explicitly, we find along the critical line (4.1) (approaching it from above), the baryon charge density and the chemical potential are related by

$$\mu_q - m_q^{(T)} = -B(T)\epsilon \log \epsilon + A(T)\epsilon + O(\epsilon^2) \tag{4.2}$$

where ϵ is the quark charge density (normalized to be dimensionless) and $A(T), B(T)$ are some functions of temperature. In the zero temperature limit, $B(T)$ goes to

---

[4]We have obtained our results both analytically and numerically with agreement.

[5]Note that this reasoning does not by itself imply that the transition should be continuous, it only indicates that the transition is not an exchange of dominance as is normally the case for a first order transition. Our explicit calculation shows that there is no jump in the baryon charge density across the transition line in the infinite 't Hooft coupling limit.

zero and $A(T)$ goes to a finite constant, and one recovers the second transition at $T = 0$ (found in [41]), where various exponents are given by their mean field values. At any finite temperature, however, it is always the logarithmic term on RHS of (4.2) that dominates at small enough densities and as a result the transition becomes third order. The logarithmic behavior does not appear to have a mean field counterpart, and thus this is an example of continuous phase transition from gravity which does not obey the Landau-Ginzburg behavior. Such log terms however do appear to be a common feature of the renormalization group analysis of condensed matter systems at their upper critical dimension.

There also exists a temperature T_c at which $B(T_c) = 0$ and beyond which $B(T) < 0$. At T_c the transition is again second order. For $T > T_c$, the transition becomes first order since for a given μ_q close to, but *smaller* than $m_q^{(T)}$, now there are two black hole type embeddings with $\epsilon \neq 0$ in addition to the Minkowski type embedding. Connecting a continuous critical line and a first order transition line, the point $(T = T_c, \mu_q = m_q^{(T)}(T_c))$ is thus a tricritical point. Again the critical behavior near the tricritical point is *not* the same as that of a Landau-Ginzburg type effective theory.

While it is natural to connect the first transition near the tricritical point with that near the vertical axis at $\mu_q = 0$, our approximation in (4.2) which applies to small densities does not extend all the way to $\mu_q = 0$. Thus that part of the phase diagram remains a conjecture at the moment. Also numerical work at *finite* density by other authors [42] suggest this should be the case, however a conclusive argument remains to be made.

The phase diagram in Fig. 4-1 is for the $\lambda = \infty$ limit, where the quark charge density is identically zero inside the transition curve. At finite λ, as pointed out in [143], for any $\mu_q \neq 0$ at any finite temperature, the baryon charge density is in fact nonzero, given by a dilute Boltzmann gas of quarks. This immediately raises the question whether the transition along (4.1) is an artifact of the infinite λ limit and will be smoothed into a crossover at any finite λ. To settle this question requires summing over the worldsheet instantons found in [143] and will be pursued in a separate publication.

The plan of the chapter is as follows. In section 4.2 we discuss the gravity description of the gauge theory system. In sec. 4.2.1 we review how to introduce a finite baryon chemical potential. In sec. 4.2.2 we argue that the phase transition is driven by string worldsheet instantons. In sec 4.3 we give a detailed analytically derivation of equation (4.2) and verify it numerically. In sec. 4.4 we discuss the thermodynamics of the system which can be gathered from equation (4.2). In the conclusion sec. 4.5 we discuss the connection of the critical point to the first order dissociation transition at $\mu_q = 0$. We also discuss what happens to the phase diagram at finite λ.

4.2   Gravity description of the gauge theory

4.2.1   General setup - finite baryon chemical potential

The general setup has been described in Chapter 1 section 3, including the introduction of a chemical potential by turning on the gauge field on the D-brane. Our staring point is the DBI action (1.15) which can be written explicitly in terms of $y(\rho), A_0(\rho)$ as

$$S = -N_f T_7 \int d^8\xi \, \rho^3 q^{3/2} \left[fq \left(1 + (y')^2 \right) - a'^2 \right]^{\frac{1}{2}}, \qquad (4.3)$$

where prime denotes derivative with respect to ρ, and we have introduced

$$a(\rho) = 2\pi\alpha' A_0 . \qquad (4.4)$$

We will denote the integrand of (4.3) as $\mathcal{L}$. Since (4.3) does not depend on a (only a') we have a conserved quantity ϵ:

$$\epsilon = \frac{\partial \mathcal{L}}{\partial a'} = \frac{a'\rho^3 q^{3/2}}{\left(fq(1 + (y')^2) - a'^2 \right)^{\frac{1}{2}}} \qquad (4.5)$$

$$a'^2 = fq \left(1 + y'^2 \right) \frac{\epsilon^2}{\rho^6 q^3 + \epsilon^2} . \qquad (4.6)$$

From (1.26), we thus find the charge density in the boundary gauge theory is given by

$$n_q = N_f T_7 (2\pi\alpha')(2\pi^2)\epsilon \tag{4.7}$$

where the factor $2\pi^2$ comes from the volume of the three sphere.

Since we will be expanding in terms of small density later, it will be convenient to scale coordinates and ϵ so that they are dimensionless, i.e.

$$u, y, \rho \rightarrow L_0(u, y, \rho), \quad \epsilon \rightarrow L_0^3 \epsilon, \quad a(\rho) \rightarrow L_0 a(\rho) \tag{4.8}$$

where L_0 is the location of the tip of the brane (1.20) *before* turning on a chemical potential[6]. From now on, $u, y, \rho, \epsilon, a(\rho)$ are all dimensionless. After the scaling (1.18) become

$$u^2 = y^2 + \rho^2, \quad q(u) \equiv 1 + \frac{\eta^4}{u^4}, \quad f \equiv \left(\frac{u^4 - \eta^4}{u^4 + \eta^4}\right)^2, \quad \eta \equiv \frac{u_0}{L_0} < 1 . \tag{4.9}$$

The boundary conditions for $y(\rho)$ and $a(\rho)$ now are

$$y(\infty) = \frac{L}{L_0}, \quad a(\infty) = \frac{2\pi\alpha'}{L_0}\mu_q \tag{4.10}$$

and equation (1.21) becomes

$$m_q^{(T)} = \frac{L_0}{2\pi\alpha'} \int_\eta^1 dy \sqrt{fq}\bigg|_{\rho=0} .T \tag{4.11}$$

To obtain the equation of motion for y it is convenient to perform a Legendre transformation on (4.3) to express it in terms of ϵ. The transformed action is

$$\mathcal{H} \equiv \epsilon a' + \mathcal{L} = \sqrt{\epsilon^2 + \rho^6 q^3}\sqrt{fq(1 + y'^2)} \tag{4.12}$$

---

[6]One can also choose to normalize them using L (1.19) which is more directly related to the field theory mass. But in our calculation below using L_0 is slightly more convenient. L_0 is fixed once the ratio m_q/T is given. Another alternative is to use the temperature but that will make the zero temperature limit more subtle.

which leads to equation of motion

$$\frac{y''}{1+y'^2} + \frac{3y'}{\rho} + \frac{8}{u^2}\frac{\rho y' - y}{u^8\eta^{-8}-1} - \frac{\epsilon^2}{\epsilon^2+\rho^6 q^3}\left[\frac{3y'}{\rho} - \frac{6}{u^2}\frac{\rho y'-y}{1+u^4\eta^{-4}}\right] = 0 \ . \qquad (4.13)$$

When $\epsilon = 0$ (i.e. zero density), equation (4.13) becomes

$$\frac{y''}{1+y'^2} + \frac{3y'}{\rho} + \frac{8}{u^2}\frac{\rho y' - y}{u^8\eta^{-8}-1} = 0 \qquad (4.14)$$

whose solution is given by $y_0(\rho)$ described earlier around equation (1.20).[7] In Fig. 4-2 we plot how L_0/L and η change with temperature for an embedding governed by $y_0(\rho)$.
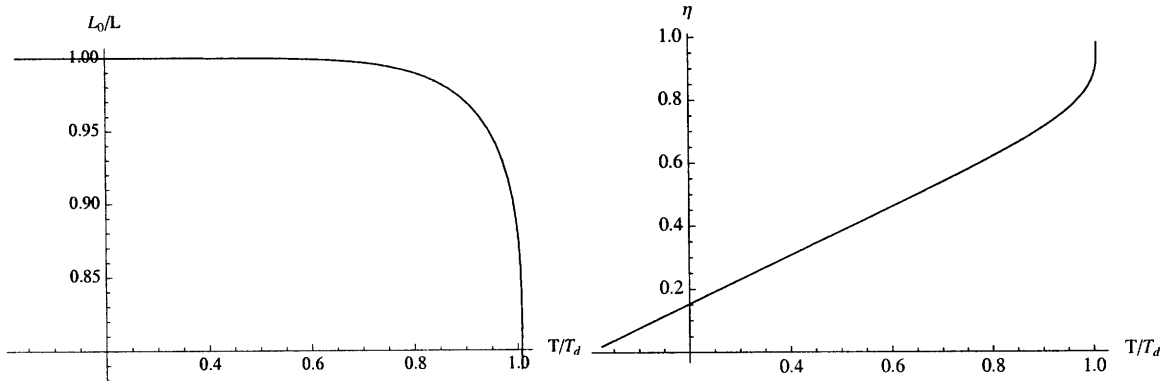
Figure 4-2: L_0/L and η for the Minkowski solution ($\epsilon = 0$) as a function of T/T_d.

4.2.2 Phase transition driven by string worldsheet instantons

For *any* value of μ_q (and $T < T_d$), one can always have the following solution to equations of motion (4.6) and (4.13) with

$$A_0 = \mu_q = \text{const}, \qquad \epsilon = 0, \qquad y(\rho) = y_0(\rho) \qquad (4.15)$$

for which (4.13) reduces to (4.14). This solution is somewhat peculiar, since it implies that the quark charge density n_q is zero even at a finite temperature and finite chemical potential μ_q. This appears to contradict with field theory expectation

---

[7]As stated earlier we will only consider $T < T_d$ for which there is only one Minkowski embedding solution.

120

that the density for quark and anti-quark should be given (at low density) by the Boltzmann distribution $n_\pm \sim e^{-\beta(m_q^{(T)} \pm \mu_q)}$ which gives a nonzero net charge density $n_q = n_+ - n_- \neq 0$ for a nonzero μ_q. There is in fact no contradiction, since (4.15) is the result in the $\lambda = \infty$ limit (supergravity limit) and in this limit due to (1.22),

$$n_\pm \sim n_q \sim e^{-\sqrt{\lambda}}, \quad \text{for} \quad \mu_q < m_q^{(T)} \,. \tag{4.16}$$

The charge density is thus exponentially small in the large λ limit and not visible to any order in the $1/\sqrt{\lambda}$ (or α') expansion.

In [143], it was found for the embedding (4.15) there are non-perturbative open string worldsheet instanton corrections to the DBI action (1.15) which accounts for the exponentially small quark density. More explicitly, the instantons are given by open strings stretching between the tip of the D7-branes and the black hole horizon and winding around the Euclidean time direction, as indicated in the left plot of Fig. 4-3. They are classified a winding number n. From the spacetime point of view, these instantons generate tiny virtual necks which connect the tip of the branes to the black hole horizon. The total Euclidean action for the D7-branes, which gives the thermodynamic potential of the boundary gauge theory in the grand canonical ensemble, can be written as

$$S = S_{DBI} + \sum_{n=\pm 1, \pm 2, \cdots} D_n \exp\left(-|n|\beta(m_q^{(T)} - \mathrm{sgn}[n]\mu_q)\right) + \cdots \tag{4.17}$$

where n sums over the instanton contributions, D_n arises from the worldsheet determinant for each instanton[8], and $\cdots$ denotes other perturbative $1/\sqrt{\lambda}$ (or α') corrections. These string worldsheet instantons have a simple interpretation in the boundary gauge theory as representing thermal medium quarks. In particular, the $n = \pm 1$ terms in (4.17) are precisely what one expects of a dilute Boltzmann gas of quarks and anti-quarks.[9]

---

[8]It also includes possible integrations over instanton moduli space.

[9]Higher n contributions should encode corrections due to Bose-Einstein or Fermi-Dirac statistics and other corrections due to interactions.

Due to (1.22), when $\mu_q < m_q^{(T)}$ the instanton contributions in (4.17) are exponentially small in $\sqrt{\lambda}$ compared with the DBI action S_{DBI}. But for

$$\mu_q \geq m_q^{(T)} \tag{4.18}$$

the instanton sum will be exponentially large compared with the DBI action and the solution (4.15) can no longer be trusted. In particular, since the instanton contributions are dominating, we expect them to "condense" and create a genuine neck between the brane and the black hole. This implies in the range (4.18) a new solution to the DBI action with the branes going into the black hole should emerge, as indicated in the right plot of Fig. 4-3. Thus in the infinite λ limit we have a phase transition at $\mu_q = m_q^{(T)}$ where the Minkowski-type embedding (4.15) goes over to a black-hole-type embedding. The transition also has a simple interpretation from the gauge theory point of view; when μ_q satisfies (4.18), the quarks have negative free energies and will thus condense and generate a finite charge density.

The possibility for such a phase transition has been studied before in [42, 40, 39], where a single[10] black hole embedding solution was found for $\mu_q > m_q^{(T)}$ and it was concluded in [42] that the transition was *first order*. One reason for the conclusion was that it appeared that the Minkowski embedding solution (4.15) was still valid for $\mu_q > m_q^{(T)}$ and thus the transition appeared to be a change of dominance between different solutions. As we discussed above, the Minkowski embedding solution should be *replaced* by a black hole embedding solution in the parameter region (4.18). Thus if there is only a single black hole embedding solution for $\mu_q > m_q^{(T)}$ the transition is most likely to be continuous. Indeed we will show in section 4.4, the transition is *third order* for temperature not too high, but then becomes first order through a *tricritical point*.[11]

---

[10] at a temperature not too high

[11] Beyond the tricritical point it becomes possible to have multiple black hole embedding solutions for a given μ_q. See section 4.4.
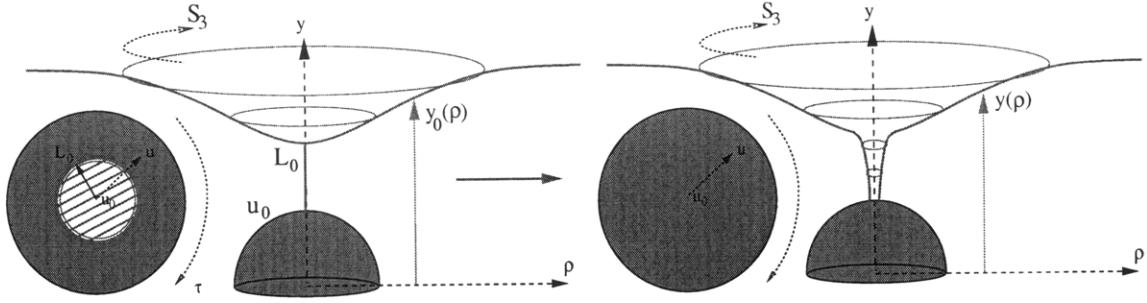
Figure 4-3: Left plot: For Minkowski type embedding (4.15), there exist worldsheet instantons which correspond to semi-classical strings stretching between the tip of the D7-branes to the black hole horizon and winding around the Euclidean time direction represented as the angle on the inset disk. The radial direction on the disk is the same as the radial direction in the $y - \rho$ plane. Right plot: for $\mu_q > m_q^{(T)}$ instantons dominate over the DBI contributions and will condense to form a genuine neck between the branes and the horizon, i.e. one should have a black hole type embedding.

4.2.3 Black hole embedding at finite density

As discussed in last subsection, for $\mu_q \geq m_q^{(T)}$ we expect a black hole type embedding for D7-branes in the gravity side and a nonzero quark charge density on the gauge theory side. That the quark density for a black hole type embedding should be zero can be seen as follows. For a black hole type embedding, one should impose an additional boundary condition $A_0 = 0$ for the gauge field at the horizon in order to ensure the regularity of the solution. From (1.25) this implies that A_0 should evolve nontrivially from the boundary to the horizon, i.e. there is a nontrivial electric field in the radial direction on the branes, which from (1.26) in turn implies $n_q \neq 0$ (and thus $\epsilon \neq 0$). Thus we should now consider equation (4.13) with $\epsilon \neq 0$. Conversely it has also been argued previously in [139] that for any $\epsilon \neq 0$, only black hole type of embeddings are allowed since for a Minkowski type embedding it is not possible to have a non-singular distribution of a finite charge density on the branes[12].

Let us now consider the boundary conditions for $y(\rho)$ at the horizon for a black hole type embedding. We will denote the point that the brane enters the horizon ρ_c

---

[12]See also [41] for a discussion at zero temperature

and $y_c \equiv y(\rho_c)$. Note that

$$y_c^2 + \rho_c^2 = u_0^2 \qquad (4.19)$$

and in order for the the third term in (4.13) to be nonsingular at the horizon, we will also need that

$$y'(\rho_c) = \frac{y_c}{\rho_c} \qquad (4.20)$$

i.e. the brane should be perpendicular to the horizon. The precise of value of ρ_c is determined by the boundary condition (4.10).

For regularity we will also require the gauge potential vanish at the horizon[13], i.e. $a(\rho_c) = 0$. From equation (4.6), we can express the chemical potential in terms of density ϵ as

$$\mu_q = \frac{L_0}{2\pi\alpha'}\epsilon \int_{\rho_c}^{\infty} d\rho \, \frac{\sqrt{fq(1+y'^2)}}{\sqrt{\epsilon^2 + \rho^6 q^3}} \; . \qquad (4.21)$$

The main technical task of the chapter is to determine the behavior of μ_q in the limit of small ϵ, which will be carried out in next section. Once the expansion of μ_q in terms of ϵ is known, we will be able to determine the order of the phase transition and other thermodynamic properties of the system. This will be carried out in section 4.4.

4.3 Small density expansion of the chemical potential

In this section we study the behavior of (4.21) in the small ϵ limit. Expanding (4.21) in small ϵ is somewhat complicated since the solution $y(\rho)$ depends nontrivially on ϵ. The expansion of $y(\rho)$ in terms of small ϵ is also involved; one cannot treat the ϵ-dependent term in (4.13) as a small perturbation of (4.14) uniformly for all values of ρ since the term becomes of $O(1)$ for sufficiently small ρ (when $\rho^6 q^3 \sim O(\epsilon^2)$).

The main result of the section is equation (4.45). Readers who are not interested in the detailed derivation can go directly to (4.45) and subsequent discussions.

---

[13]Otherwise the one-form $A_0 dt$ will be singular at the horizon since the norm for $\frac{\partial}{\partial t}$ vanishes there.

4.3.1 Expansion of the solution

Since the perturbation in ϵ is not uniform in ρ one needs to divide the ρ axis into different regions, treating the perturbations in each region separately, and matching them together at the end. For our purpose, it turns out enough to split the ρ-axis into two regions:

- **Inner** $\rho = \varepsilon^{\frac{1}{2}}\sigma$ for $\sigma_c < \sigma < \Lambda$

- **Outer** $\rho_\Lambda < \rho < \infty$

where

$$\rho_c = \epsilon^{\frac{1}{2}}\sigma_c, \qquad \rho_\Lambda = \epsilon^{\frac{1}{2}}\Lambda . \tag{4.22}$$

The reason for the choice of scaling in the inner region can be seen by letting $\rho = \epsilon^\alpha \sigma$ in (4.13) and one finds that for $\epsilon = \frac{1}{2}$ a nontrivial scaling limit exists, which results differential equation in (4.29) below. Also see Appendix B for a discussion of the $T = 0$ solution where this scaling is evident.

We will consider the limit

$$\epsilon \to 0, \qquad \sigma = \text{finite}, \qquad \Lambda \to \infty, \qquad \rho_\Lambda \to 0 . \tag{4.23}$$

We expand the solution in the inner and outer regions as[14]

$$y_\mathcal{I}(\sigma) \;=\; Y_0(\sigma) + \varepsilon Y_1(\sigma) + \varepsilon^2 Y_2(\sigma) + \cdots \tag{4.24}$$

$$y_\mathcal{O}(\rho) \;=\; y_0(\rho) + \varepsilon y_1(\rho) + \varepsilon^2 y_2(\rho) + \cdots . \tag{4.25}$$

Plugging (4.24) and (4.25) respectively into (4.13) and expanding the equation in ϵ, we obtain a series of differential equations for various functions in (4.24) and (4.25). These equations are rather complicated and not exactly solvable. We will work out the behavior of $Y_0(\sigma), Y_1(\sigma)$ in the large σ limit and $y_0(\rho), y_1(\rho)$ in the small ρ limit

---

[14]While it is not a priori obvious the expansion parameter should be ε and not some other power, the expansions below do yield consistent results.

and match them in the overlapping region. Fortunately it turns out this is enough to find the leading expansion of μ_q in the small ϵ limit analytically.

Let us first examine the outer region. y_0 is simply the solution to (4.14) which describes the embedding at zero density. It satisfies the boundary condition (4.10) at the boundary and near $\rho = 0$ has the following expansion

$$y_0(\rho) = 1 + \frac{\rho^2}{\eta^{-8} - 1} - \frac{\eta^8(5 + 5\eta^8 - 3\eta^{16})}{3(1 - \eta^8)^3}\rho^4 + O(\rho^6) \ . \tag{4.26}$$

y_1 satisfies a homogeneous linear equation obtained by linearizing (4.14). For small ρ it has an expansion,

$$y_1 = b_{-1}\rho^{-2} + b_0 \log \rho + b_1 + O(\rho) \tag{4.27}$$

where b_{-1} and b_1 are integration constants and

$$b_0 = -\frac{28\eta^8}{(1 - \eta^4)^2(1 + \eta^4)^2}b_{-1} \ . \tag{4.28}$$

Note that the first two terms diverge in the $\rho \to 0$ limit. The coefficient b_{-1} of the quadratically divergent term will be fixed later by matching with the inner solution. b_1 should be determined by requiring $y_1(\rho \to \infty) \to 0$ since y_0 already satisfies the required boundary condition (4.10) there.

Now we look at the inner region. $Y_0(\sigma)$ satisfies a second order *non-linear* differential equation (primes below denotes derivative w.r.t. σ)

$$\frac{Y_0''}{Y_0'^2} + 3\left(1 + \frac{\eta^4}{Y_0^4}\right)^3 \sigma^5 Y_0' + \frac{8}{Y_0^2}\frac{\sigma Y_0' - Y_0}{Y_0^8\eta^{-8} - 1} + \frac{6}{Y_0^2}\frac{\sigma Y_0' - Y_0}{1 + Y_0^4\eta^{-4}} = 0 \tag{4.29}$$

From (4.19) and (4.20) the boundary condition at the horizon is

$$Y_0(\sigma_0) = \eta, \qquad Y_0'(\sigma_0) = \frac{\eta}{\sigma_0} \tag{4.30}$$

where σ_0 is an integration constant. σ_0 is the zero-th order term in the expansion in ϵ of $\sigma_c = \rho_c/\epsilon^{1/2}$ (where again it is a non trivial fact that this expansion begins at $\mathcal{O}(1)$ in ϵ)

$$\sigma_c = \sigma_0 + \epsilon\,\sigma_1 + \cdots \tag{4.31}$$

and can be determined by the boundary condition at infinity,

$$Y_0(\sigma) \to 1 \qquad \text{as} \qquad \sigma \to \infty\,. \tag{4.32}$$

The above condition is fixed by comparing with the leading term in (4.26). At large σ, Y_0 has the expansion

$$
\begin{aligned}
Y_0(\sigma) \quad &= 1 - \frac{1}{2(1+\eta^4)^{3/2}}\sigma^{-2} + \frac{\eta^4(-3+5\eta^4)}{4(-1+\eta^4)(1+\eta^4)^4}\sigma^{-4} \\
&+ \frac{\eta^4(27 - 131\eta^4 + 153\eta^8 - 105\eta^{12})}{24(-1+\eta^4)^2(1+\eta^4)^{13/2}}\sigma^{-6} + O(\sigma^{-8}) + O(\sigma^{-8}\log\sigma)
\end{aligned}
\tag{4.33}
$$

Note that the coefficient before σ^{-8} is an integration constant which can be fixed by (4.30). We will not need its value below.

$Y_1(\sigma)$ satisfies a second order *linear* differential equation with coefficients that depend on $Y_0(\sigma)$. It is not homogeneous and rather complicated. We will not write it here. For large σ we find the expansion

$$Y_1(\sigma) = a_{-1}\sigma^2 + a_0\log\sigma + a_1 + O(\sigma^{-1}) \tag{4.34}$$

where a_1 is an integration constant (the other integration constant presumably appears at higher order in the expansion) and

$$a_{-1} = \frac{\eta^8}{1-\eta^8}, \qquad a_0 = \frac{14\eta^8}{(1-\eta^4)^2(1+\eta^4)^{\frac{7}{2}}}\,. \tag{4.35}$$

Note the first two terms of (4.34) are divergent as $\sigma \to \infty$. The constant a_1 can be determined by matching with the solution of the outer region. The *other* boundary condition is determined by the regularity condition (4.19-4.20) (expanded to this

127

order) at the horizon, this gives only one boundary condition on Y_1 and its derivative because the first order correction σ_1 in (4.31) is a free parameter. This parameter σ_1 would then be determined by the resulting solution.

We will now determine various integration constants above by matching the solutions in the inner and outer regions around ρ_Λ. Note given the relation $\rho = \epsilon^{\frac{1}{2}} \sigma$, the ϵ expansion in the outer region is reshuffled compared to that in the inner region. Comparing the first term in (4.27) to the second term of (4.33) we find that

$$b_{-1} = -\frac{1}{2(1 + \eta^4)^{3/2}}, \qquad b_0 = \frac{14 \eta^8}{(1 - \eta^4)^2 (1 + \eta^4)^{\frac{7}{2}}} \tag{4.36}$$

where we have used (4.28) in obtaining the second equation. From (4.36) and (4.35) we see that the logarithmic term in (4.27) precisely match with that in (4.34); this is a nontrivial self-consistency check of our expansion. It now remains to match the constant terms in (4.27) and (4.34). Given the difference in the argument of logarithmic term in (4.27) and (4.34), we thus find that

$$a_1 = b_1 + \frac{1}{2} b_0 \log \epsilon = b_1 + \frac{7 \eta^8}{(1 - \eta^4)^2 (1 + \eta^4)^{\frac{7}{2}}} \log \epsilon \; . \tag{4.37}$$

As remarked below (4.28), b_1 is determined by the boundary condition $y_1(\infty) = 0$ and since the equation for y_1 is independent of ϵ, so is b_1.[15] Thus we see from (4.37) that the integration constant a_1 for inner solution Y_1 now contains a $\log \epsilon$ piece![16] This will be important in our determination of the leading order behavior for μ_q below.

As a check on our above results we can make sure that the exact (numerical) solution at small densities matches well onto our expansions in the two different regions. This is demonstrated in Fig. (4-4). The agreement is very precise suggesting the two regions we have used are sufficient. Higher order corrections in the two regions would appear as divergences toward the exact solution.

---

[15]Determining b_1 requires solving the two-point boundary value problem for y_1.
[16]This in turn implies that σ_1 in (4.31) also contains $\log \epsilon$.
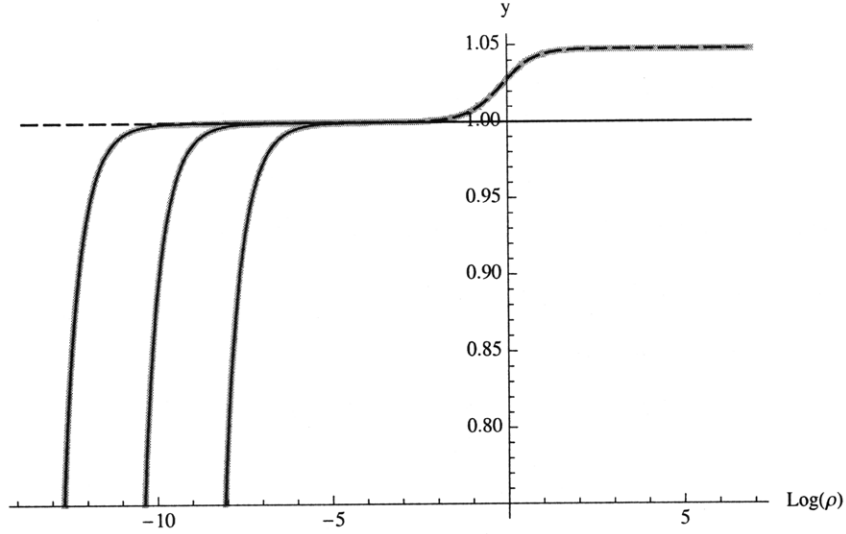
Figure 4-4: The exact embeddings for $\epsilon = 10^{-11}, 10^{-9}, 10^{-7}$ shown in green. To clearly show the two regions we have plotted $y(\rho)$ as a function of $\log(\rho)$. These are compared to the zeroth order inner (*solid*) and outer (*dashed*) solutions. The inner solution $Y_0(\sigma)$ is a function of $\sigma = \rho \epsilon^{-1/2}$ so for the various fixed densities the curve is simply shifted along the $\log(\rho)$ axis. The agreement between the three curves on the overlapping regions is very precise.

4.3.2 Expansion of the chemical potential

We now look at the small ϵ expansion of (4.21). We will give the main steps and final results, leaving further details to Appendix D.

The μ_q integral (4.21) can be split into integrals over the inner and outer regions

$$\mu_q = \int_{\rho_c}^{\rho_\Lambda} (\cdots) + \int_{\rho_\Lambda}^{\infty} (\cdots) \equiv \mu_{\mathcal{I}} + \mu_{\mathcal{O}} . \tag{4.38}$$

$\mu_{\mathcal{I}}$ and $\mu_{\mathcal{O}}$ can now be expanded in terms of ϵ using (4.24) and (4.25). The outer region contribution $\mu_{\mathcal{O}}$ starts with order ϵ, i.e.

$$\mu_{\mathcal{O}} = \epsilon \mu_{\mathcal{O}}^{(1)} + O(\epsilon^2) \tag{4.39}$$

and for $\mu_{\mathcal{O}}^{(1)}$ only y_0 is needed. Using the small ρ expansion of y_0 (4.26) we find that the integral for $\mu_{\mathcal{O}}^{(1)}$ contains a quadratic and a logarithmic divergent term in the limit

129

$\rho_\Lambda \to 0$,

$$\mu_\mathcal{O}^{(1)} = \frac{L_0}{2\pi\alpha'} \left(\frac{1-\eta^4}{2(1+\eta^4)^2 \rho_\Lambda^2} - \frac{2\eta^4(3-\eta^4+3\eta^8)}{(1-\eta^4)(1+\eta^4)^4} \log(\rho_\Lambda) + K_\mathcal{O}(\eta, L/L_0) \right) \qquad (4.40)$$

where $K_\mathcal{O}$ denotes the part which remains finite in the limit $\rho_\Lambda \to 0$ $K_\mathcal{O}$, whose explicit expression is given in Appendix D, depends on the full solution $y_0(\rho)$ and can only be evaluated numerically.

The inner region contribution also contains an $O(1)$ piece

$$\mu_\mathcal{I} = \mu_\mathcal{I}^{(0)} + \epsilon \mu_\mathcal{I}^{(1)} + \cdots \qquad (4.41)$$

with (recall that $\sigma = \epsilon^{-\frac{1}{2}}\rho$)

$$\mu_\mathcal{I}^{(0)} = \frac{L_0}{2\pi\alpha'} \int_{\sigma_c}^{\Lambda} d\sigma \, Y_0'(\sigma) \frac{Y_0^4 - \eta^4}{Y_0^2 \sqrt{Y_0^4 + \eta^4}} = \int_{\sigma_c}^{\infty} (\cdots) - \int_{\Lambda}^{\infty} (\cdots) \qquad (4.42)$$

where in the second equality we have separated the expression into two pieces by splitting the integral. Now changing the integration variable of the first integral into Y_0 and comparing it with (4.11), we find that it is precisely $m_q^{(T)}$. The second term can be evaluated in power series of $1/\Lambda$ by using the expression (4.33) for Y_0 at large σ, leading to

$$\mu_\mathcal{I}^{(0)} = m_q^{(T)} - \frac{L_0}{2\pi\alpha'} \frac{(1-\eta^4)}{2(1+\eta^4)^2 \Lambda^2} + \mathcal{O}(\Lambda^{-4}) . \qquad (4.43)$$

To evaluate $\mu_\mathcal{I}^{(1)}$ one also needs Y_1. Using the expansion (4.34) of Y_0 and Y_1 for large σ, we find that the integral for $\mu_\mathcal{I}^{(1)}$ contains a logarithmic divergence (in the $\Lambda \to \infty$ limit) from the upper end of the integral and can be written as

$$\mu_\mathcal{I}^{(1)} = \frac{L_0}{2\pi\alpha'} \left(\frac{2\eta^4(3-\eta^4+3\eta^8)}{(1-\eta^4)(1+\eta^4)^4} \log(\Lambda) + \frac{7\eta^8 \log\epsilon}{(1-\eta^4)(1+\eta^4)^4} + K_\mathcal{I}(\eta, L/L_0) \right) . \qquad (4.44)$$

Note that in the finite part we have isolated a piece proportional to $\log\epsilon$ which comes from the integration constant a_1 of Y_1 through equation (4.37) (see Appendix D for details). $K_\mathcal{I}$ is finite and independent of ϵ. Its explicit expression is given in D and

can only be evaluated numerically.

Now adding (4.40) and (4.43), (4.44) together we find that the second term in (4.43) precisely cancels the quadratic divergence in (4.40) and the logarithmic divergence in (4.44) precisely cancels with that in (4.40), leaving a finite piece proportional to $\epsilon \log \epsilon$. We thus find that

$$\mu = m_q^{(T)} - B(T)\epsilon \log \epsilon + A(T)\epsilon + O(\epsilon^2) \tag{4.45}$$

where

$$B(T) = B_1(T) + B_2(T) = \frac{L_0}{2\pi\alpha'} \frac{\eta^4 \left(3 - 8\eta^4 + 3\eta^8\right)}{(1 - \eta^4)(1 + \eta^4)^4}, \qquad A(T) = \frac{L_0}{2\pi\alpha'}\left(K_{\mathcal{O}} + K_{\mathcal{I}}\right) \tag{4.46}$$

and

$$B_1(T) = \frac{L_0}{2\pi\alpha'} \frac{\eta^4(3 - \eta^4 + 3\eta^8)}{(1 - \eta^4)(1 + \eta^4)^4}, \qquad B_2(T) = -\frac{L_0}{2\pi\alpha'} \frac{7\eta^8}{(1 - \eta^4)(1 + \eta^4)^4} \tag{4.47}$$

Note that in writing (4.46) and (4.47) we have emphasized that the coefficient of $\epsilon \log \epsilon$ receives contributions from two different sources; B_1 from cancellation of the logarithmic divergence and B_2 from the finite piece in (4.44). The expressions for $K_{\mathcal{O}}$ and $K_{\mathcal{I}}$ are given in Appendix D, which can only be evaluated numerically. We also note that in the $\epsilon \to 0$ limit it is the $\epsilon \log \epsilon$ which dominates and whose coefficient we have determined exactly. Note that L_0, which gives of the location of the tip of the D7-branes in the absence of a charged density (1.20), is also temperature-dependent.

Again we can use exact (numerical) solutions for small densities to check our analysis. The $\log \epsilon$ dependence is not easy to see, so we must push our analysis to very small densities with a wide range of densities. Then the best way to extract the behavior is to plot the function $x(\epsilon)$ defined by,

$$x(\epsilon) \quad = \quad \frac{d \log(\mu_q - m_q^{(T)})}{d \log \epsilon} \tag{4.48}$$

$$\approx \quad \frac{A(T) - B(T)(\log \epsilon + 1)}{A(T) - B(T) \log \epsilon} \tag{4.49}$$

131
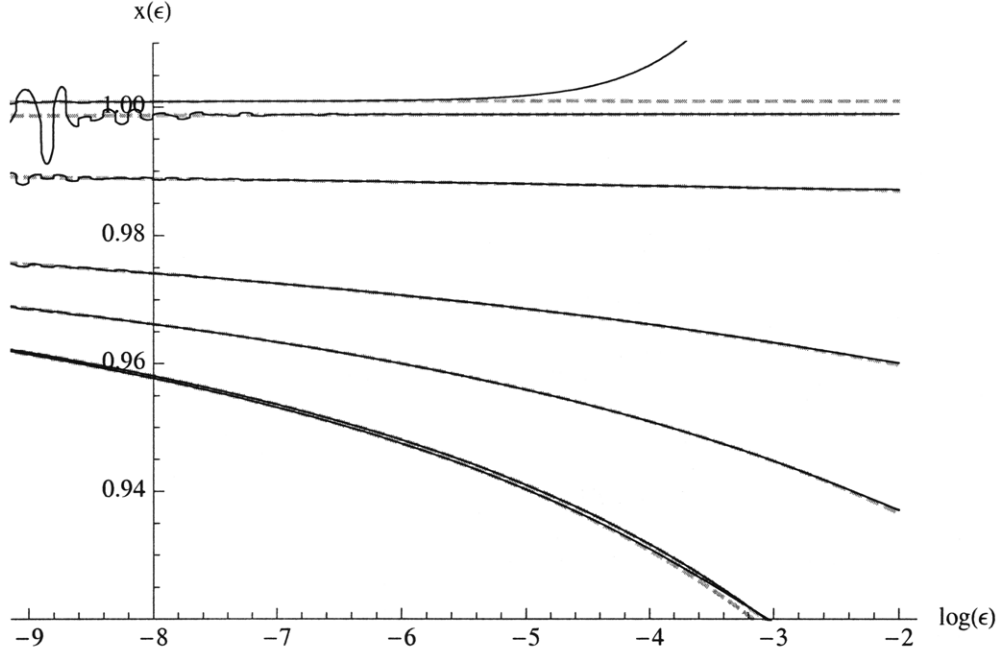
Figure 4-5: Plots of the exponent $x(\epsilon)$ as defined in (4.48), for various values of the temperature. At zero temperature the exponent is simply 1 and all these curves should eventually limit to 1 at small enough densities. The slow running of this exponent is a consequence of the $\log \epsilon$ behavior of the chemical potential. The dashed line is a (1 parameter) fit to the numerical curve using (4.49).

where for the last equality we have used our derived small ϵ expression (4.45). We can fit this later form to the numerical result and find the ratio $A(T)/B(T)$, after which we can use the overall normalization of $\mu_q - m_q^{(T)}$ to fix $A(T)$ and $B(T)$ separately. This agreement in the form of the solution is shown in Fig. 4-5.

4.3.3 Behavior of $B(T)$ and $A(T)$

Let us now examine the behavior of $B(T)$ and $A(T)$ as we vary T. In the $T \to 0$ (i.e. $\eta \to 0$) limit, from (4.46)

$$m_q(T) = m_q, \qquad A(T) = m_q \frac{\kappa^3}{2}, \qquad B(T) = 0 \tag{4.50}$$

which reduces to the correct zero temperature behavior (C.4) in Appendix C. In the above equation κ is a number defined by the integral $\kappa = \int_0^\infty dx/(x^6 + 1)$. For general temperature T, the behavior of $A(T), B(T)$ and $m_q^{(T)}$ are plotted in Fig. 4-6. Note

132
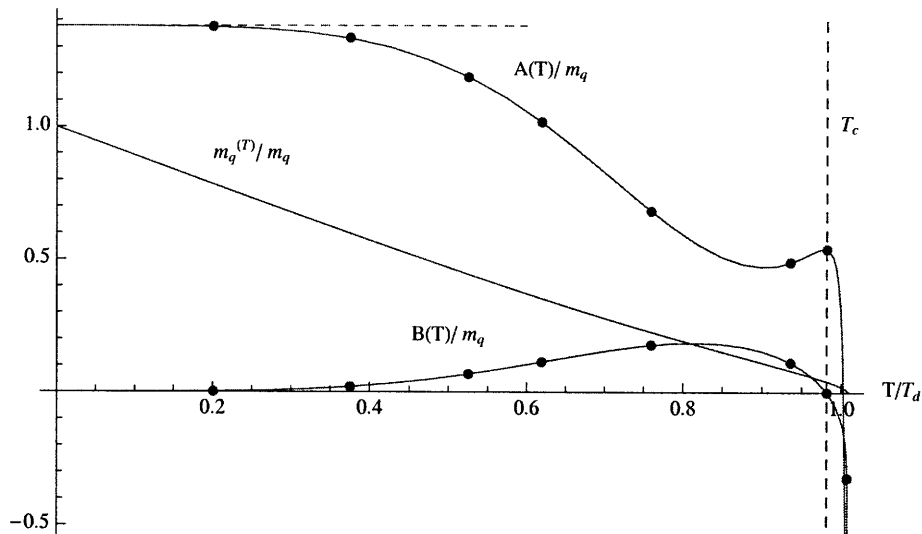
Figure 4-6: The quantities in (4.45) are plotted as a function of T/T_d. The dots represent the values of $A(T)$ and $B(T)$ obtained through fitting the numerical results to the form of the small density expansion. The actual curves come from the results of section III (which also require numerics to calculate $A(T)$.) The consistency is gratifying.

that in obtaining Fig. 4-6 we have converted the dependence on η into T and also the temperature dependence of L_0 using the relations demonstrated in Fig. 4-2.

Note that $B(T)$ is positive at small temperature and becomes negative for

$$\eta > \eta_c, \qquad \eta_c = (\frac{1}{3}(4 - \sqrt{7}))^{\frac{1}{4}}, \quad \text{i.e.} \quad T > T_c, \qquad T_c \approx .982T_d, \qquad B(T_c) = 0 \quad (4.51)$$

Also note that $A(T)$ becomes negative at some temperature higher than T_c. Furthermore it can be shown that $A(T)$ diverges at a temperature T_m ($T_m 1.008T_d$), beyond which Minkowski embedding no longer exists; clearly our analysis does not apply since there is no zero density solution about which to perturb in ϵ.

4.4 Thermodynamics

From our small ϵ analysis we can now extract some important aspects of the thermo-dynamics of this gauge theory. We will mostly work in the grand canonical ensemble, where we fix T, μ_q and use the pressure $P(\mu_q, T)$ as the appropriate thermodynamic

133

potential.

4.4.1 A third order phase transition for $0 < T < T_c$

As noted above $B(T) > 0$ for $0 < T < T_c$. In this case (4.45) may be inverted to find $\epsilon(\mu_q)$ which is then a single-valued function of μ_q for $\mu_q > m_q^{(T)}$. In other words there is only a single black hole embedding for a given fixed $\mu_q > m_q^{(T)}$. Thus for $B(T) > 0$ we conclude there is a continuous phase transition at $\mu_c = m_q^{(T)}$. For $\mu_q < m_q^{(T)}$ we have a single Minkowski embedding with $\epsilon = 0$.

Examining derivatives of the pressure on either side of $m_q^{(T)}$ one finds for $\mu_q < m_q^{(T)}$,

$$P(T,\mu) = P_0(T), \qquad n_q = \frac{\partial P_0}{\partial \mu_q} = 0, \qquad \frac{\partial^n P_0}{\partial \mu_q^n} = 0, \quad \text{for all } n \geq 1 \qquad (4.52)$$

and for $\mu_q > m_q^{(T)}$, we find

$$\frac{\partial^2 P}{\partial \mu_q^2} \propto \left(\frac{\partial \mu_q}{\partial \epsilon} \right)^{-1} = \frac{1}{A - B - B \log \epsilon} \qquad (4.53)$$

and

$$\frac{\partial^3 P}{\partial \mu_q^3} \propto -\frac{\partial^2 \mu_q}{\partial \epsilon^2} \left(\frac{\partial \mu_q}{\partial \epsilon} \right)^{-2} = \frac{B}{\epsilon} \frac{1}{(A - B - B \log \epsilon)^2} \qquad (4.54)$$

In the limit $\epsilon \to 0$, $\frac{\partial^2 P}{\partial \mu_q^2} \to 0$ and $\frac{\partial^3 P}{\partial \mu_q^3} \to \infty$. This implies that there is a third order phase transition since the third derivative of the pressure is discontinuous across the phase boundary. Also since $\frac{\partial P^2}{\partial \mu_q^2} > 0$, the system is thermodynamically stable.

Note that exactly for $B(T) = 0$ the transition becomes second order, since (4.53) is then discontinuous across the phase boundary. This happens at two places, the first is the zero temperature critical point which was studied in [41]. The second is a new critical point at $(T, \mu) = (T_c, \mu_c)$ where T_c is given in (4.51) and $\mu_c = m_q^{(T=T_c)} \approx .0418 m_q$. We will discuss the phase structure around this point in the next subsection.

In Fig. (4-1) we display the phase diagram in the $\mu_q - T$ plane, where this 3rd order phase transition is the predominant feature.

4.4.2 First order phase transition for $T > T_c$

Beyond the critical point $T > T_c$ we find that $B(T)$ becomes negative. From (4.53) this implies that $\frac{\partial^2 P}{\partial \mu_q^2}$ becomes negative in the limit of small ϵ indicating a thermodynamic instability.

To see what happens beyond T_c, let us plot μ_q at fixed T as a function of ϵ. As indicated in the left plot of Fig. 4-7 the curve drops below $\mu_q = m_q^{(T)}$. Since we expect the curve will go up again for sufficiently large density, there must be at least one minimum somewhere, which we call will $\mu_{\min}$. This minimum satisfies $\mu_{\min} < m_q^{(T)}$. That is there will be multiple black hole embeddings for a fixed $\mu_q > \mu_{\min}$ and which appear as a function of μ_q before one reaches $\mu_q = m_q^{(T)}$. This allows for the possibility of a first order phase transition from the Minkowski embedding with $\epsilon = 0$ to a black hole embedding with $\epsilon = \epsilon_d(T) \neq 0$ for some chemical potential $\mu_q = \mu_d(T)$ between $\mu_{\min} < \mu_d < m_q^{(T)}$. In this way one circumvents the thermodynamically unstable solution.
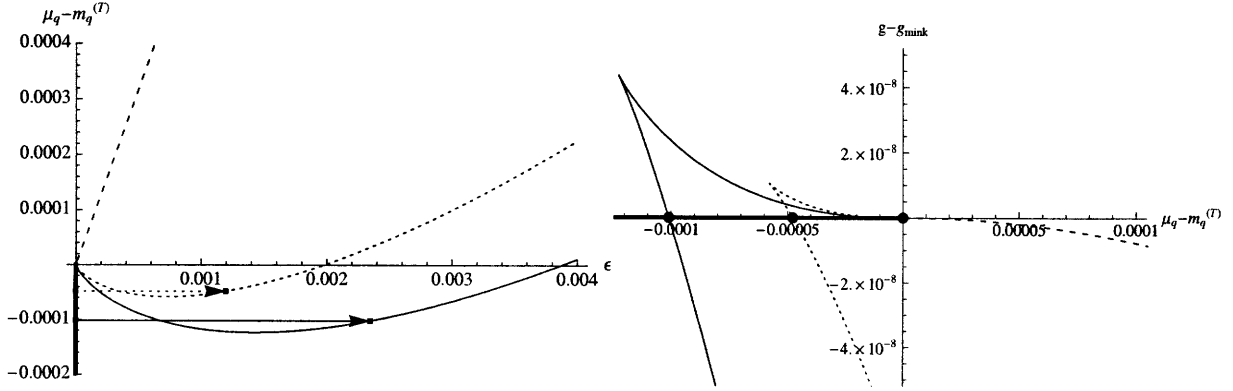
Figure 4-7: *(left)* The quark chemical potential as a function of quark density, for three temperatures $T/T_d = .980, .995, .996$. The first (long dashes) is below T_c and has no minimum. For the other two we have indicated the chemical potential at which the transition occurs. *(right)* The grand potential density (related to the pressure by $P = -g$) as a function of chemical potential for the same temperatures as the left figure.

Although this discussion was quite general for $T > T_c$, we can make it more explicit by considering temperatures $|T - T_c| \ll T_c$, then the minimum and the other black hole embedding still lie at small enough values of ϵ that (4.45) applies with only small corrections. The left plot of Fig. 4-7 gives the behavior of the chemical potential as

a function of quark density near T_c and the right plot of Fig. (4-7) demonstrates the swallow tail behavior of the pressure for this first order transition. Using (4.45), the first order transition point μ_d and the discontinuity in the density ϵ_d can be expressed in terms of the functions $A(T)$ and $B(T)$ as

$$\epsilon_d(T) \approx \exp\left(\frac{A - B/2}{B}\right) \qquad \mu_d(T) - m_q^{(T)} \approx \frac{1}{2}B\epsilon_d(T) \tag{4.55}$$

and very close to T_c we can expand $A(T)$ and $B(T)$

$$A = A_c + \mathcal{O}(T - T_c), \qquad B = -B_c'(T - T_c) + \mathcal{O}(T - T_c)^2 \tag{4.56}$$

to find

$$\varepsilon_d(T) \approx \exp\left(-\frac{A_c}{B_c'(T - T_c)}\right) = \exp(-.12T_d/(T - T_c)) \tag{4.57}$$

In Fig. (4-8) we plot ϵ_d and μ_d as functions of T near T_c using (4.55).
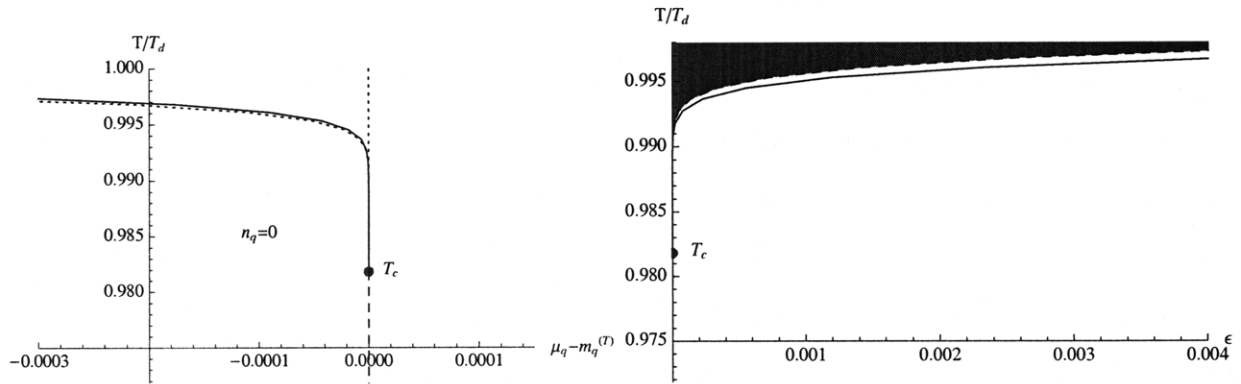
Figure 4-8: (*left*) The first order phase transition line (solid) close to the critical point, in the $(\mu_q - m_q^{(T)}) - T$ plane. Also shown (dashed) is the region where multiple embeddings are available at fixed μ_q. (*right*) The behavior of $\varepsilon_d(T)$ above the critical temperature The shaded region represents the onset of a thermodynamic instability. In the canonical ensemble this region is circumvent as usual by the Maxwell construction.

To conclude this section we note that our analysis near T_c relies on the small density behavior (4.45). An implicit assumption in our discussion is that various curves in the left plot of Fig. 4-7 does not turn back down at larger densities. While our small ϵ analysis itself does not rule out this possibility, we believe it does not

happen for temperature sufficiently close to T_c from our own numerical study of embedding solutions and from the finite density analysis of [139].[17] Our analysis of the first order phase transition cannot be trusted for temperatures too high above T_c - since then the density at the first order phase transition will lie out of the range of applicability of (4.45). Note that (4.45) is likely to break down much earlier than simply when $\epsilon \sim 1$. The reason for this is that at some temperature multiple embeddings for a fixed *density* should appear, something which our analysis has not allowed for. This is clearly the case (as discussed earlier) for zero density, where there exists a temperature $T_{bh} < T_d$ above which multiple embeddings are allowed (the original Minkowski embedding and two new black hole embeddings). [18] One expects this to be the case for small densities. Indeed these new embeddings will be continuous deformations of black hole embeddings away from zero density, so our starting point (Minkowski embeddings) is not good for seeing these multiple embeddings. As we will discuss later the reason for this break down is closely related to how this line of first order phase transition connects to the zero density dissociation transition.

4.5   Conclusions and Discussions

In this chapter we showed that in the plane of temperature v.s. baryon chemical potential there is a critical line of third order phase transition which ends at a tri-critical point after which the transition becomes first order. The critical behavior at the critical line is given by (4.45) which contains an intriguing logarithmic behavior. It would be interesting to have a microscopic understanding of this behavior, and more generally the structure of the whole phase diagram. In particular, it would be interesting to see whether the logarithmic behavior is related to the spiral behavior observed in [36, 37] at zero chemical potential. Below we discuss in more detail two open issues of our investigation.

---

[17]At some higher temperature, this could happen.

[18]Note that $T_{bh} = 0.9975 T_d$ is far enough away from $T_c = .982 T_d$ that one can trust that multiple embeddings do not appear then.

4.5.1 Connection to the dissociation transition

To complete the phase diagram, we need to address whether the first order phase transition slightly above T_c discussed in sec. 4.4.2 connects to the first order phase transition along the vertical axis at $T = T_d$ and $\mu_q = 0$, and if yes, how. Note that such a conclusion is suggested by numerical work in [40] and is consistent with the numerical work in [42].

For convenience of discussion let us first briefly review some important aspects of the transition at $\mu_q = 0$. At a low temperature there is only a single Minkowski embedding. As one increases T to a temperature T_{bh}, two new black hole embeddings appear and when one further increases the temperature to $T_d > T_{bh} = 0.997 T_d$, a first order phase transition occurs, above which one of the black hole embedding thermodynamically dominates over the Minkowski embedding. For all the embedding solutions, the baryon density is zero. Thus the discontinuity $\epsilon_d(T)$ at the phase transition is trivially zero.

We now return to the question at hand, which unfortunately our analysis for small density cannot directly answer. To see this, if we were to extrapolate our analysis of the 1st order phase transition line (the solid line in the left figure of Fig. 4-8), we find that the line $\mu_d(T)$ crosses the $\mu_q = 0$ axis at some temperature. This temperature is slightly higher than T_d and hence would seem to give an estimate of T_d itself, subject to ϵ corrections. This small difference from T_d might not seem like a problem, and one might guess we have a nice description of the physics of the zero density dissociation transition. However it is qualitatively wrong, since we also find $\epsilon_d(T)$ grows monotonically along this line. This is qualitatively wrong because on the axis $\mu_q = 0$, the phase transition should occur at zero density. This demonstrates that (4.45) must have broken down quite drastically somewhere before $\mu_d(T) = 0$ is reached.

We will now consider the simplest possibility, i.e. *assuming* that 1st order transition line from T_c does smoothly connect with the transition at zero μ_q. For this to happen the transition density $\epsilon_d(T)$ should first increase as we increase T from
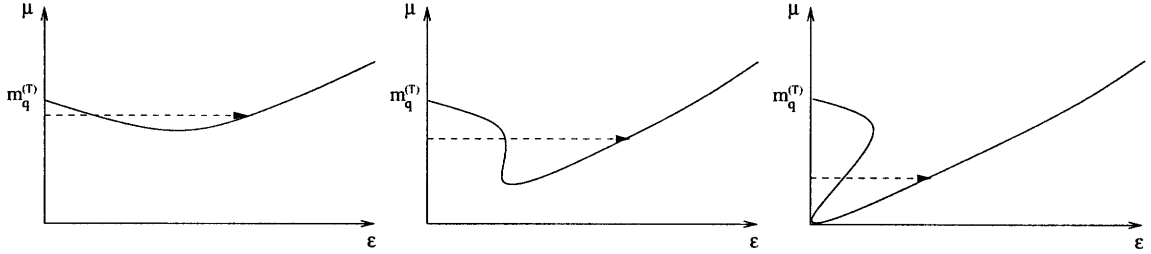
Figure 4-9: The qualitative behavior of $\mu_q(\epsilon)$ at different temperatures in order for the 1st order phase transition near T_c discussed in last section to connect to the transition at $\mu_q = 0, \varepsilon = 0$. Left plot: for a temperature T slightly above T_c. Middle plot: for a temperature T above T_c and below T_{bh}. Right plot: for $T \geq T_{bh}$.

T_c (consistent with the behavior derived from (4.45)) and then decrease to zero as T_d is approached. In turn this implies that the minimum of the curve $\mu_q(\epsilon)$ should approach the $\epsilon = 0$ axis as the temperature is increased to $T = T_{bh}$. In Fig.4-9 we plot qualitatively, at different temperatures, what is required of the curve $\mu_q(\epsilon)$ for this to happen. In particular, the minimum of the curve will hit the origin $\epsilon = \mu_q = 0$, exactly at the temperature $T = T_{bh}$, where two black hole embeddings appear at zero density. For temperatures above $T > T_{bh}$ moving towards $T = T_d$ the curve $\mu_q(\epsilon)$ is similar to that at $T = T_{bh}$. However now the point at which the 1st order phase transition occurs (which we have called (μ_d, ε_d)) should move towards the origin. Note that plots of form of Fig. 4-9 were found numerically in [39].

An important feature of the last two plots in Fig.4-9 is that when the temperature is sufficiently high, μ can be multi-valued for a fixed ϵ. For $T > T_{bh}$, this is consistent with our expectation that there should be three black hole embeddings at small ϵ, two from small density perturbations of the black hole embeddings at zero density one from the small perturbation of the Minkowski embedding which we discussed earlier in this paper. We have done some preliminary study of the behavior of the $\mu - \varepsilon$ plot near the origin for $T \sim T_{bh}$ from perturbing two black hole embeddings at zero density and confirmed the qualitative behavior presented in the last two plots. But the extrapolation to the branch we studied in this paper requires studying the finite density solution and that part of the curve is pure speculation at the moment. We leave the full exploration to future work.

Since, for high enough temperatures, there are multiple embeddings with different

chemical potentials and the same density, if we examine the thermodynamics in the canonical ensemble, there will be an interesting set of phase transitions unrelated to the one identified above that can occur between embeddings with *different* chemical potentials, but the same density. These phase transitions are quite strange, and as discussed in [139] occur between solutions which are potential thermodynamically unstable. These transitions should involve embeddings with chemical potentials higher than that at which the 1st order phase transition in the grand canonical ensemble occurs. Hence such transitions will be hidden from the point of view of the grand canonical ensemble. Since thermodynamics should be consistent in the two different ensembles one would expect that a proper consideration of the canonical ensemble using for example, the Maxwell construction of inhomogeneous phases, should remove these differences.

4.5.2   Transition at finite λ
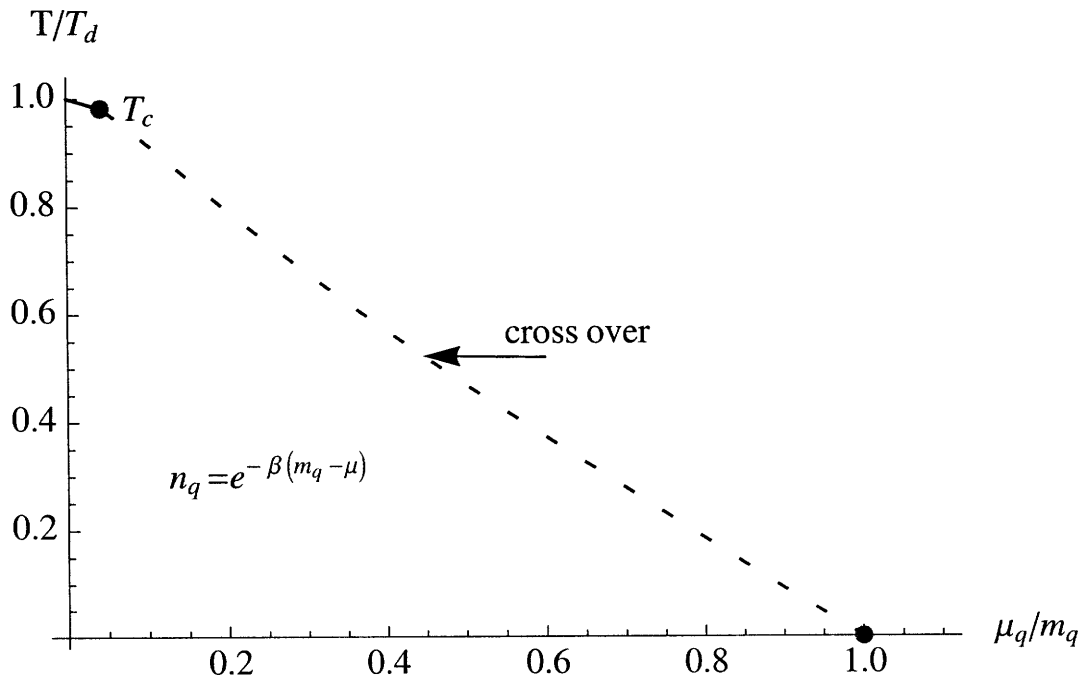
Figure 4-10: Possible phase diagram at finite λ. The lower region consists of a Boltzmann gas of quarks and anti-quarks. The third order phase transition of Fig. 4-1 is potentially smoothed to a cross over.

Another important question is what could happen to the phase diagram at finite

't Hooft coupling λ. At finite λ, as pointed out in [143] and commented upon earlier in [42], for any $\mu_q \neq 0$ at any finite temperature, the baryon charge density is in fact *nonzero*, given by a dilute Boltzmann gas of quarks. Thus in the phase diagram Fig. 4-1, the region below the critical line also has a finite density. This is of course expected for a deconfined plasma. In particular the value of quark density at the transition line should be nonzero and continuous at finite λ. This immediately raises the possibility whether the transition is smoothed into a crossover at any finite λ. To have a definite answer to this question requires summing over the instanton contributions in (4.17) for all n and then taking the limit $\mu_q \to m_q^{(T)}$ in the resulting expression. This is certainly beyond the scope of the current paper. In Fig 4-10 we plot qualitatively the structure of the phase diagram if the transition is smoothed out.

Here we mention another indirect indication that the transition might be smoothed out. In [143] we have argued that at any finite λ, in the region below the transition line in the phase diagram, the mesons have a width proportional to the sum of quark and anti-quark densities,

$$\Gamma = \frac{32\pi^3 \sqrt{\lambda}}{N_c m_q^2} |\psi(\theta = 0)|^2 (n_+ + n_-) . \tag{4.58}$$

where $n_\pm \propto \exp(-(m_q^{(T)} \pm \mu_q)/T)$ and are exponentially small in $\sqrt{\lambda}$ as argued in sec.4.2.2. $\psi(\theta = 0)$ is the meson wave function at the tip of the brane. We have also performed [144] a calculation of the meson width on the critical line from above and found at small densities exactly the same answer as (4.58).[19] Note that one of the key signatures of the phase transition at zero density (in fact potentially the defining signature) is the spectrum of mesons (quark and anti-quark bound states)[38, 37]. Here we find the meson widths and thus the spectrum are continuous across the critical line indicating that the transition might be smoothed out.

---

[19]The meson widths at small density have also been studied numerically in [126].

Appendix A

General discussion of brane embedding and fluctuations

In this appendix we present a general discussion of brane embedding in a curved spacetime (in the absence of fluxes) and its small fluctuations. We then specialize to the case of D7-branes embedded in the $AdS_5 \times S_5$ black hole geometry.

A.1   General discussion

Consider a $p + 1$-dimensional brane in a D-dimensional target space whose action is

$$S_{Dp} = -\mu_p \int d^{p+1}\xi \sqrt{-\det \tilde{h}_{ij}} \, , \tag{A.1}$$

where $\xi^i, i = 0, 1, \ldots, p$ denote the worldvolume coordinates and $\tilde{h}_{ij}$ is the induced metric in the worldvolume

$$\tilde{h}_{ij} = G_{\mu\nu}(X)\frac{\partial X^\mu}{\partial \xi^i}\frac{\partial X^\nu}{\partial \xi^j}, \qquad \mu = 0, 1, \ldots, D - 1 \, . \tag{A.2}$$

Suppose that $X_0^\mu(\xi^i)$ solves the equations of motion following from (A.1), thus describing an embedding of the brane in the target spacetime. We are interested in

understanding the behavior of small fluctuations around X_0. For this purpose, let

$$X^\mu(\xi) = X_0^\mu(\xi^i) + \delta X^\mu(\xi^i) \,. \tag{A.3}$$

The action for δX^μ can then be obtained straightforwardly from (A.1). The resulting action and equations of motion for δX^μ are, however, not geometrically transparent. This is due to the fact that $\delta X^\mu(\xi^i)$ is the difference between coordinates and thus does not have good properties under coordinate transformations. A more convenient way to parameterize $\delta X^\mu(\xi)$ is to use the exponential map to express it in terms of a vector in the tangent space at X_0^μ, as we now describe. (Such techniques have also been used in the calculation of string worldsheet beta functions [114].) Given a vector η^μ, we shoot out geodesics of unit affine parameter from X_0 with tangent η^μ. The end point of such a geodesic is identified with $X_0^\mu + \delta X^\mu$. Such a map should be one-to-one within a small neighborhood of X_0. To second order in η one may solve the geodesic differential equation, finding

$$\delta X^\mu = \eta^\mu - \frac{1}{2}\Gamma^\mu_{\alpha\beta}(X_0)\eta^\alpha\eta^\beta + \dots \,. \tag{A.4}$$

Note that the appearance of Γ is consistent with the coordinate dependence of δX; they can both be shown to have the same variation under a coordinate transformation.

Using the parametrization (A.4), we find that

$$\tilde{h}_{ij} = G_{\mu\nu}(X_0 + \delta X)\partial_i(X_0^\nu + \delta X^\nu)\partial_j(X_0^\mu + \delta X^\mu) \tag{A.5}$$

$$= h_{ij} + 2G_{\mu\nu}\lambda^\mu_{(i}\nabla_{j)}\eta^\mu + G_{\mu\nu}\nabla_i\eta^\mu\nabla_j\eta^\nu + \eta^\alpha\eta^\beta\lambda^\mu_{(i}\lambda^\nu_{j)}R_{\nu\beta\alpha\mu}$$

with

$$h_{ij} = G_{\mu\nu}(X_0)\partial_i X_0^\mu \partial_j X_0^\nu = \lambda_i^\mu\lambda_{j\mu}, \qquad \nabla_i = \lambda_i^\mu\nabla_\mu, \qquad \lambda_i^\mu = \partial_i X_0^\mu \,. \tag{A.6}$$

The simplest way to find (A.5) is to use the Riemann Normal coordinates at X_0 in which the Christoffel symbols vanish. h_{ij} is the induced metric in the worldvolume

theory and below indices i, j will be raised and lowered by h. To quadratic order in η we have

$$\sqrt{-\det \tilde{h}_{ij}} = \sqrt{-\det h_{ij}} \left(1 + \lambda^i_\nu \nabla_j \eta^\nu + \frac{1}{2} \nabla^i \eta^\mu \nabla_i \eta_\mu - (\lambda_{i\mu} \nabla_j \eta^\mu)(\lambda^{(i}_\nu \nabla^{j)} \eta^\nu) \right.$$
$$\left. + \frac{1}{2} (\lambda^i_\nu \nabla_i \eta^\nu)^2 + \frac{1}{2} \eta^\alpha \eta^\beta h^{ij} \lambda^\mu_i \lambda^\nu_j R_{\alpha\mu\nu\beta} \right) . \qquad (A.7)$$

We now take η^μ to be orthogonal to the brane worldvolume (which corresponds to choosing the static gauge), i.e.

$$\eta^\mu = \chi_s n^\mu_s(X_0), \qquad s = 1, \ldots, D - p - 1 , \qquad (A.8)$$

where $n_s(X_0)$ are unit vectors orthogonal to the worldvolume direction. Note that λ^μ_i and n^μ_s together span the full tangent space at X_0. i.e.

$$\lambda^\mu_i n_{s\mu} = 0, \qquad n_{s\mu} n^\mu_t = \delta_{st}, \qquad \lambda^\mu_i \lambda^j_\mu = \delta^j_i , \qquad (A.9)$$

and

$$\delta^\mu_\nu = \lambda^\mu_i \lambda^i_\nu + n^\mu_s n_{s\nu} . \qquad (A.10)$$

We now introduce

$$K_{sij} = \lambda^\mu_i \lambda^\nu_j \nabla_\mu n_{s\nu}, \qquad K_s = K_{sij} h^{ij}, \qquad U^i_{st} = n^\nu_s \nabla_i n_{t\nu} = n^\nu_s \lambda^\mu_i \nabla_\mu n_{t\nu} . \qquad (A.11)$$

K_{sij} is the extrinsic curvature of the brane in the s-direction, and is symmetric in i, j. (This follows from the fact that a surface orthogonal to n^μ_s satisfies $\nabla_{[\mu} n^t_{\nu]} = \sum_s v^s_{[\mu} n^s_{\nu]}$ for some one-form v^s_μ. Note also that K_{sij} can be written as $K_{sij} = \frac{1}{2} L_{n_s} h_{ij}$, where L_n is the Lie derivative along n-direction.) U^i_{st}, which is antisymmetric in s, t, is an $SO(D - 1 - p)$ connection for the transverse directions. Note that the choice of n^μ_s (and thus χ_s) is not unique. One can choose a different set of basis vectors by making an arbitrary local $SO(D - 1 - p)$ transformation. Thus χ_s transforms as a vector under the $SO(D - 1 - p)$ "gauge" symmetry and U^i_{st} transform as a connection. Note

145

that this gauge symmetry is not dynamical. With these definitions we can now write

$$\nabla_i \eta_\mu = (D_i \chi_s) n_{s\mu} + K_{sij} \chi_s \lambda^j_\mu \,, \tag{A.12}$$

where

$$D_i \chi_s = \partial_i \chi_s + U_{ist} \chi_t \tag{A.13}$$

is an $SO(D-p-1)$ covariant derivative. Using (A.12) in (A.7), we now find that

$$S_{Dp} = -\mu_p \int d^{p+1}\xi \sqrt{-\det h_{ij}} \left(1 + \chi_s K_s + \frac{1}{2} D_i \chi_s D^i \chi^s + \frac{1}{2} \chi_s \chi_t \left(-K_{sij} K_t^{ij} + R_{sijt} h^{ij} + K_s K_t \right) \right) \tag{A.14}$$

with $R_{sijt} = n_s^\alpha n_t^\beta \lambda_i^\mu \lambda_j^\nu R_{\alpha\mu\nu\beta}$. For X_0 to satisfy the equations of motion, the terms in (A.14) that are linear in the χ's have to vanish. This implies that

$$K_s = K_{sij} h^{ij} = 0, \qquad s = 1, \ldots, D-p-1 \,. \tag{A.15}$$

These are the embedding equations for the background. Thus, the action (A.14) for the small fluctuations to quadratic order becomes

$$S_{Dp} = \mu_p \int d^{p+1}\xi \sqrt{-\det h_{ij}} \left(-\frac{1}{2} D_i \chi_s D^i \chi^s - \frac{1}{2} \chi_s \chi_t \left(-K_{sij} K_t^{ij} + R_{sijt} h^{ij} \right) \right) \,. \tag{A.16}$$

We have used both the embedding equations (A.15) and the action for the small fluctuations (A.16) in Section 4.

The action (A.16) can be further simplified if n_s^μ satisfies additional constraints. For example, if n_s^μ is proportional to a Killing vector, then

$$K_{sij} = 0 \,. \tag{A.17}$$

This follows from the fact that n_s^μ satisfies $\nabla_{(\mu} n^s_{\nu)} = v_{(\mu} n^s_{\nu)}$ for some v_μ. If in addition n_s^μ is a hypersurface orthogonal, i.e. if it satisfies $\nabla_{[\mu} n^s_{\nu]} = w_{[\mu} n^s_{\nu]}$ for some one form

w_μ, then

$$U_{ist} = 0, \quad \text{for all } t . \tag{A.18}$$

We have used this simplification in Section 4.

Finally, note that equation (A.16) was written using the coordinate split (A.9). One can write it and other equations in a more covariant way by introducing

$$h_{\mu\nu} = h^{ij}\lambda_{i\mu}\lambda_{j\nu}, \qquad h_\mu{}^\nu = h^{ij}\lambda_{i\mu}\lambda_j^\nu, \qquad h^{\mu\nu} = h^{ij}\lambda_i^\mu\lambda_j^\nu , \tag{A.19}$$

and using these objects in place of h_{ij} and λ_i^μ in various places. $h_{\mu\nu} = g_{\mu\nu} - n_{s\mu}n_{s\nu}$ is the covariant induced metric on the brane and $h_\mu{}^\nu$ is the projector onto the world-volume directions.

A.2   D7-branes in $AdS_5 \times S_5$ black hole

We now specialize to the case of D7-branes considered in the main text, where we have two transverse directions with

$$n_1^\nu = \frac{1}{N_1}\left(\left(\frac{\partial}{\partial y}\right)^\nu - y_0'(\rho)\left(\frac{\partial}{\partial\rho}\right)^\nu\right) , \quad n_2^\nu = \frac{1}{N_2}\left(\frac{\partial}{\partial\phi}\right)^\nu , \tag{A.20}$$

where $N_{1,2}$ are normalization factors. In this case U_{st}^i is proportional to the two-dimensional antisymmetric tensor ϵ_{st}. It is easy to see that n_2^ν is both hypersurface orthogonal and proportional to a Killing vector (since nothing depends on ϕ). We thus have $K_{2ij} = 0$ and $U_{12}^i = 0$. The action (A.16) now reduces to the form we have used in Section 4, namely

$$S_{D7} = \mu_7 \int d^8\xi\sqrt{-h}\left(1 + \frac{1}{2}(\partial\phi_1)^2 + \frac{1}{2}(\partial\phi_2)^2 + \frac{1}{2}m_1^2\phi_1^2 + \frac{1}{2}m_2^2\phi_2^2\right) , \tag{A.21}$$

where the "masses" are given by

$$m_1^2 = -R_{11} - R_{2112} - K_{1ij}K_1^{ij} , \tag{A.22}$$

$$m_2^2 = -R_{22} - R_{2112} , \tag{A.23}$$

147

with R_{2112}, R_{11} and R_{22} as defined in (2.62). In writing (A.21)–(A.23) we have used the identities

$$R_{sijt}h^{ij} = n_s^\alpha n_t^\beta h^{ij}\lambda_i^\mu \lambda_j^\nu R_{\alpha\mu\nu\beta} = -R_{st} - R_{s11t} - R_{s22t}, \qquad s,t = 1,2 \qquad \text{(A.24)}$$

and the fact that $R_{12} = 0$ for the $AdS_5 \times S_5$ black hole spacetime. We can also use the generalization of the Gauss-Codazzi relation for a codimension two surface which we derive in Section A.3, see Eq. (A.28), to write

$$K_{1ij}K_1^{ij} = -\,^{(8)}R + R - 2R_{11} - 2R_{22} - 2R_{2112} \;. \qquad \text{(A.25)}$$

Therefore, m_1^2 in (A.22) can equivalently be written as

$$m_1^2 = R_{11} + R_{2112} + 2R_{22} + \,^{(8)}R - R \;, \qquad \text{(A.26)}$$

which is the form that we used in Section 4.

A.3 Gauss-Codazzi relations for co-dimension 2

Define the covariant derivative on the D7 brane as

$$D_\alpha s^\beta \equiv h_\alpha^\mu h_\nu^\beta \nabla_\mu s^\nu \;. \qquad \text{(A.27)}$$

This is equivalent to the covariant derivative defined with respect to h_{ij}. We can now use D_α to define the curvature of the D7-brane and then relate it to the curvature of the full space. Calculations similar to those in [115] reveal that

$$^{(8)}R_{ijk}{}^l = P(R)_{ijk}{}^l + (K^s)_{ik}(K^s)_j^l - (K^s)_{jk}(K^s)_i^l \;, \qquad \text{(A.28)}$$

148

where s labels the two directions perpendicular to the brane and is summed over. $P(R)$ is the projection of the full Riemann tensor onto the D7-brane,

$$P(R)_{ijk}{}^{l} = \lambda_i^\mu \lambda_j^\nu \lambda_k^\alpha \lambda_\beta^l R_{\mu\nu\alpha}{}^{\beta} \ . \tag{A.29}$$

Taking further contractions of Eq. (A.28) with δ_j^l and h^{ik} and using Eq.(A.10) gives

$$^{(8)}R = R - 2R_{ss} - R_{tsst} + K_s K_s - \left(K_{sij} K_s^{ij}\right), \tag{A.30}$$

where s, t are both summed. In the case of interest, where $K_{2ij} = 0$ because n_2^μ is proportional to a Killing vector and where $K_s = 0$ is the embedding equation, we obtain (A.25).

Appendix B

Dp-Dq-Brane Theories

It will be of interest in future to study the degree to which the meson dispersion relations that we have derived, together with their consequences like (2.128) and (2.129), change as one modifies the gauge theory to make it more QCD-like. In this appendix, we report on a check that we have mentioned in Section 6 in which the gauge theory is modified, albeit not in the direction of QCD. We consider the $(p+1)$-dimensional gauge theories described by N Dp-branes [110] into which fundamental quarks, and hence mesons, have been introduced by embedding N_f Dq-branes [111, 105, 36, 37]. The Dp-branes fill coordinates $0, 1, \ldots, p$. The Dq-branes fill coordinates $0, 1, \ldots, d$, where $d \leq p$, as well as $q - d$ of the remaining $9 - p$ coordinates. In the large-N limit, the near horizon geometry of the Dp-branes is dual to a $(p+1)$-dimensional supersymmetric Yang-Mills theory with 16 supercharges that is nonconformal for $p \neq 3$. We will restrict to $p < 5$. In the $N_f/N \to 0$ approximation, the Dq-branes live in the background Dp-brane geometry, and their back-reaction on the geometry can be neglected. Strings which stretch between the Dq- and the Dp-branes are dual to N_f fundamental quarks in the gauge theory. We shall set $N_f = 1$. And, scalar mesons in the gauge theory are represented by fluctuations of the position of the Dq-brane. The specific case that we have analyzed throughout most of this paper is $p = d = 3$, $q = 7$. In this more general setting, as in the specific case, there is a dissociation transition at some T_{diss} at which the spectrum of meson fluctuations changes from discrete to continuous.

The background Dp-brane geometry is described by the metric [110]

$$ds^2 = R^2 \left(\frac{R}{L_0}\right)^{(3-p)/2} \left(-fdt^2 + r^{(7-p)/2}dx_p^2 + \frac{r^{(p-3)/2}}{u^2}\left(d\rho^2 + dy^2 + \rho^2 d\Omega^2_{q-d-1} + y^2 d\Omega^2_{8-p-q+d}\right)\right)$$

(B.1)

and the dilaton

$$e^\phi = \left(\frac{L_0}{R}\right)^{(p-3)(7-p)/4} g_s r^{(p-3)(7-p)/4} ,$$

(B.2)

where

$$f = u^{-(7-p)/2} \frac{\left(u^{7-p} - \varepsilon^{(7-p)/2}\right)^2}{u^{7-p} + \varepsilon^{(7-p)/2}} ,$$

(B.3)

$$r^{(7-p)/2} = u^{-(7-p)/2}\left(u^{7-p} + \varepsilon^{(7-p)/2}\right) ,$$

(B.4)

$$u^2 = y^2 + \rho^2 ,$$

(B.5)

and where we are using dimensionless coordinates as in (2.44). The black hole horizon is located at $u = u_0 \equiv \sqrt{\varepsilon}$. L_0 specifies the position where the Dq-brane that we introduce will sit, as follows. We shall embed a Dq-brane described, in the absence of fluctuations, by a curve $y(\rho)$ with the Dq-brane placed such that its tip is located at $\rho = 0$ and $y = L_0$, and then use L_0 to rescale metric coordinates such that the tip of the Dq-brane is at $y(0) = 1$. After this rescaling, the metric and dilaton are given by (B.1) and (B.2). The holographic dictionary determines the coupling, number of colors, and temperature in the gauge theory via

$$\lambda = \frac{(16\pi^3)^{(p-3)/2}}{\Gamma\left(\frac{7-p}{2}\right)} R^{7-p}\alpha'^{p-5} ,$$

(B.6)

$$\frac{\lambda}{N} = 2^{p-1}\pi^{p-2}g_s\alpha'^{(p-3)/2} ,$$

(B.7)

$$T = \frac{(7-p)2^{(5-p)/(7-p)}}{4\pi} u_0^{(5-p)/2}R^{-1}\left(\frac{L_0}{R}\right)^{(5-p)/2} .$$

(B.8)

Note that λ has dimension $p-3$, making it useful to define the dimensionless coupling

$$\lambda_{\text{eff}} \equiv \lambda T^{p-3} .$$

(B.9)

The differential equation that specifies the shape of the embedding curve $y(\rho)$ can be derived as we did in obtaining (2.40). For the special case in which $p-d+q-d=4$, the embedding equation simplifies, becoming

$$\frac{y''}{1+y'^2} + \frac{(q-d-1)y'}{\rho} = \frac{2\varepsilon^{(7-p)/2}(y-y'\rho)}{u^2}\left(\frac{(3-d)u^{7-p}+(q-d)\varepsilon^{(7-p)/2}}{u^{2(7-p)}-\varepsilon^{7-p}}\right).$$

(B.10)

We have scaled our variables so that the tip of the Dq-brane is at $y(0)=1$; in order to have a smooth embedding we require $y'(0)=0$; using these boundary conditions, we can then solve the embedding equation and obtain $y(\infty)$, which defines ϵ_∞ via $y(\infty)=\sqrt{\varepsilon/\epsilon_\infty}$, . Finally, we can determine what the mass m_q of the quarks that we are analyzing is via

$$m_q^2 = \frac{\varepsilon L_0^2}{4\pi^2\epsilon_\infty \alpha'^2}.$$

(B.11)

From (B.6), (B.8) and (B.11) we find that

$$\epsilon_\infty = a_p\left(\frac{T}{m_q}\right)^2 \lambda_{\text{eff}}^{2/(5-p)} = a_p\frac{\lambda^{2/(5-p)}T^{4/(5-p)}}{m_q^2},$$

(B.12)

where the constant a_p is given by

$$a_p = \frac{2^{(10-2p)/(7-p)}\pi^{(3-p)/(5-p)}}{(7-p)^{4/(5-p)}}\left(\Gamma\left(\frac{7-p}{2}\right)\right)^{2/(5-p)}.$$

(B.13)

We also note that the energy density of the plasma is given by [110]

$$\rho = b_p N^2 T^{p+1}\lambda_{\text{eff}}^{(p-3)/(5-p)} = b_p N^2 \lambda^{(p-3)/(5-p)}T^{(14-2p)/(5-p)},$$

(B.14)

where the constant b_p is given by

$$b_p = \frac{(9-p)\,2^6\,\pi^{(13-3p)/(5-p)}}{(7-p)^{(19-3p)/(5-p)}}\left(\Gamma\left(\frac{7-p}{2}\right)\right)^{2/(5-p)}.$$

(B.15)

This means that

$$\left(\frac{\epsilon_\infty}{\epsilon_\infty^{\text{diss}}}\right)^{(7-p)/2} = \frac{\rho(T)}{\rho_{\text{diss}}},$$

(B.16)

where the zero-velocity mesons dissociate at a temperature T_{diss} corresponding to $\rho = \rho_{\text{diss}}$ and $\epsilon_\infty = \epsilon_\infty^{\text{diss}}$, with $\epsilon_\infty^{\text{diss}}$ a constant of order unity.

We shall not repeat our construction of the meson wave functions and dispersion relations for the Dp-Dq system here. Instead, we shall assume that in the large-k limit the meson wave functions become localized at the tip of the Dq brane at $\rho = 0$ and $y = 1$, as we found for the D3-D7 system. As a consequence, the limiting meson velocity will be given by the local speed of light at the tip of the Dq-brane. This velocity can be read from the metric (B.1), and is given by

$$v_0 = \left(\frac{1 - \varepsilon^{(7-p)/2}}{1 + \varepsilon^{(7-p)/2}} \right) . \tag{B.17}$$

In Section 6 we have analyzed this result in the small ε limit, showing that in this limit it takes on the form (2.131) for any p. This illustrates the generality of the result (2.128) when it is phrased in terms of the energy density. Here, we shall analyze (B.17) at arbitrary $\varepsilon < 1$, seeking to compare it to (2.129). From (B.17) and (B.16) we see that the critical velocity satisfies

$$\frac{1 - v_0}{1 + v_0} = \frac{1 - v_0^2}{(1 + v_0)^2} = \varepsilon^{(7-p)/2} = \frac{\rho}{\rho_{\text{diss}}} \left(\epsilon_\infty^{\text{diss}} \frac{\varepsilon}{\epsilon_\infty} \right)^{(7-p)/2} . \tag{B.18}$$

Recall that $\epsilon_\infty^{\text{diss}}$ is a constant of order unity and that $\varepsilon/\epsilon_\infty$ is a weak function of temperature and hence of ρ, obtained by solving the embedding equation and making a plot of ϵ_∞ vs. ε as in Fig. 2-2, and reading off the ratio.

Much as we did in Section 6, we can see (B.18) either as giving the limiting velocity v_0 as a function of ρ, or as giving $\rho_{\text{diss}}(v)$, the energy density above which no mesons with velocity v exist, via

$$\rho_{\text{diss}}(v) = (1 - v^2)\rho_{\text{diss}} \left[\frac{1}{(1 + v)^2} \left(\epsilon_\infty^{\text{diss}} \frac{\varepsilon}{\epsilon_\infty} \right)^{(p-7)/2} \right] . \tag{B.19}$$

This is the generalization of (2.129) to the Dp-Dq system. It is written somewhat implicitly, since $\varepsilon/\epsilon_\infty$ which occurs within the square brackets is a weak function of $\rho_{\text{diss}}(v)$. It is nevertheless manifest that the entire expression in the square brackets

is a weak function of v, varying from one constant of order one at $v = 0$ to some different constant of order one at $v = 1$. As in (2.125), we can then define a function $f(v)$ by rewriting (B.19) as

$$\rho_{\text{diss}}(v) = [f(v)]^{(14-2p)/(5-p)} \frac{\rho_{\text{diss}}(0)}{\gamma^2}, \tag{B.20}$$

where $\gamma = 1/\sqrt{1 - v^2}$ is the Lorentz boost factor. Equivalently, using (B.14) we can write

$$T_{\text{diss}}(v) = f(v) \frac{T_{\text{diss}}(0)}{\gamma^{(5-p)/(7-p)}} . \tag{B.21}$$

We have seen in Fig. 2-12 that for the D3-D7 brane system, $f(v)$ is everywhere close to 1, with $f(1) = 0.924$ being the farthest it gets from 1. We have also done the exercise of solving the embedding equations for $p = 4$, the D4-D6 brane system with $d = 3$, and find in that case that the farthest that $f(v)$ gets from $f(v) = 1$ is $f(1) = 1.048$.

Given its derivation via (B.18), it would have been reasonable to try writing

$$\rho_{\text{diss}}(v) = \left[\tilde{f}(v)\right]^{(14-2p)/(5-p)} \rho_{\text{diss}}(0) \frac{1-v}{1+v} \tag{B.22}$$

instead of (B.20). This does not work as well, yielding a $\tilde{f}(v)$ that reaches 1.306 for the D3-D7 system and 1.261 for the D4-D6 system. So although there is no important parametric difference between (B.22) and (B.20), we have focussed on the form (B.20), and hence (B.21), throughout this paper.

The most important conclusion from our Dp-Dq investigation in this Appendix comes by comparing (B.20) and (B.21). We see that in all the Dp-Dq systems we analyze, the leading velocity dependence of $\rho_{\text{diss}}(v)$ is that it is proportional to $1/\gamma^2$, as if the mesons see a boosted energy density as we discussed in Section 2. In contrast, $T_{\text{diss}}(v)$ scales with a power of γ that depends on p.

Appendix C

The zero temperature solution at small densities

One way to motivate the scaling of the inner region $\rho = \sigma \epsilon^{1/2}$ is to look at the zero temperature solution in detail, where the exact solution is known.

This solution is:

$$y'(\rho) = \frac{c}{\sqrt{\rho^6 + \epsilon^2 - c^2}} \qquad a'(\rho) = \frac{\epsilon}{c} y'(\rho) \tag{C.1}$$

where c is an integration constant related to the expectation of the mass operator dual to the field y on the gravity side. The boundary conditions are $y(0) = a(0) = 0$.

We can fix c in terms of the quark mass, or equivalently in terms of L. After rescaling as (4.8) by $L_0 = L$ the condition $y(\infty) = 1$ fixes the quark mass. Integrating (C.1) one finds for c,

$$\kappa^3 c^3 = \left(\epsilon^2 - c^2 \right)$$

where κ is a number defined by the integral, $\kappa = \int_0^\infty dx/(x^6 + 1)$. For small densities the condensate c approaches ϵ as,

$$c \approx \epsilon - (\kappa/L)^3 \epsilon^2 \,, \qquad \epsilon^2 - c^2 \approx \epsilon^3 (\kappa/L)^3 \tag{C.2}$$

Note that by small densities we really mean $\epsilon \ll L^3$ or equivalently $n_q/(N_c \sqrt{\lambda}) \ll m_q^3$.

157

From (C.1) it is clear the cross over scale for $y(\rho)$ between a flat Minkowski embedding and the curved solution going to the (AdS) horizon is $\rho^6 \sim \epsilon^2 - c^2$ or $\rho \sim \epsilon^{1/2}$ at small densities. This is the scaling that we set out to demonstrate.

Rescaling $\sigma = \rho/\epsilon^{1/2}$ we find the zero temperature *inner* solution becomes,

$$\frac{dY_0}{d\sigma} \approx \frac{1}{\sqrt{\sigma^6 + (\kappa)^3}} \tag{C.3}$$

In this limit the chemical potential to order ϵ receives contributions only from inner region with the result

$$\mu_q = \frac{L}{2\pi\alpha'} \left(1 + \frac{1}{2}\kappa^3\epsilon + \mathcal{O}(\epsilon^2) \right) \tag{C.4}$$

Appendix D

Detailed analysis of the chemical potential

In this appendix we give some details in the small ϵ-expansion of μ_q, equation (4.21), which we copy here for convenience

$$\mu_q = \frac{L_0}{2\pi\alpha'}\epsilon \int_{\rho_c}^{\infty} d\rho\, \frac{\sqrt{fq(1+y'^2)}}{\sqrt{\epsilon^2 + \rho^6 q^3}}\ . \tag{D.1}$$

Various functions in (D.1) were introduced in (4.9). We split the above integral into those over the inner and outer regions

$$\mu_q = \int_{\rho_c}^{\rho_\Lambda}(\cdots) + \int_{\rho_\Lambda}^{\infty}(\cdots) \equiv \mu_\mathcal{I} + \mu_\mathcal{O} \tag{D.2}$$

which can then be expanded in terms of ϵ using the expansions (4.24), (4.25) of $y(\rho)$ in inner and outer regions respectively.

Let us first look at $\mu_\mathcal{O}$. We find that it starts with order ϵ

$$\mu_\mathcal{O} = \epsilon\, \mu_\mathcal{O}^{(1)} + O(\epsilon^2) \tag{D.3}$$

with

$$\frac{2\pi\alpha'}{L_0}\mu_\mathcal{O}^{(1)} = \int_{\rho_\Lambda}^{\infty} d\rho \frac{(1 - \eta^4/u^4)\sqrt{1 + y_0'^2}}{(1 + \eta^4/u^4)^2\, \rho^3} \tag{D.4}$$

159

and $u^2 = \rho^2 + y_0^2(\rho)$. Using the expansion (4.26) of y_0 at small ρ, we find that the integral contains a quadratic and a logarithmic divergent term in the limit $\rho_\Lambda \to 0$, given by

$$\frac{2\pi\alpha'}{L_0}\mu_{\mathcal{O}}^{(1)} = \frac{1 - \eta^4}{2(1 + \eta^4)^2\rho_\Lambda^2} - \frac{2\eta^4(3 - \eta^4 + 3\eta^8)}{(1 - \eta^4)(1 + \eta^4)^4}\log(\rho_\Lambda) + K_{\mathcal{O}} \qquad (D.5)$$

where $K_{\mathcal{O}}$ denotes the finite part of the integral. It can be defined more precisely by

$$K_{\mathcal{O}} = \lim_{\rho_\Lambda \to 0} \left[\int_{\rho_\Lambda}^{\infty} d\rho \frac{(1 - \eta^4/u^4)\sqrt{1 + y_0'^2}}{(1 + \eta^4/u^4)^2\rho^3} - \frac{(1 - \eta^4)}{2(1 + \eta^4)^2\rho_\Lambda^2} - \frac{2\eta^4(3 - \eta^4 + 3\eta^8)}{(-1 + \eta^4)(1 + \eta^4)^4}\log(\rho_\Lambda) \right]$$
$$(D.6)$$

Once $y_0(\rho)$ is known numerically, $K_{\mathcal{O}}$ can be calculated numerically.

We now look at $\mu_{\mathcal{I}}$ which can be expanded as

$$\mu_{\mathcal{I}} = \mu_{\mathcal{I}}^{(0)} + \epsilon\mu_{\mathcal{I}}^{(1)} + \cdots \qquad (D.7)$$

Bibliography

[1] D. Teaney, "Effect of shear viscosity on spectra, elliptic flow, and Hanbury Brown-Twiss radii," Phys. Rev. C **68**, 034913 (2003) [arXiv:nucl-th/0301099];

[2] K. Dusling and D. Teaney, "Simulating elliptic flow with viscous hydrodynamics," Phys. Rev. C **77**, 034905 (2008) [arXiv:0710.5932 [nucl-th]].

[3] M. Luzum and P. Romatschke, "Conformal Relativistic Viscous Hydrodynamics: Applications to RHIC results a: sqrt(sNN) = 200 GeV," Phys. Rev. C **78**, 034915 (2008) [Erratum-ibid. C **79**, 039903 (2009)] [arXiv:0804.4015 [nucl-th]].

[4] D. T. Son and A. O. Starinets, "Visocisty, Black Holes, and Quantum Field theory" Ann. Rev. Nucl. Part. Sci. **57**, 95 (2007) [arXiv:0704.0240 [hep-th]].

[5] G. Policastro, D. T. Son and A. O. Starinets, "From AdS/CFT correspondence to hydrodynamics," JHEP **0209**, 043 (2002) [arXiv:hep-th/0205052].

[6] G. Policastro, D. T. Son and A. O. Starinets, "The shear viscosity of strongly coupled N = 4 supersymmetric Yang-Mills plasma," Phys. Rev. Lett. **87**, 081601 (2001) [arXiv:hep-th/0104066].

[7] C. P. Herzog, A. Karch, P. Kovtun, C. Kozcaz and L. G. Yaffe, "Energy loss of a heavy quark moving through N = 4 supersymmetric Yang-Mills plasma," JHEP **0607**, 013 (2006) [arXiv:hep-th/0605158].

[8] S. S. Gubser, "Drag force in AdS/CFT," Phys. Rev. D **74**, 126005 (2006) [arXiv:hep-th/0605182];

[9] H. Liu, K. Rajagopal and U. A. Wiedemann, "Calculating the jet quenching parameter from AdS/CFT," Phys. Rev. Lett. **97**, 182301 (2006) [arXiv:hep-ph/0605178];

[10] H. Liu, K. Rajagopal and U. A. Wiedemann, "An AdS/CFT calculation of screening in a hot wind," Phys. Rev. Lett. **98**, 182301 (2007) [arXiv:hep-ph/0607062].

[11] H. Liu, K. Rajagopal and U. A. Wiedemann, "Wilson loops in heavy ion collisions and their calculation in AdS/CFT," JHEP **0703**, 066 (2007) [arXiv:hep-ph/0612168].

[12] K. Peeters, J. Sonnenschein and M. Zamaklar, "Holographic melting and related properties of mesons in a quark gluon plasma," Phys. Rev. D **74**, 106008 (2006) [arXiv:hep-th/0606195];

[13] M. Chernicoff, J. A. Garcia and A. Guijosa, "The energy of a moving quark-antiquark pair in an N = 4 SYM plasma," JHEP **0609**, 068 (2006) [arXiv:hep-th/0607089]; see also Appendix A of

[14] T. Matsui and H. Satz, "J / Psi Suppression By Quark - Gluon Plasma Formation," Phys. Lett. B **178**, 416 (1986).

[15] O. Kaczmarek and F. Zantow, "Static quark anti-quark interactions in zero and finite temperature QCD. I: Heavy quark free energies, running coupling and quarkonium binding," Phys. Rev. D **71**, 114510 (2005) [arXiv:hep-lat/0503017].

[16] For a review, see H. Satz, "Colour deconfinement and quarkonium binding," J. Phys. G **32** (2006) R25 [arXiv:hep-ph/0512217].

[17] F. Karsch, D. Kharzeev and H. Satz, "Sequential charmonium dissociation," Phys. Lett. B **637**, 75 (2006) [arXiv:hep-ph/0512239].

[18] J. M. Maldacena, "The large N limit of superconformal field theories and supergravity," Adv. Theor. Math. Phys. **2**, 231 (1998) [Int. J. Theor. Phys. **38**, 1113 (1999)] [arXiv:hep-th/9711200];

[19] E. Witten, "Anti-de Sitter space and holography," Adv. Theor. Math. Phys. **2**, 253 (1998) [arXiv:hep-th/9802150];

[20] S. S. Gubser, I. R. Klebanov and A. M. Polyakov, "Gauge theory correlators from non-critical string theory," Phys. Lett. B **428**, 105 (1998) [arXiv:hep-th/9802109];

[21] O. Aharony, S. S. Gubser, J. M. Maldacena, H. Ooguri and Y. Oz, "Large N field theories, string theory and gravity," Phys. Rept. **323**, 183 (2000) [arXiv:hep-th/9905111].

[22] E. Witten, "Anti-de Sitter space, thermal phase transition, and confinement in gauge theories," Adv. Theor. Math. Phys. **2** *ibid.* 505 (1998); [arXiv:hep-th/9803131];

[23] P. K. Kovtun and A. O. Starinets, "Quasinormal modes and holography," Phys. Rev. D **72**, 086009 (2005) [arXiv:hep-th/0506184].

[24] R. C. Myers and S. E. Vazquez, "Quark Soup al dente: Applied Superstring Theory," Class. Quant. Grav. **25**, 114008 (2008) [arXiv:0804.2423 [hep-th]].

[25] S. S. Gubser, I. R. Klebanov and A. A. Tseytlin, "Coupling constant dependence in the thermodynamics of N = 4 supersymmetric Yang-Mills theory, " Nucl. Phys. B **534**, 202 (1998) [arXiv:hep-th/9805156]

[26] A. Bazavov *et al.* "Equation of state and QCD transition at finite temperature," arXiv:0903.4379 [hep-lat]

[27] J. M. Maldacena, "Wilson loops in large N field theories," Phys. Rev. Lett. **80**, 4859 (1998) [arXiv:hep-th/9803002].

[28] S. J. Rey and J. T. Yee, "Macroscopic strings as heavy quarks in large N gauge theory and anti-de Sitter supergravity," Eur. Phys. J. C **22**, 379 (2001) [arXiv:hep-th/9803001].

[29] S. J. Rey, S. Theisen and J. T. Yee, "Wilson-Polyakov loop at finite temperature in large N gauge theory and anti-de Sitter supergravity," Nucl. Phys. B **527**, 171 (1998) [arXiv:hep-th/9803135];

[30] A. Brandhuber, N. Itzhaki, J. Sonnenschein and S. Yankielowicz, "Wilson loops in the large N limit at finite temperature," Phys. Lett. B **434**, 36 (1998) [arXiv:hep-th/9803137];

[31] M. C. Chu and T. Matsui, "Dynamic Debye screening for a heavy anti-quark pair traversing a quark gluon plasma," Phys. Rev. D **39**, 1892 (1989).

[32] F. Karsch, E. Laermann and A. Peikert, "The pressure in 2, 2+1 and 3 flavour QCD," Phys. Lett. B **478**, 447 (2000) [arXiv:hep-lat/0002003];

[33] F. Karsch, "Lattice results on QCD thermodynamics," Nucl. Phys. A **698**, 199 (2002) [arXiv:hep-ph/0103314].

[34] E. Caceres, M. Natsuume and T. Okamura, "Screening length in plasma winds," JHEP **0610**, 011 (2006) [arXiv:hep-th/0607233].

[35] H. Liu, K. Rajagopal and Y. Shi, "Robustness and Intrared Sensitivity of Various Observables in the Application of AdS/CFT to Heavy Ion Collisions," JHEP **8080**, 048 (2008) [arXiv:0803.3214 [hep-ph]].

[36] D. Mateos, R. C. Myers and R. M. Thomson, "Holographic phase transitions with fundamental matter," Phys. Rev. Lett. **97**, 091601 (2006) [arXiv:hep-th/0605046].

[37] D. Mateos, R. C. Myers and R. M. Thomson, "Thermodynamics of the brane," JHEP **0705**, 067 (2007) [arXiv:hep-th/0701132].

[38] C. Hoyos, K. Landsteiner and S. Montero, "Holographic Meson Melting," JHEP **0704**, 031 (2007) [arXiv:hep-th/0612169].

[39] S. Nakamura, Y. Seo, S. J. Sin and K. P. Yogendran, "Baryon-charge Chemical Potential in AdS/CFT," Prog. Theor. Phys. **120**, 51 (2008) [arXiv:0708.2818 [hep-th]].

[40] K. Ghoroku, M. Ishihara and A. Nakamura, "D3/D7 holographic Gauge theory and Chemical potential," Phys. Rev. D **76**, 124006 (2007) [arXiv:0708.3706 [hep-th]].

[41] A. Karch and A. O'Bannon, "Holographic Thermodynamics at Finite Baryon Density: Some Exact Results," JHEP **0711**, 074 (2007) [arXiv:0709.0570 [hep-th]].

[42] D. Mateos, S. Matsuura, R. C. Myers and R. M. Thomson, "Holographic phase transitions at finite chemical potential," JHEP **0711**, 085 (2007) [arXiv:0709.1225 [hep-th]].

[43] J. Babington, J. Erdmenger, N. J. Evans, Z. Guralnik and I. Kirsch, "Chiral symmetry breaking and pions in non-supersymmetric gauge / gravity duals," Phys. Rev. D **69**, 066007 (2004) [arXiv:hep-th/0306018].

[44] I. Kirsch, "Generalizations of the AdS/CFT correspondence," Fortsch. Phys. **52**, 727 (2004) [arXiv:hep-th/0406274].

[45] T. Albash, V. G. Filev, C. V. Johnson and A. Kundu, "A topology-changing phase transition and the dynamics of flavour," Phys. Rev. D **77**, 066004 (2008) [arXiv:hep-th/0605088].

[46] J. Sonnenschein, "What does the string / gauge correspondence teach us about Wilson loops?," arXiv:hep-th/0003032.

[47] J. Kuti, J. Polonyi and K. Szlachanyi, "Monte Carlo Study Of SU(2) Gauge Theory At Finite Temperature," Phys. Lett. B **98** (1981) 199;

[48] L. D. McLerran and B. Svetitsky, "A Monte Carlo Study Of SU(2) Yang-Mills Theory At Finite Temperature," Phys. Lett. B **98** (1981) 195;

[49] L. D. McLerran and B. Svetitsky, "Quark Liberation At High Temperature: A Monte Carlo Study Of SU(2) Gauge Phys. Rev. D **24** (1981) 450;

[50] O. Kaczmarek, F. Karsch, P. Petreczky and F. Zantow, "Heavy quark anti-quark free energy and the renormalized Polyakov loop," Phys. Lett. B **543** (2002) 41 [arXiv:hep-lat/0207002].

[51] O. Kaczmarek, F. Karsch, F. Zantow and P. Petreczky, "Static quark anti-quark free energy and the running coupling at finite temperature," Phys. Rev. D **70**, 074505 (2004) [Erratum-ibid. D **72**, 059903 (2005)] [arXiv:hep-lat/0406036].

[52] P. Petreczky and K. Petrov, "Free energy of a static quark anti-quark pair and the renormalized Polyakov loop in three flavor QCD," Phys. Rev. D **70** (2004) 054503 [arXiv:hep-lat/0405009].

[53] Y. Maezawa, S. Ejiri, T. Hatsuda, N. Ishii, N. Ukita, S. Aoki and K. Kanaya, "Static quark free energies at finite temperature with two flavors of improved Wilson quarks," PoS **LAT2006**, 141 (2006) [arXiv:hep-lat/0610013].

[54] For a review, see F. Karsch, d"Properties of the quark gluon plasma: A lattice perspective," Nucl. Phys. A **783**, 13 (2007) [arXiv:hep-ph/0610024].

[55] M. Asakawa, T. Hatsuda and Y. Nakahara, "Maximum entropy analysis of the spectral functions in lattice QCD," Prog. Part. Nucl. Phys. **46** (2001) 459 [arXiv:hep-lat/0011040];

[56] T. Umeda, R. Katayama, O. Miyamura and H. Matsufuru, "Study of charmonia near the deconfining transition on an anisotropic lattice with O(a) improved quark action," Int. J. Mod. Phys. A **16** (2001) 2215 [arXiv:hep-lat/0011085];

[57] T. Umeda, K. Nomura and H. Matsufuru, "Charmonium at finite temperature in quenched lattice QCD," Eur. Phys. J. C **39S1**, 9 (2005) [arXiv:hep-lat/0211003];

[58] M. Asakawa and T. Hatsuda, "J/psi and eta/c in the deconfined plasma from lattice QCD," Phys. Rev. Lett. **92**, 012001 (2004) [arXiv:hep-lat/0308034];

[59] S. Datta, F. Karsch, P. Petreczky and I. Wetzorke, "Behavior of charmonium systems after deconfinement," Phys. Rev. D **69**, 094507 (2004) [arXiv:hep-lat/0312037];

[60] H. Iida, T. Doi, N. Ishii and H. Suganuma, "J/psi at high temperatures in anisotropic lattice QCD," PoS **LAT2005** (2006) 184 [arXiv:hep-lat/0509129];

[61] A. Jakovac, P. Petreczky, K. Petrov and A. Velytsky, "Quarkonium correlators and spectral functions at zero and finite temperature," Phys. Rev. D **75**, 014506 (2007) [arXiv:hep-lat/0611017].

[62] R. Morrin *et al.*, "Charmonium spectral functions in N(f) = 2 QCD," PoS **LAT2005**, 176 (2005) [arXiv:hep-lat/0509115];

[63] G. Aarts *et al.*, "Charmonium spectral functions in $N_f = 2$ QCD at high temperature," PoS **LAT2006**, 126 (2006) [arXiv:hep-lat/0610065];

[64] G. Aarts *et al.*, "Charmonium at high temperature in two-flavor QCD," arXiv:0705.2198 [hep-lat];

[65] M. B. Oktay *et al.*, "Charmonium properties in the quark-gluon plasma," arXiv:0710.2795 [hep-lat].

[66] M. Laine, O. Philipsen, P. Romatschke and M. Tassler, "Real-time static potential in hot QCD," JHEP **0703**, 054 (2007) [arXiv:hep-ph/0611300];

[67] M. Laine, "A resummed perturbative estimate for the quarkonium spectral function in hot QCD," JHEP **0705**, 028 (2007) [arXiv:0704.1720 [hep-ph]];

[68] M. Laine, O. Philipsen and M. Tassler, "Thermal imaginary part of a real-time static potential from classical lattice gauge theory simulations," JHEP **0709**, 066 (2007) [arXiv:0707.2458 [hep-lat]];

[69] Y. Burnier, M. Laine and M. Vepsalainen, "Heavy quarkonium in any channel in resummed hot QCD," arXiv:0711.1743 [hep-ph].

[70] B. Alessandro *et al.* [NA50 Collaboration], "A new measurement of J/psi suppression in Pb - Pb collisions at 158-GeV per nucleon," Eur. Phys. J. C **39**, 335 (2005) [arXiv:hep-ex/0412036];

[71] R. Arnaldi *et al.* [NA60 Collaboration], "J/psi suppression in In In collisions at 158-GeV/nucleon," Nucl. Phys. A **783** (2007) 261 [arXiv:nucl-ex/0701033].

[72] A. Adare *et al.* [PHENIX Collaboration], "J/psi production vs centrality, transverse momentum, and rapidity in Au+ Au collisions at s(NN)**(1/2) = 200-GeV," Phys. Rev. Lett. **98** (2007) 232301 [arXiv:nucl-ex/0611020].

[73] F. Carminati *et al.* [ALICE Collaboration], "Alice: Physics Performance Report, Volume I," J. Phys. G **30**, 1517 (2004);

[74] B. Alessandro *et al.* [ALICE Collaboration], "ALICE: Physics performance report, volume II," J. Phys. G **32**, 1295 (2006);

[75] D. d'Enterria *et al.* [CMS Collaboration], "CMS physics technical design report: Addendum on high density QCD with heavy ions," J. Phys. G **34**, 2307 (2007).

[76] K. Adcox *et al.* [PHENIX Collaboration], "Formation of dense partonic matter in relativistic nucleus nucleus collisions at RHIC: Experimental evaluation by the PHENIX collaboration," Nucl. Phys. A **757** (2005) 184 [arXiv:nucl-ex/0410003];

[77] B. B. Back *et al.* [PHOBOS Collaboration], "The PHOBOS perspective on discoveries at RHIC," Nucl. Phys. A **757** (2005) 28 [arXiv:nucl-ex/0410022];

[78] I. Arsene *et al.* [BRAHMS Collaboration], "Quark gluon plasma and color glass condensate at RHIC? The perspective from the BRAHMS experiment," Nucl. Phys. A **757** (2005) 1 [arXiv:nucl-ex/0410020];

[79] J. Adams *et al.* [STAR Collaboration], "Experimental and theoretical challenges in the search for the quark gluon plasma: The STAR collaboration's critical assessment of the evidence from RHIC collisions," Nucl. Phys. A **757** (2005) 102 [arXiv:nucl-ex/0501009].

[80] J. W. Qiu, "Factorization for hadronic heavy quarkonium production," Nucl. Phys. A **783** (2007) 309 [arXiv:nucl-th/0610128].

[81] J. W. Qiu, J. P. Vary and X. f. Zhang, "J/psi suppression in nucleus nucleus collisions," Phys. Rev. Lett. **88** (2002) 232301 [arXiv:hep-ph/9809442].

[82] D. Kharzeev and K. Tuchin, "Signatures of the color glass condensate in J/psi production off nuclear targets," Nucl. Phys. A **770** (2006) 40 [arXiv:hep-ph/0510358].

[83] R. L. Thews, M. Schroedter and J. Rafelski, "Enhanced J/psi production in deconfined quark matter," Phys. Rev. C **63** (2001) 054905 [arXiv:hep-ph/0007323];

[84] L. Grandchamp and R. Rapp, "Thermal versus direct J/psi production in ultrarelativistic heavy-ion collisions," Phys. Lett. B **523** (2001) 60 [arXiv:hep-ph/0103124];

[85] A. Andronic, P. Braun-Munzinger, K. Redlich and J. Stachel, "Statistical hadronization of charm in heavy-ion collisions at SPS, RHIC and LHC," Phys. Lett. B **571** (2003) 36 [arXiv:nucl-th/0303036].

[86] F. Karsch and R. Petronzio, "chi and J/ psi supression in heavy ion collision and a model for its momentum dependence," Z. Phys. C **37**, 627 (1988).

[87] S. J. Brodsky and A. H. Mueller, Phys. Lett. B **206** (1988) 685;

[88] S. Gavin, M. Gyulassy and A. Jackson, "Hadronic J/psi Suppression in Ultrarelativistic Nuclear Collisions," Phys. Lett. B **207** (1988) 257;

[89] N. Armesto and A. Capella, "A quantitative reanalysis of J/psi suppression in nuclear collisions," Phys. Lett. B **430** (1998) 23 [arXiv:hep-ph/9705275].

[90] D. Kharzeev and H. Satz, "Quarkonium interactions in hadronic matter," Phys. Lett. B **334** (1994) 155 [arXiv:hep-ph/9405414];

[91] S. G. Matinyan and B. Muller, "A model of charmonium absorption by light mesons," Phys. Rev. C **58** (1998) 2994 [arXiv:nucl-th/9806027];

[92] L. Maiani, F. Piccinini, A. D. Polosa and V. Riquer, "J/psi absorption in heavy-ion collisions," Nucl. Phys. A **741** (2004) 273 [arXiv:hep-ph/0402275].

[93] D. Kharzeev and H. Satz, "Charmonium interaction in nuclear matter," Phys. Lett. B **356** (1995) 365 [arXiv:hep-ph/9504397].

[94] S. S. Adler *et al.* [PHENIX Collaboration], "J/psi production and nuclear effects for d + Au and p + p collisions at s(NN)**(1/2) = 200-GeV," Phys. Rev. Lett. **96** (2006) 012304 [arXiv:nucl-ex/0507032].

[95] G. Policastro, D. T. Son and A. O. Starinets, "The shear viscosity of strongly coupled N = 4 supersymmetric Yang-Mills plasma," Phys. Rev. Lett. **87**, 081601 (2001) [arXiv:hep-th/0104066].

[96] D. Bak, A. Karch and L. G. Yaffe, "Debye screening in strongly coupled N=4 supersymmetric Yang-Mills plasma," JHEP **0708**, 049 (2007) [arXiv:0705.0994 [hep-th]].

[97] I. Amado, C. Hoyos-Badajoz, K. Landsteiner and S. Montero, "Absorption Lengths in the Holographic Plasma," JHEP **0709**, 057 (2007) [arXiv:0706.2750 [hep-th]].

[98] S. D. Avramis, K. Sfetsos and D. Zoakos, "On the velocity and chemical-potential dependence of the heavy-quark interaction in N = 4 SYM plasmas," Phys. Rev. D **75**, 025009 (2007) [arXiv:hep-th/0609079].

[99] M. Natsuume and T. Okamura, "Screening length and the direction of plasma winds," JHEP **0709**, 039 (2007) [arXiv:0706.0086 [hep-th]].

[100] A. Karch and E. Katz, "Adding flavor to AdS/CFT," JHEP **0206**, 043 (2002) [arXiv:hep-th/0205236].

[101] M. Kruczenski, D. Mateos, R. C. Myers and D. J. Winters, "Meson spectroscopy in AdS/CFT with flavour," JHEP **0307**, 049 (2003) [arXiv:hep-th/0304032].

[102] M. Kruczenski, D. Mateos, R. C. Myers and D. J. Winters, "Towards a holographic dual of large-N(c) QCD," JHEP **0405**, 041 (2004) [arXiv:hep-th/0311270].

[103] S. Hong, S. Yoon and M. J. Strassler, "Quarkonium from the fifth dimension," JHEP **0404**, 046 (2004) [arXiv:hep-th/0312071].

[104] I. Kirsch and D. Vaman, "The D3/D7 background and flavor dependence of Regge trajectories," Phys. Rev. D **72**, 026007 (2005) [arXiv:hep-th/0505164].

[105] R. C. Myers and R. M. Thomson, "Holographic mesons in various dimensions," JHEP **0609**, 066 (2006) [arXiv:hep-th/0605017].

[106] R. C. Myers, A. O. Starinets and R. M. Thomson, "Holographic spectral functions and diffusion constants for fundamental arXiv:0706.0162 [hep-th].

[107] K. Peeters and M. Zamaklar, "Dissociation by acceleration," arXiv:0711.3446 [hep-th].

[108] J. Erdmenger, N. Evans, I. Kirsch and E. Threlfall, "Mesons in Gauge/Gravity Duals - A Review," arXiv:0711.4467 [hep-th].

[109] See Eqs. 22.7.1-3 in M. Abramowitz and I. A. Stegun, eds., **Handbook of Mathematical Functions**, U.S. Government Printing Office, Washington, DC,1964.

[110] N. Itzhaki, J. M. Maldacena, J. Sonnenschein and S. Yankielowicz, "Supergravity and the large N limit of theories with sixteen supercharges," Phys. Rev. D **58**, 046004 (1998) [arXiv:hep-th/9802042].

[111] D. Arean and A. V. Ramallo, "Open string modes at brane intersections," JHEP **0604**, 037 (2006) [arXiv:hep-th/0602174].

[112] M. A. Lisa, S. Pratt, R. Soltz and U. Wiedemann, "Femtoscopy in relativistic heavy ion collisions," Ann. Rev. Nucl. Part. Sci. **55**, 357 (2005) [arXiv:nucl-ex/0505014].

[113] R. Lednicky, V. L. Lyuboshits, B. Erazmus and D. Nouais, "How to measure which sort of particles was emitted earlier and which later," Phys. Lett. B **373** (1996) 30.

[114] For a review, see C. G. Callan and L. Thorlacius, "Sigma Models And String Theory," in **Particles, strings and supernovae: proceedings of TASI Institute in Elementary Particle Physics**, A. Jevicki and C.-I. Tan, eds. (Worlds Scientific: 1989).

[115] See Chapter 10 and in particular Eq. (10.2.23) in R. M. Wald, **General Relativity**, (University of Chicago Press, 1984).

[116] H. B. Meyer, "Energy-momentum tensor correlators and viscosity," arXiv:0809.5202 [hep-lat].

[117] P. Kovtun, D. T. Son and A. O. Starinets, "Holography and hydrodynamics: Diffusion on stretched horizons," JHEP **0310**, 064 (2003) [arXiv:hep-th/0309213];

[118] A. Buchel and J. T. Liu, "Universality of the shear viscosity in supergravity," Phys. Rev. Lett. **93**, 090602 (2004) [arXiv:hep-th/0311175];

[119] P. Kovtun, D. T. Son and A. O. Starinets, "Viscosity in strongly interacting quantum field theories from black hole physics," Phys. Rev. Lett. **94**, 111601 (2005) [arXiv:hep-th/0405231];

[120] C. P. Herzog, "Energy loss of heavy quarks from asymptotically AdS geometries," JHEP **0609**, 032 (2006) [arXiv:hep-th/0605191];

[121] J. Casalderrey-Solana and D. Teaney, "Heavy quark diffusion in strongly coupled $N = 4$ Yang Mills," Phys. Rev. D **74**, 085012 (2006) [arXiv:hep-ph/0605199];

[122] J. Casalderrey-Solana and D. Teaney, "Transverse momentum broadening of a fast quark in a $N = 4$ Yang Mills plasma," JHEP **0704**, 039 (2007) [arXiv:hep-th/0701123];

[123] D. T. Son and A. O. Starinets, JHEP **0209**, 042 (2002) [arXiv:hep-th/0205051].

[124] Q. J. Ejaz, T. Faulkner, H. Liu, K. Rajagopal and U. A. Wiedemann, "A limiting velocity for quarkonium propagation in a strongly coupled plasma via AdS/CFT," JHEP **0804**, 089 (2008) [arXiv:0712.0590 [hep-th]].

[125] S. Nakamura, Y. Seo, S. J. Sin and K. P. Yogendran, "A new phase at finite quark density from AdS/CFT," arXiv:hep-th/0611021.

[126] R. C. Myers and A. Sinha, "The fast life of holographic mesons," arXiv:0804.2168 [hep-th].

[127] J. Erdmenger, M. Kaminski and F. Rust, "Holographic vector mesons from spectral functions at finite baryon or isospin density," Phys. Rev. D **77**, 046005 (2008) [arXiv:0710.0334 [hep-th]].

[128] J. Mas, J. P. Shock, J. Tarrio and D. Zoakos, "Holographic Spectral Functions at Finite Baryon Density," arXiv:0805.2601 [hep-th].

[129] E. S. Fradkin and A. A. Tseytlin, "Nonlinear Electrodynamics From Quantized Strings," Phys. Lett. B **163**, 123 (1985).

[130] M. Dine, N. Seiberg, X. G. Wen and E. Witten, "Nonperturbative Effects on the String World Sheet," Nucl. Phys. B **278**, 769 (1986);

[131] E. Witten, "World-sheet corrections via D-instantons," JHEP **0002**, 030 (2000) [arXiv:hep-th/9907041].

[132] K. Dusling, J. Erdmenger, M. Kaminski, F. Rust, D. Teaney and C. Young, JHEP **0810**, 098 (2008) [arXiv:0808.0957 [hep-th]].

[133] D. Mateos and L. Patino, "Bright branes for strongly coupled plasmas," JHEP **0711**, 025 (2007) [arXiv:0709.2168 [hep-th]].

[134] J. Casalderrey-Solana and D. Mateos, "Prediction of a Photon Peak in Heavy Ion Collisions," arXiv:0806.4172 [hep-ph].

[135] A. Karch, D. T. Son and A. O. Starinets, "Zero Sound from Holography," arXiv:0806.3796 [hep-th].

[136] M. Kulaxizi and A. Parnachev, "Comments on Fermi Liquid from Holography," Phys. Rev. D **78**, 086004 (2008) [arXiv:0808.3953 [hep-th]].

[137] M. Kulaxizi and A. Parnachev, "Holographic Responses of Fermion Matter," arXiv:0811.2262 [hep-th].

[138] K. Y. Kim and I. Zahed, "Baryonic Response of Dense Holographic QCD," arXiv:0811.0184 [hep-th].

[139] S. Kobayashi, D. Mateos, S. Matsuura, R. C. Myers and R. M. Thomson, "Holographic phase transitions at finite baryon density," JHEP **0702**, 016 (2007) [arXiv:hep-th/0611099].

[140] J. Erdmenger, M. Kaminski, P. Kerner and F. Rust, "Finite baryon and isospin chemical potential in AdS/CFT with flavor," JHEP **0811**, 031 (2008) [arXiv:0807.2663 [hep-th]].

[141] N. Horigome and Y. Tanii, "Holographic chiral phase transition with chemical potential," JHEP **0701**, 072 (2007) [arXiv:hep-th/0608198].

[142] K. Y. Kim, S. J. Sin and I. Zahed, "Dense hadronic matter in holographic QCD," arXiv:hep-th/0608046.

[143] T. Faulkner and H. Liu, "Meson widths from string worldsheet instantons," arXiv:0807.0063 [hep-th].

[144] T. Faulkner and H. Liu, to appear.